Vol. 1, No. 3, September 2025
jams.hsu.ac.ir

JOURNAL OF APPLIED MATERIAL SCIENCE

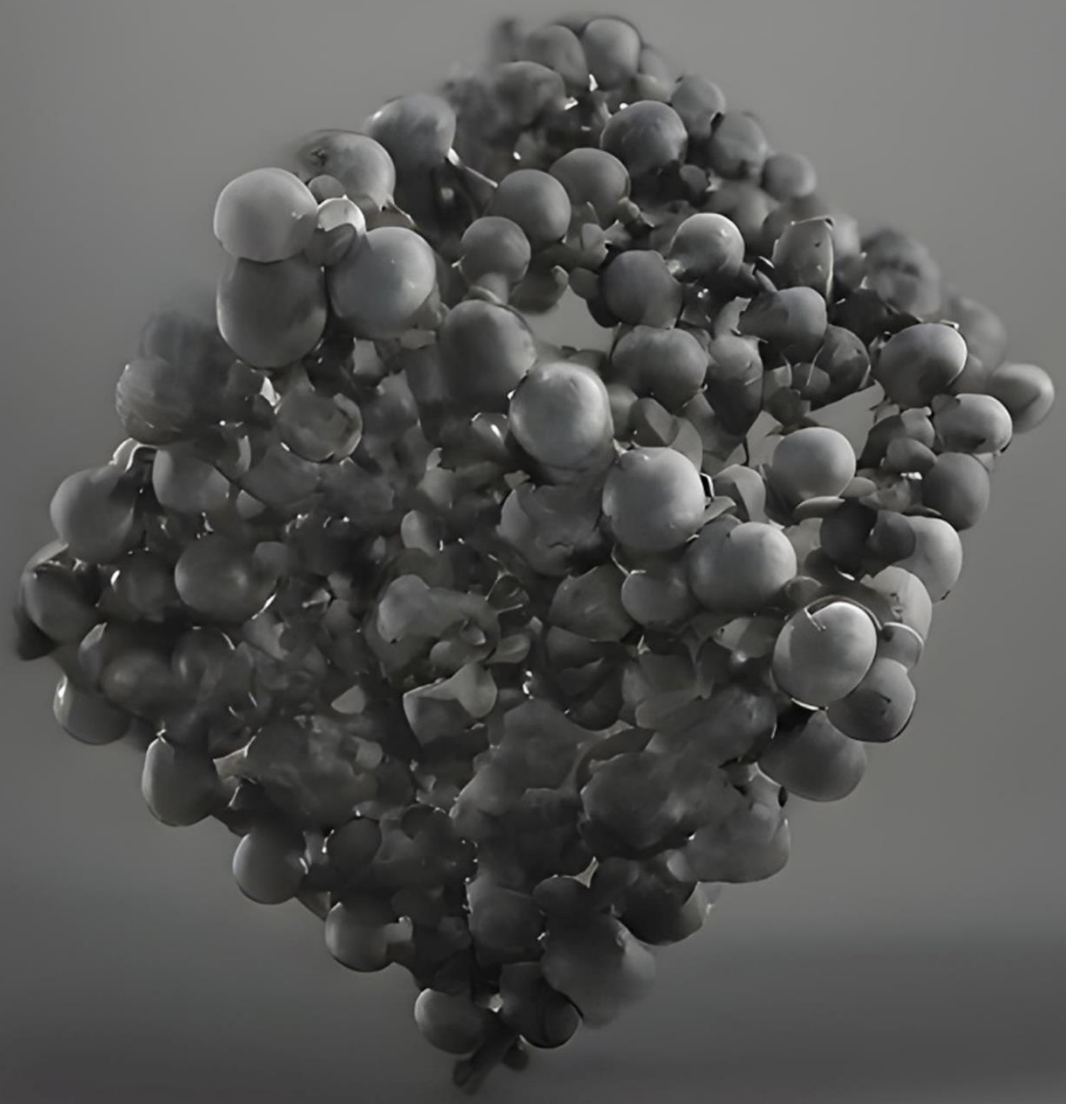

Hakim Sabzevari University

JOURNAL OF
APPLIED
MATERIAL
SCIENCE
jams.hsu.ac.ir

Contents

Volume 1, No. 3, September 2025

Editorial **210142**

Aims and scope of the journal, a brief submission guideline, and the list of the editorial board.

Ahmad Allahbakhsh

doi: 10.22034/jams.2025.210142

Microplastics: Pollution of the Modern World **210143**

Microplastics, due to their small size and lightweight nature, have raised significant health concerns in recent years. They can influence our lives both directly and indirectly, making responsible management of plastic waste more important than ever. In this invited mini-review, Sheydaei discusses microplastic pollution and its sources, as well as the effects of microplastics on marine organisms.

Milad Sheydaei

doi: 10.22034/jams.2025.210143

Fluoride Adsorption Behavior in Cost-effective Plant-based Bio-sorbents **210144**

The detrimental effects of excessive fluoride on the health of both humans and animals through drinking-water sources are evident, particularly regarding dental and skeletal fluorosis. This underscores the critical need for stringent control of fluoride concentration levels in drinking water. In their study, Visarapu et al. presented various plant-based biosorbents for fluoride removal, and their results demonstrated that Hibiscus leaves achieved a high fluoride removal efficiency with an impressively low dosage of just 1 g.

Malathi Visarapu, Anna Tanuja Safala B., Bharath Kumar Ch., Madhavi Vemula

doi: 10.22034/jams.2025.210144

© 2025 *J. Appl. Mater. Sci.* This material is licensed under a Creative Commons Attribution 4.0 International License.

A Theoretical and Experimental Analysis of the Complexation Process Between Progesterone and Cyclodextrin Nanosponge 210145

In this study, Hadadian et al. synthesized cyclodextrin nanosponges using hexamethylene diisocyanate as the crosslinker and investigated the complexation of progesterone within the nanosponge structure of these carriers. Their experimental and theoretical findings suggest the formation of a 1:2 (drug:host) molar ratio complex, indicating that hydrogen bonding is the primary driving force behind this phenomenon.

Mehrdad Hadadian, Behnam Mahdavi, Esmail Rezaei-Seresht

doi: 10.22034/jams.2025.210145

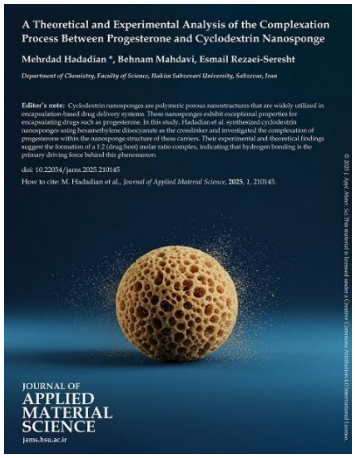

Antibacterial/Magnetic Iron Oxide Nanoparticles: A Comprehensive Review of Synthesis Methods, Doping Effects, Antibacterial Properties, and Applications in Medical and Food Industries 210146

In this systematic review, Hosseinzadeh provided a detailed overview of recent studies on the effects of various dopants on the antibacterial mechanisms of magnetic nanoparticles. These dopants boosted the antibacterial activity of these nanoparticles for a variety of applications in clinical, food, and environmental fields, such as drug delivery systems, coatings for implants, wound healing, and antimicrobial packaging.

Hamid Hosseinzadeh

doi: 10.22034/jams.2025.210146

Effect of $CoCl_2$ Doping on the Optical and Electrical Properties of PEO Polymer Films for Optoelectronic Applications 210147

Roopa K. V. and Subramanya K. investigated the doping of PEO films with cobaltous chloride ($CoCl_2$) at various concentrations. Their findings indicated that the interaction between Co^{2+} ions and the ether groups of PEO results in the formation of metal-ligand coordination bonds within the doped PEO films. This interaction significantly enhances the electrical conductivity and ion mobility of the $CoCl_2$-doped PEO films and results in a redshift in the absorption edge of these films.

Roopa K. V., Subramanya Kilarkaje

doi: 10.22034/jams.2025.210147

© 2025 *J. Appl. Mater. Sci.* This material is licensed under a Creative Commons Attribution 4.0 International License.

Investigation of Wear Resistance and Corrosion of Ni-PTFE Composite Coatings Prepared by Electrodeposition Method 210148

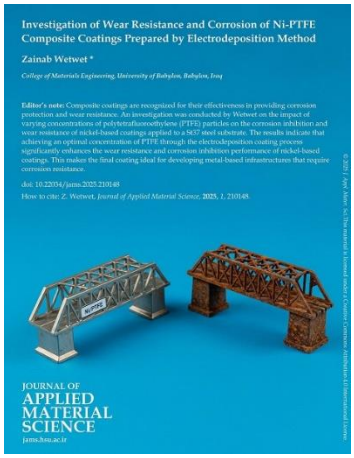

An investigation was conducted by Wetwet on the impact of varying concentrations of polytetrafluoroethylene (PTFE) particles on the corrosion inhibition and wear resistance of nickel-based coatings applied to a St37 steel substrate. The results indicate that achieving an optimal concentration of PTFE through the electrodeposition coating process significantly enhances the wear resistance and corrosion inhibition performance of nickel-based coatings. This makes the final coating ideal for developing metal-based infrastructures that require corrosion resistance.

Zainab Wetwet

doi: 10.22034/jams.2025.210148

ABOUT COVER

The proper selection of elements in a unit cell directly influences the predictions made by an analytical model. Various classes of elements, which represent the solid and fluid phases involved in thermal and electrical conductivity, have been used in the literature to develop different types of analytical models. The cover features a regenerated image based on a unit cell containing spherical elements, aimed at predicting the thermal conductivity of porous materials.

(Note: The covers of this journal are created in part using artificial intelligence (AI) technologies, with direct human supervision. AI and AI-assisted technologies are permitted only for generating graphical abstract suggestions. If such technologies are used in the manuscript preparation, it must be clearly disclosed in the Acknowledgments section.)

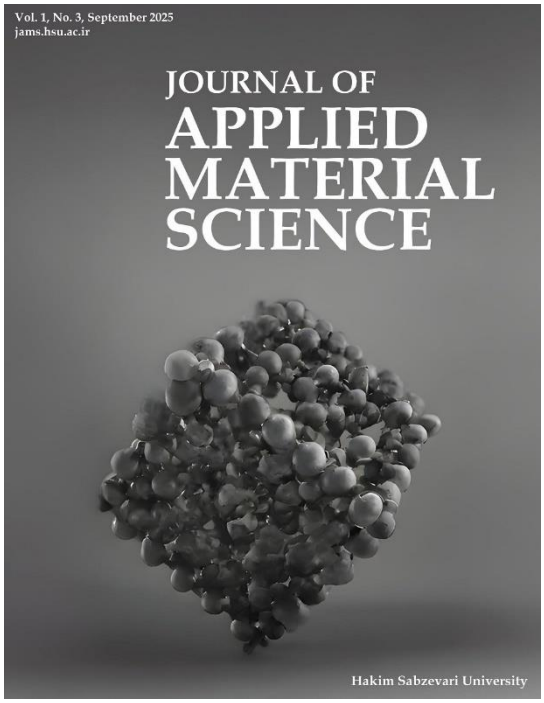

© 2025 *J. Appl. Mater. Sci.* This material is licensed under a Creative Commons Attribution 4.0 International License.

jams.hsu.ac.ir JOURNAL OF APPLIED MATERIAL SCIENCE

Journal of Applied Material Science:

an *open-access* platform to publish scientific developments in all aspects of material science under the *highest publication standards* and *the fastest peer-review process*

The Journal of Applied Material Science publishes original research in the form of ***communications*** and ***full papers***, as well as ***reviews***, invited ***mini-reviews***, and invited research news. Publication in this journal is **entirely free of charge**, and all accepted papers will be available online immediately after typesetting. Dr. Ahmad Allahbakhsh, along with an international team of editors, leads the journal to meet the highest publication standards. We are looking forward to receiving your submissions.

Editor-in-Chief: Dr. Ahmad Allahbakhsh (Hakim Sabzevari University)

Director in charge: Prof. Gholamali Farzi (Hakim Sabzevari University)

International Editorial Board Members:

Prof. Ahmad Reza Bahramian (Tarbiat Modares University),
Prof. Mohammadhosein (Momo) Safari (Hasselt University),
Prof. Denis Rodrigue (Laval University),
Prof. Ursula Windberger (Medical University of Vienna),
Prof. Gholamali Farzi (Hakim Sabzevari University),
Prof. Sabu Thomas (Mahatma Gandhi University),
Dr. Hamidreza Oveisi (Hakim Sabzevari University),
Prof. Manoj Balachandran (CHRIST University),
Dr. Rasoul Esmaeely Neisiany (Hakim Sabzevari University),
Prof. Raffaella Mancuso (University of Calabria),
Dr. Ahmad Allahbakhsh (Hakim Sabzevari University)

Journal of Applied Material Science is an open-access journal, which means that all content is freely available without charge to the users and institutions. Users are allowed to read, download, copy, distribute, print, search, or link to the full texts of the articles, or use them for any other lawful purpose, without asking prior permission from the publisher or the author. This is in accordance with the BOAI definition of open access. Authors are free to deposit a copy of their paper (Published version, Version of Record) in an institutional or other repository of their choice.

To submit a manuscript: Please consult the **aim and scope** of the journal at: https://jams.hsu.ac.ir/journal/aim_scope

Guide for Authors is available at: https://jams.hsu.ac.ir/journal/authors.note

To **submit** your paper, please visit: https://jams.hsu.ac.ir/author

https://doi.org/10.22034/jams.2025.210142
J. Appl. Mater. Sci., **2025**, *1*, 210142.
© 2025 *J. Appl. Mater. Sci.* This material is licensed under a Creative Commons Attribution 4.0 International License.

Microplastics: Pollution of the Modern World

Milad Sheydaei *

Department of Chemical Engineering, Faculty of Engineering, University of Garmsar, Garmsar, Iran

Editor's note: Microplastics, due to their small size and lightweight nature, have raised significant health concerns in recent years. They can influence our lives both directly and indirectly, making responsible management of plastic waste more important than ever. In this invited mini-review, Sheydaei discusses microplastic pollution and its sources, as well as the effects of microplastics on marine organisms.

doi: 10.22034/jams.2025.210143

How to cite: M. Sheydaei. *Journal of Applied Material Science*, **2025**, *1*, 210143.

JOURNAL OF
APPLIED
MATERIAL
SCIENCE
jams.hsu.ac.ir

© 2025 *J. Appl. Mater. Sci.* This material is licensed under a Creative Commons Attribution 4.0 International License.

Journal of Applied Material Science **2025**, *1*, 210143
How to cite: M. Sheydaei, *Journal of Applied Material Science*, **2025**, *1*, 210143.
Journal homepage: **jams.hsu.ac.ir**

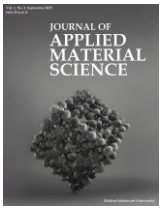

Invited Review

Microplastics: Pollution of the Modern World

Milad Sheydaei *

Department of Chemical Engineering, Faculty of Engineering, University of Garmsar, Garmsar, Iran

Abstract

With the progress of industry and economy in societies, unfortunately, we are witnessing more pollution of the environment every day. It is believed that the progress of science and industry will bring comfort to the inhabitants of the Earth, but in reality, we are witnessing increasing pollution in many areas. Among all the pollutants, for several decades, humans have been causing a new pollution, and that is microplastics. Simply put, plastic particles smaller than 5 mm are called microplastics. They can be found everywhere, and, unfortunately, they have a long shelf life and high stability, so they slowly degrade. They have a high potential for fragmentation, which is why they are constantly decreasing in size, and this increases the scope of pollution. Also, they absorb many pollutants and can be considered as carriers of other pollutants. Microplastics easily accumulate in many organisms through ingestion and breathing, leading to physical damage. However, many of them contain chemical additives and can cause toxic effects. This review paper discusses microplastic pollution and its sources. The effects of microplastics on marine organisms are also addressed.

Keywords: Environmental pollution; Removal method; Marine organisms.

1. Introduction

The progress of industry and society has brought prosperity and comfort to humans, but on the other hand, it has caused great damage to the environment, which ultimately endangers the health of humans and other creatures living on earth [1-3]. Climate change, deforestation, and pollution of water resources and soil can be considered examples of this disaster [4-6]. Meanwhile, plastics are a group of polymers that are of great interest due to their unique properties, such as flexibility, cheapness, and easy molding [7, 8]. For this reason, in contemporary society, plastics can be seen in most applications. It has been reported in the literature that the annual production of plastic goods has increased from 1.5 million tons in the 1950s to 450 million tons in 2024 [9]. It can be said that the most common plastics produced are polystyrene (PS), polypropylene, polyamide (PA), polyethylene terephthalate (PET), polyethylene (PE), and polyvinyl chloride (PVC) [10]. Plastic waste pollution is of great importance because they have a long lifespan and many of them contain harmful substances such as bisphenol A [11]. Figure 1 shows the global cumulative disposal of inadequately managed plastic waste from 1950 to 2060.

Meanwhile, an uninvited guest has been a serious concern for all people on Earth for years: micro- and nano-scale plastic waste. They can be considered a new

* Corresponding author.
Email addresses: md.sheydaei@fmgarmsar.ac.ir, m.sheydaei@yahoo.com (M. Sheydaei)

Received 4 June 2025
Revised 28 June 2025
Accepted 28 June 2025
Available online 6 July 2025

https://doi.org/10.22034/jams.2025.210143
© 2025 The Authors. This article is licensed under a Creative Commons Attribution 4.0 International License.

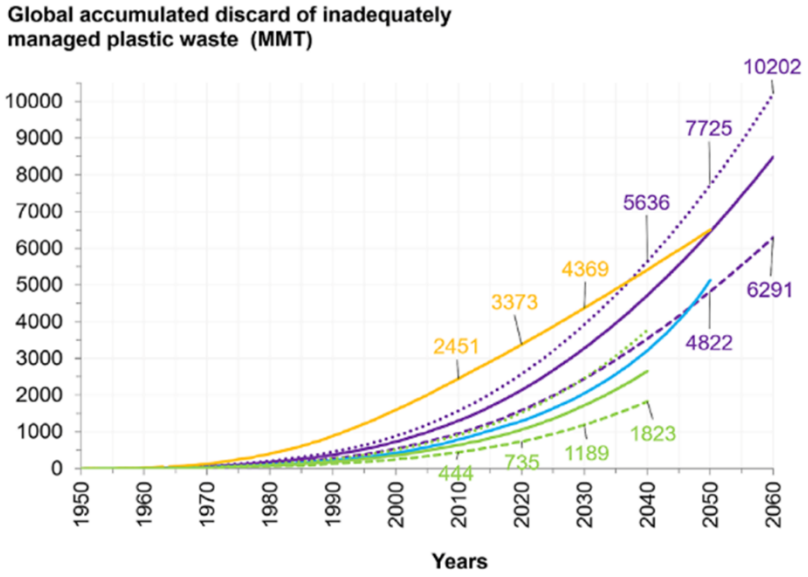

Figure 1. Global cumulative discard of plastic waste inadequately managed over 1950–2060 – The Business-As-Usual (BAU) scenario (MMT: million metric tons). Reprinted with permission from [9]. 2024, Cambridge University Press.

problem arising from plastic pollution. Due to their size, they can unfortunately easily enter the bodies of humans and fauna (see Figure 2). Due to their lightweight nature, microplastics are easily transported and can contaminate locations far from where they were produced [12]. Microplastics readily contaminate soil and water, and in recent years, their presence in the oceans has significantly increased, with concentrations reported to reach up to 100,000 particles per cubic meter [13]. The National Oceanic and Atmospheric Administration

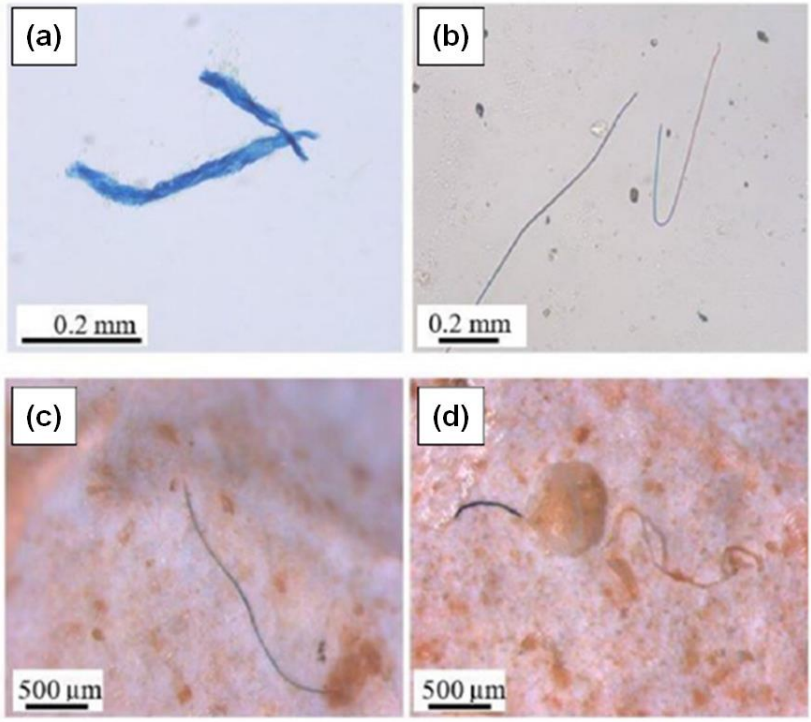

Figure 2. Microplastic fibers and filaments in the gastrointestinal tracts of myctophid fish (a-d). Reprinted with permission from [12]. 2023, MDPI.

© 2025 The Authors. This article is licensed under a Creative Commons Attribution 4.0 International License.

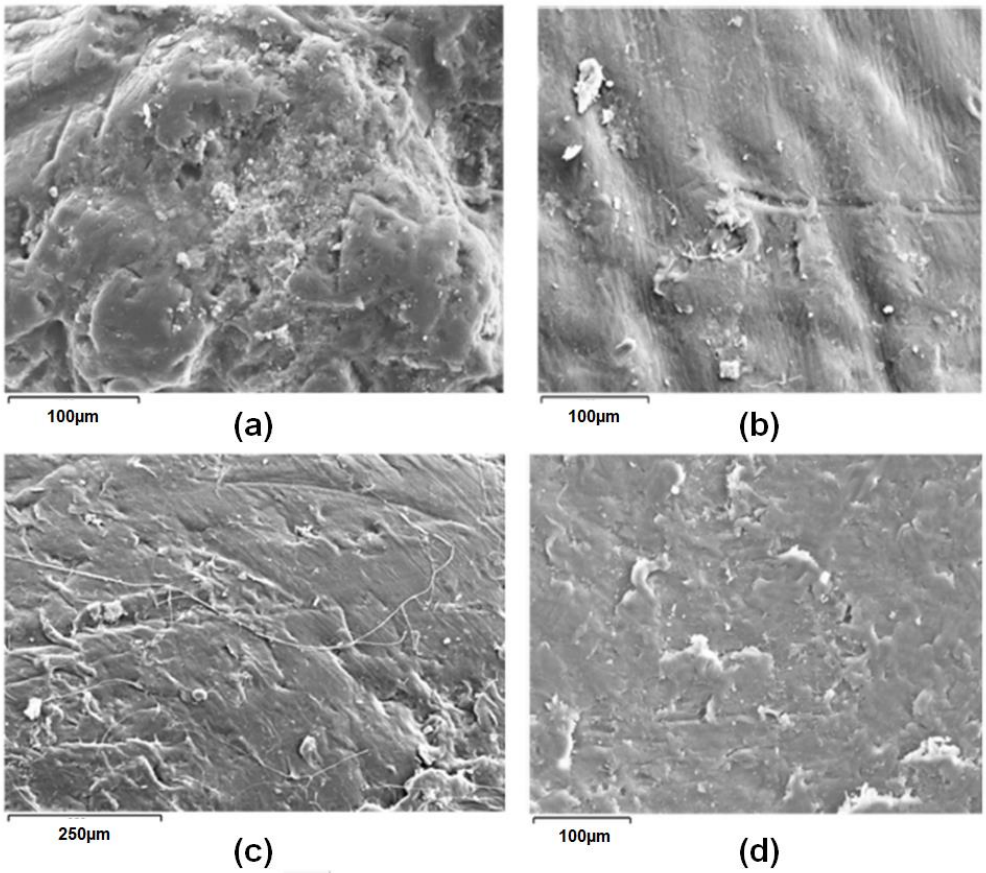

Figure 3. SEM images of pellets: (a) Before clean-up, (b) After the spill, (c) 5 months after the spill, and (d) 6 months after the spill. Reprinted with permission from [15]. 2022, MDPI.

defines microplastics as particles smaller than 5 mm in size [14].

Microplastics can be the result of the fragmentation of larger items, or they can be particles that are purposefully manufactured to a microscopic size. In October 2018, a storm in the Durban harbour (South Africa) resulted in the spillage of about 2,000 tons of polyethylene pellets, raising environmental concerns, and Mofokeng and Glassom [15] investigated this contamination.

Scanning electron microscopy (SEM) results (see Figures 3 and 4) showed that the old pellets had cracks while the newer pellets were smooth with little abrasion. After five and six months in the environment, the pellets showed signs of surface abrasion and deterioration, respectively. Bacterial and fungal growth was also observed on the surface of the old pellets after two months. Also, no heavy metal contamination was observed in the pellets over time.

In recent years, the use of alternatives to plastics, including glass and biodegradable packaging, has increased, but this approach requires a global agreement [16]. However, raising public awareness and reducing the use of plastic products and their release into the environment is far more valuable than plastic alternatives. This paper addresses microplastics and their negative effects on marine organisms and the research conducted in this field.

2. Microplastic sources

The reports show that the production of plastics derived from fossil fuels is increasing yearly, and plastic waste has become a global problem due to poor management. Microplastics pose a threat to many aquatic species, especially planktonic and invertebrate organisms, as they easily accumulate in their bodies (see

© 2025 The Authors. This article is licensed under a Creative Commons Attribution 4.0 International License.

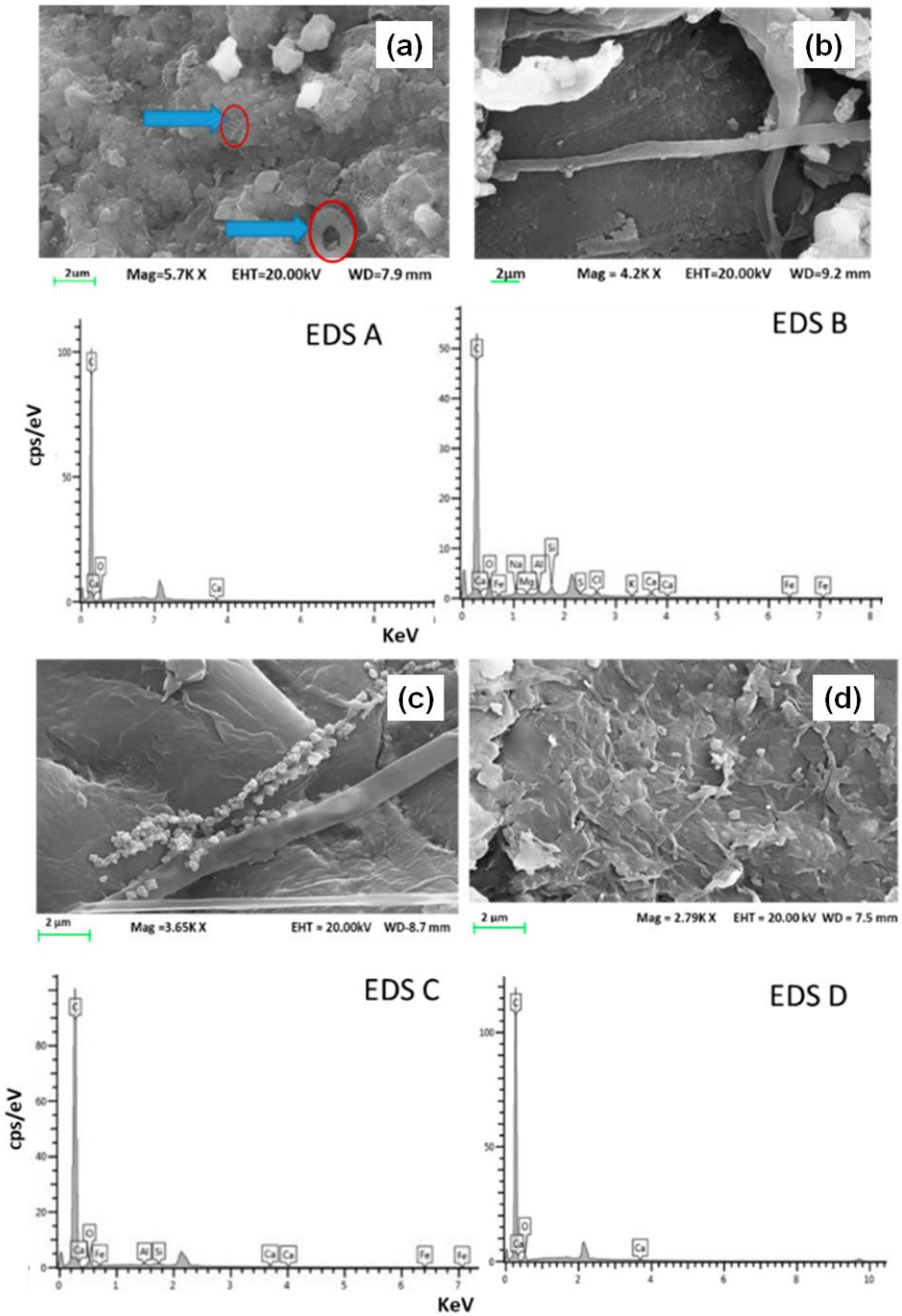

Figure 4. SEM images of pellets collected show surface metal concentrations. (a) Before clean-up (C, Ca, O, Ca), (b) after two months of exposure (C, Ca, O, Fe, Mg, Al, Si, S, Cl, K, Ca, Ca, Fe, Fe), (c) after three months of exposure (C, Ca, Fe, Al, Si, Ca, Ca), and (d) after six months of exposure (C, Ca, O, Ca). The red circles indicate the presence of diatoms on pellets. Reprinted with permission from [15]. 2022, MDPI.

Figure 5) [17, 18]. Many reports suggest that microplastics have the potential to cause chronic toxicity [19, 20]. Law et al. [21] investigated the effects of PS microplastics on marine filter-feeding fish, and the

© 2025 The Authors. This article is licensed under a Creative Commons Attribution 4.0 International License.

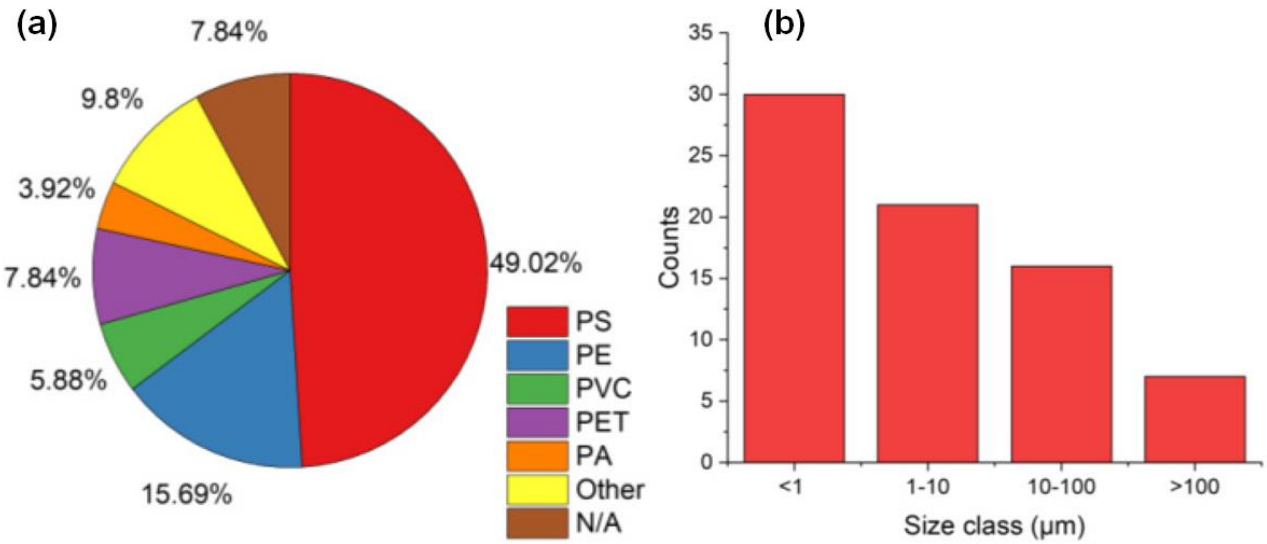

Figure 5. (a) Polymers used in different ecotoxicological tests to expose zooplankton species. (b) Average size distribution of the microplastics used. Reprinted with permission from [18]. 2023, MDPI. (Note: N/A: Studies that did not specify the type of polymer.)

results showed that PS microplastics can be transmitted through the blood and cause reproductive disorders.

The toxicity of microplastics is related to many factors, such as unreacted monomers, oligomers, and additives. These factors are leached under the influence of various factors such as UV light, long rubbing, solvents, and even ocean water [17]. For this reason, food packaging is of great importance because monomers and oligomers can easily migrate into food.

Many additives, such as plasticizers, fillers, inhibitors, and antioxidants, are toxic [17, 22-24]. Some phthalates used in baby bottles have been reported to release in the range of 50–150 μg/kg after a 120 min contact time at 70 °C [25]. This relatively easy release can be attributed to the lack of chemical reaction with the plastic structure, as most of these additives are not chemically bound to plastic structures [17, 26]. In addition to being toxic, plastics unfortunately also have the ability to absorb hydrophobic pollution from water [27]. We can say that they play the role of a Trojan horse.

Primary sources of microplastics include household and industrial sewage and feedstocks used to produce plastics (whether plastic products or granules and powders) [28]. However, secondary sources of microplastics can be identified through mechanical degradation and exposure to solvents and UV light [29]. Many wastewater treatment plants remove large plastic particles, but microplastics can pass through treatment units and enter the aquatic environment [30, 31].

Household sewage contains polymer particles from cosmetics, cleaning, and fibers (mainly polyester, acrylic, and PA) [17, 26]. It has been reported in the literature that bottled water can also contain microplastics [26]. Many foods and beverages should not be served in plastic containers, such as alcoholic beverages, as alcohol can release unreacted monomers and oligomers.

3. Effects of microplastics on marine organisms

The high production of plastics, most of which are designed for single use, has led to environmental pollution. Plastic waste is entering the environment at an uncontrollable rate, with the greatest impact on marine and freshwater ecosystems [14, 32]. They reach the oceans through wind and rivers, causing pollution [14]. One of the most important problems with plastics once they enter the environment is that they are continuously broken down into smaller particles, making them easier to transport [32]. Unfortunately, today microplastics are present even in the most remote marine environments, but gyres can be considered the main place for their accumulation [14, 33]. Brown et al. [34] evaluated the presence of microplastics on eighteen beaches on six continents, and the results showed that microplastics

© 2025 The Authors. This article is licensed under a Creative Commons Attribution 4.0 International License.

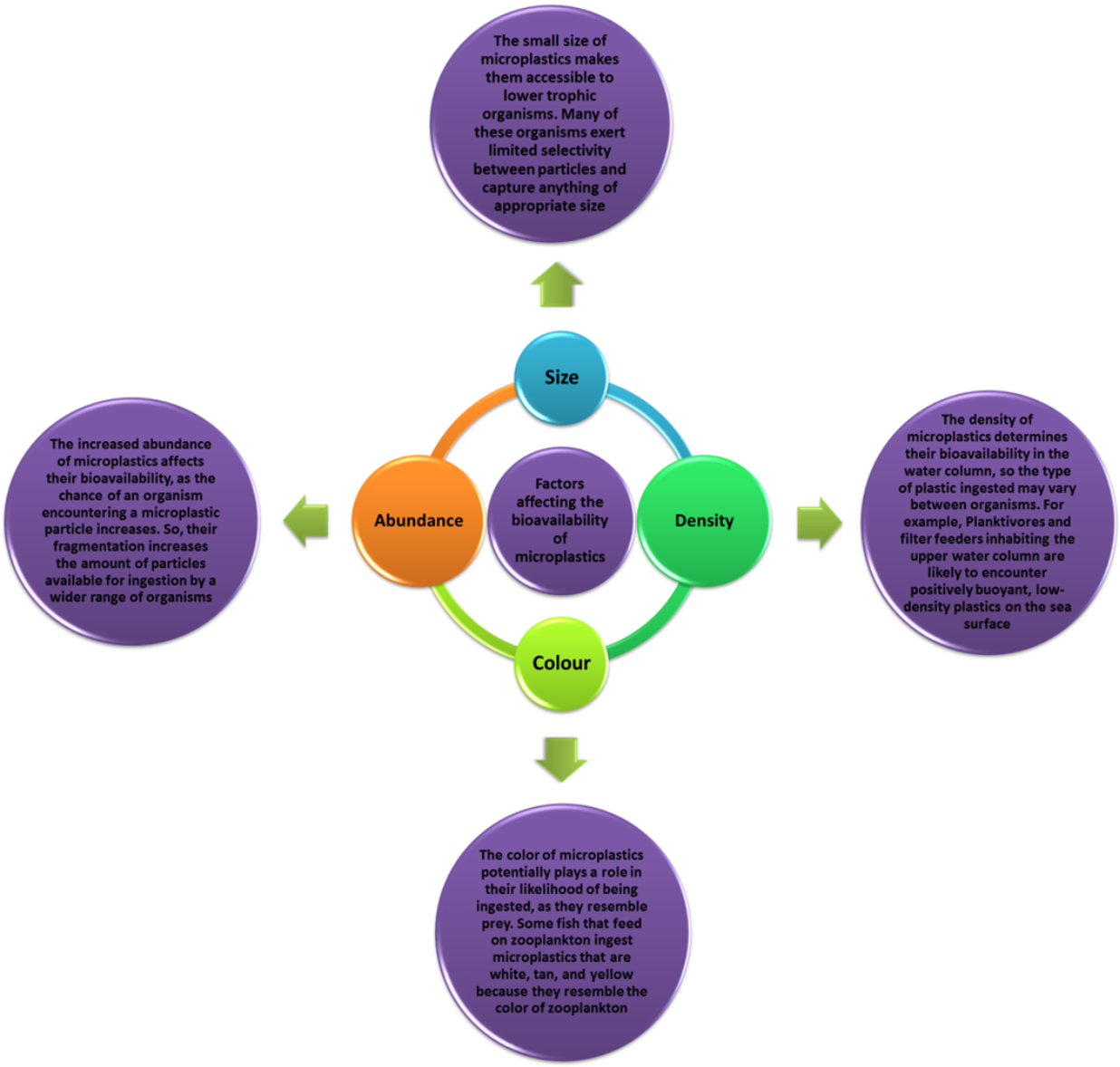

Figure 6. Factors affecting the bioavailability of microplastics.

were present in fibrous forms, with a maximum concentration of 124 fibers per liter. According to reports, microplastics are believed to be a serious threat to more than 250 marine species [14]. Figure 6 shows the factors affecting the bioavailability of microplastics in aquatic ecosystems.

In addition to freshwater, soils are also a site of accumulation of microplastic fibers [35]. They persist for a long time in layers of about 25 cm of agricultural soils treated with sewage sludge (as fertilizer). This indicates a gradual transfer in the solid media and then accumulation at depth [17]. Considering this fact, it can be said that agricultural soils have a higher probability of retaining microplastics compared to other areas [36].

Hunter et al. [37] assessed the presence of pre-production pellets (see Figure 7) in the Avon–Heathcote Estuary/Ihutai (Aotearoa–New Zealand). The results showed seven aggregation points, and a total of 3,819 pellets were identified. They were predominantly transparent (86%), 3 mm in size (54%), cylindrical (62%),

© 2025 The Authors. This article is licensed under a Creative Commons Attribution 4.0 International License.

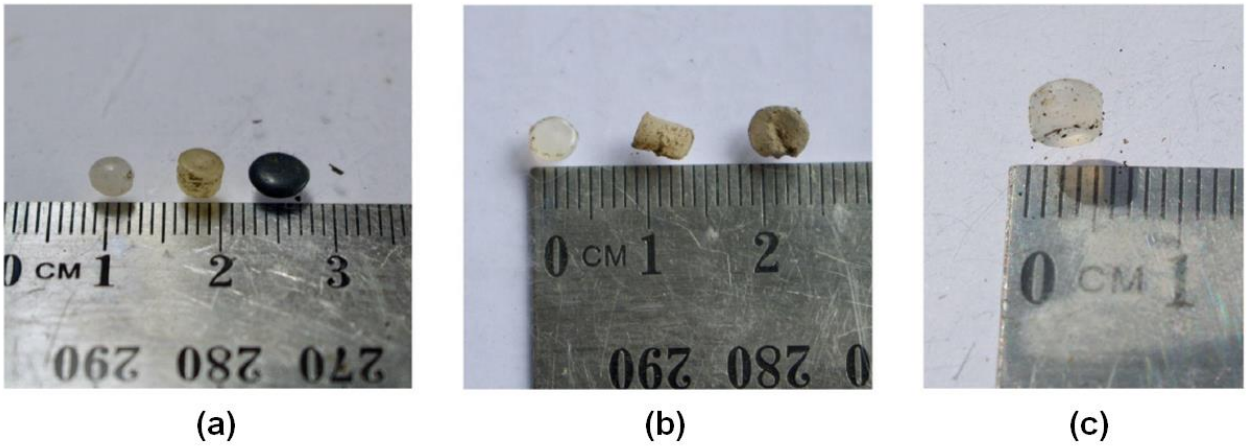

Figure 7. Pellet classification: (a) by shape, from left to right—spherical, cylindrical, lentil, (b) by weathering, from left to right—category "1" no yellowing or cracking, category "2" yellowing only, category "3" yellowing and cracking visible; (c) an exemplar pellet classified as 4 mm size, cylindrical and category "1" weathering. Reprinted with permission from [37]. 2022, MDPI.

moderately weathered (41%), and made of low-density PE (53%). The accumulation and abundance are likely influenced by the river flows along which the plastic producers are located, weather conditions, and proximity to stormwater outlets.

Rivers carry a high volume of microplastics, and in places where the energy of the river flow is low, microplastics settle together with sediments in the riverbed [38]. Riverbed sediments can always be considered an alarm for pollution because they always contain all the pollutants, such as microplastics and heavy metals, and by evaluating the sediments, the level of environmental pollution can be measured [3, 4, 38]. As shown in Figure 6, size and density are very important, as it has been reported that larger sizes with irregular shapes and jagged geometry and sharp ends and higher density of plastic lead to easy sinking in water and presence in sediment, while spherical particles tend to remain on the water surface [39-43]. Therefore, sediments in areas close to factories, densely populated cities, and densely populated coastal regions are highly polluted. Sediment-dwelling organisms such as benthic holothurians *Thyonella gemmate*, and lugworm *Arenicola marina* are always vulnerable to damage from microplastics because they generally have a non-selective feeding strategy and ingest large volumes of sediment, thus also ingesting microplastics or heavy metals [3, 4, 14]. Table 1 reports some marine organisms that are susceptible to ingesting microplastics, as well as their exposure routes to microplastics. Among aquatic organisms, mussels are filter feeders and process a high volume of water, so if the water is contaminated with pollutants, they will accumulate them [23]. They are almost sessile creatures that do not migrate, so they will be very damaged if their living environment is polluted [17, 33]. Table 2 also reports microplastics in some mussel and fish species.

Table 1. Some marine organisms and their exposure routes to microplastics (Data from [14, 33])

Species	Exposure routes
Amphipods	They directly mistake microplastics for a natural food source.
The marine polychaete A. *marina*	Selection is based on size, with smaller particles adhering and being retained by the mucous-lined proboscis papillae.
Plankton eaters	Due to the similarity in specific gravity of plastic microspheres with algae, they are mistakenly ingested by plankton eaters.
Echinoderm larvae	They ingest polymer microspheres based on their size (smaller than 3 mm).
Marine algae	Adsorbs nanoplastics, especially when positively charged.
Grazing microzooplankton	Size-based selectivity indicates the potential to ingest microplastics of appropriate size.

© 2025 The Authors. This article is licensed under a Creative Commons Attribution 4.0 International License.

Table 2. Microplastics in some species of mussel and fish

Species	Region	Polymers observed	Shape	Size (mm)	Reference
Mytilus edulis	French Atlantic coast	PE, Polypropylene (PP)	Fragment	0.05–0.1	[53]
Mytilus spp.	Norwegian coastal waters	Cellophane, Ethylene-vinyl acetate (EVA), PET, PP, PE, PA	Fiber, Fragment	0.07–3.87	[54]
Mytilus Galloprovincialis	Adriatic Sea	PE, PP, PET, PS, PVC	Fiber, Fragment	0.02–0.3	[55]
Mytilus Galloprovincialis	Turkish coasts	PET, PP, PE	Fragment, Fiber, Film	0.5–2.0	[56]
Mytilus Galloprovincialis	N Ionian Sea	PE, PP, Polytetrafluoroethylene (PTFE)	Fiber, Fragment	0.04–0.74	[57]
Mytilus edulis, Perna viridis	Coastal waters China	PET, PVC, PE, PP, Rayon	Fiber, Fragment, Bead	0.25–1.0	[58]
Sardinia pilchardus	Adriatic Sea	PP, PVC, PTFE, PA	Fragment, Fiber	0.12–0.59	[59]
Sardina pilchardus	Gulf of Lyon, France	PET, PE, PA, PP	Fiber	1.77	[60]
Solea solea	Adriatic Sea	PVC, PP, PE, PA, Polyester	Fragment, Fiber	0.1–0.5	[61]
Boops boops	Mediterranean Sea	PE, PP, PS, PVC	Fiber	0.05–4.75	[62]
Boops boops	Catalan coast, Spain	PP, PE, PS	Fragment, Fiber	< 0.1–5	[63]
Mugil cephalus	E Hong Kong	PP, PE, Polyester	Fragment, Fiber	1.21	[64]

There are many reports of the effects of microplastic ingestion in organisms, such as internal abrasions and blockages of the digestive tract. Figure 8 shows the factors affecting the physical impacts of microplastics.

Among aquatic organisms, the Red Sea giant clam (*Tridacna maxima*) can remove microplastics [17]. Arossa et al. [44] evaluated the removal of polyethylene microplastics (53 to 500 µm in size) by *Tridacna maxima*. The results showed that clams' shells played a major role in removing microplastics (through sorption on the surface, microplastics attach to the clams' shells) and resulted in a 66.03% removal from wastewater. Researchers have proposed many methods for removing microplastics. Among the methods for removing microplastics, membrane bioreactors, adsorption on green microalgae, and conventional activated sludge are among the most efficient methods [45-48]. In the membrane bioreactor method, catalysis is promoted by biological catalysts such as bacteria, enzymes, and is accompanied by a separation process carried out by a membrane system (see Figure 9) [49]. Algae-based separation technologies are very promising for the removal of pollutants. These methods are based on the mechanisms of bioadsorption, bioaccumulation, and

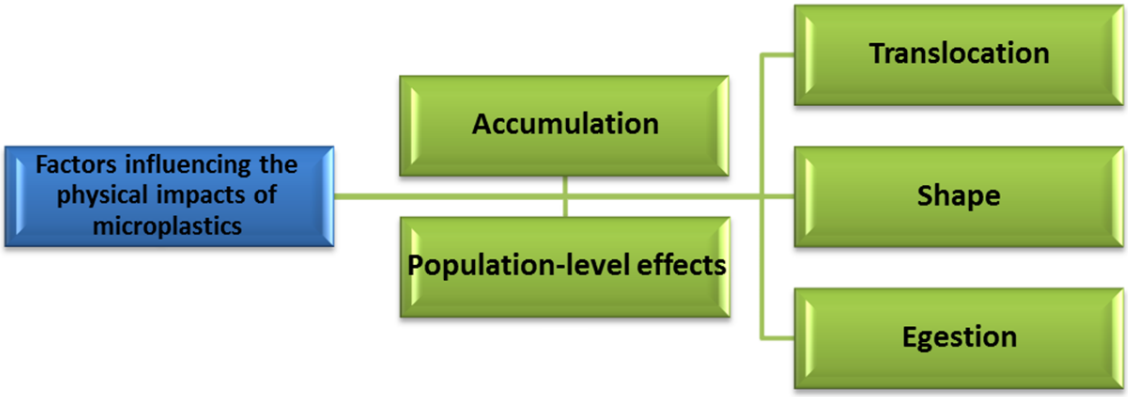

Figure 8. Factors influencing the physical impacts of microplastics.

© 2025 The Authors. This article is licensed under a Creative Commons Attribution 4.0 International License.

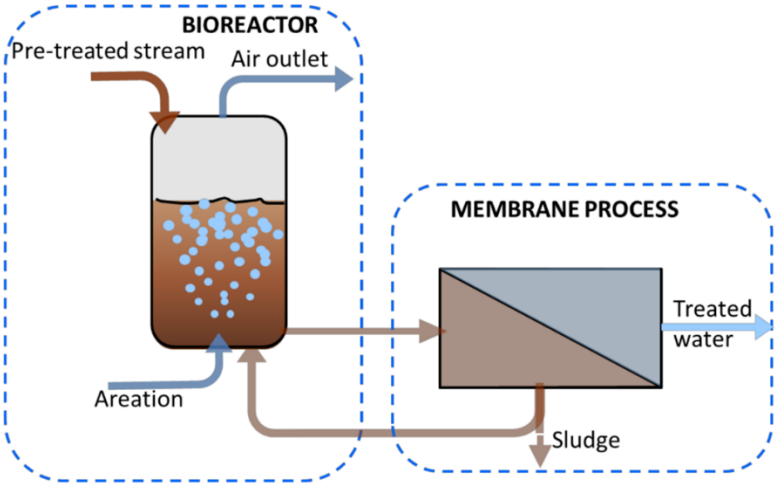

Figure 9. Schematic representation of a membrane bioreactor process. Reprinted with permission from [45]. 2019, MDPI.

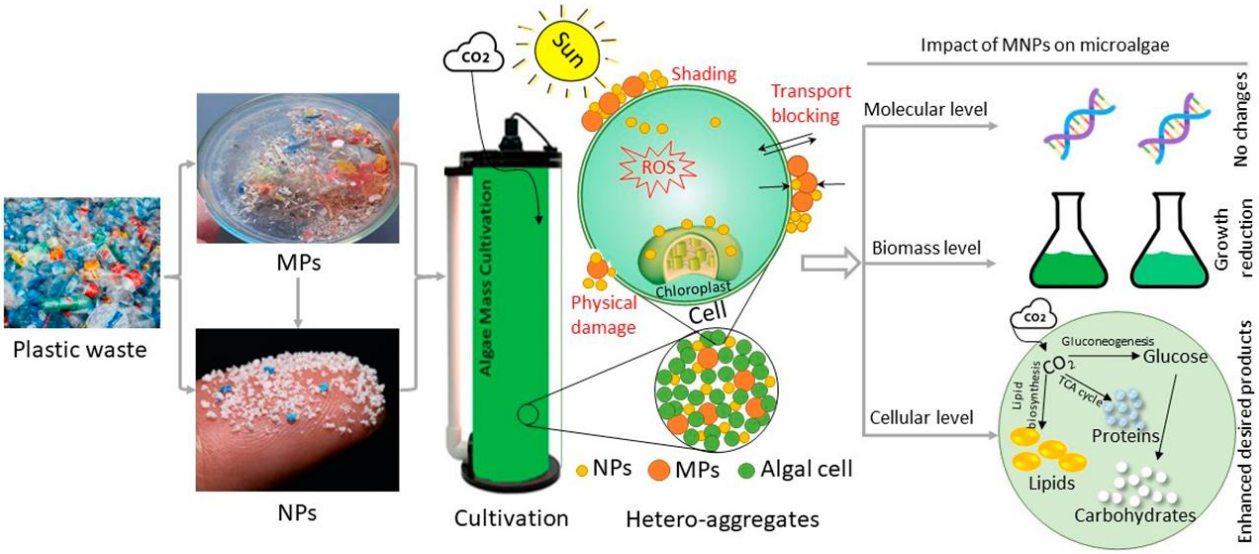

Figure 10. The modes of action and effects of microplastics and nanoplastics on microalgal cells and biomass production. Reprinted with permission from [65]. 2022, MDPI.

biodegradation. For example, studies have shown that the microalgae *Chlamydomonas* sp. and *Chlorella vulgaris* are very effective in the adsorption of pollutants [50]. Their cell walls are rich in polysaccharides, proteins, and lipids that contain functional groups that effectively interact with hydrophobic microplastic particles (see Figure 10) [46, 50]. Reports have shown that effluent and sludge contain high concentrations of microplastics [51]. Therefore, conventional activated sludge processes remove a significant fraction of microplastics, although the removal efficiency depends on the wastewater treatment plant configuration and operating parameters [52]. Figure 11 shows a comparison of these three methods.

4. Conclusions

To sum up, microplastics can be considered one of the most important pollutants in the world today, in which only humans play a direct role. Microplastics can easily cause environmental pollution, and their removal is very expensive, and in some cases, it can be said that their complete removal is not possible. The most important

© 2025 The Authors. This article is licensed under a Creative Commons Attribution 4.0 International License.

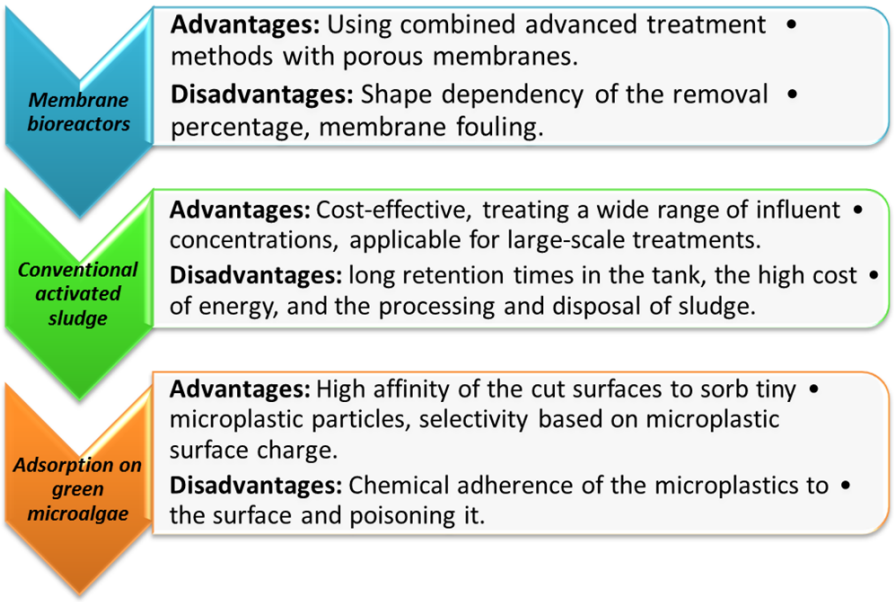

Figure 11. Comparison of some different methods for removing microplastics from the environment.

factor in controlling this pollution is the use of fewer plastics and replacing them with other materials. Proper management of plastic waste is of great importance because its entry into the environment depends on this factor. Currently, marine organisms are most harmed by microplastics because they come into contact with them in water and sediments while feeding and breathing, but in the future, humans will increasingly encounter them.

Conflict of Interest

The authors declare no conflict of interest.

References

1. S. Tong, et al. Current and future threats to human health in the Anthropocene. *Environment International*, **2022**, *158*, 106892.

2. N.P. Hariram, et al. Sustainalism: An Integrated Socio-Economic-Environmental Model to Address Sustainable Development and Sustainability. *Sustainability*, **2023**, *15*, 10682.

3. M. Sheydaei. Heavy Metals Contamination in Soil and Rice and their Removal Processes: A Brief Review. *Geomicrobiology Journal*, **2024**, *41*, 721.

4. M. Sheydaei. Investigation of Heavy Metals Pollution and Their Removal Methods: A Review. *Geomicrobiology Journal*, **2024**, *41*, 213.

5. S.C. Heath. Navigating psychosocial dimensions: understanding the intersections of adaptation strategies and well-being outcomes in the context of climate change. *Current Opinion in Environmental Sustainability*, **2025**, *72*, 101493.

6. F.R. de Paula, et al. Timing since deforestation for pastures implementation in the western Amazon: Impacts on stream water biogeochemistry. *Science of The Total Environment*, **2025**, *976*, 179320.

7. M. Sheydaei, et al. PVCS/GO nanocomposites: investigation of thermophysical, mechanical and antimicrobial properties. *Journal of Sulfur Chemistry*, **2022**, *43*, 376.

8. H.M. Magbool. Sustainability of utilizing recycled plastic fiber in green concrete: A systematic review. *Case Studies in Construction Materials*, **2025**, *22*, e04432.

9. M. Cordier, et al. Reducing plastic production: Economic loss or environmental gain? *Cambridge Prisms: Plastics*, **2024**, *2*, e2.

10. R.y. Öztekin and D.a.T. Sponza. Removal Mechanisms of Polyethylene, Polypropylene, Polyvinyl Chloride, Polyamide (Nylon), Polystyrene and Polyethylene Terephthalate in Wastewater Treatment Plants by Chemical, Photocatalytic, Biodegradation and Hybrid Processes. *International Journal of Environmental Engineering and Development*, **2023**, *1*, 206.

11. F.A.S. Islam. The Impact of Plastic Waste on Ecosystems and Human Health and Strategies for Managing It for A Sustainable Environment. *International Journal of Latest Technology in Engineering Management & Applied Science*, **2025**, *14*, 706.

© 2025 The Authors. This article is licensed under a Creative Commons Attribution 4.0 International License.

12. O. Novillo-Sanjuan, et al. Microplastics in Lampanyctus crocodilus (Risso 1810, Myctophidae), a Common Lanternfish Species from the Ibiza Channel (Western Mediterranean). *Microplastics*, **2023**, *2*, 242.

13. X. Meng, et al. A Review of Sources, Hazards, and Removal Methods of Microplastics in the Environment. *Water*, **2025**, *17*, 102.

14. S.L. Wright, R.C. Thompson, and T.S. Galloway. The physical impacts of microplastics on marine organisms: A review. *Environmental Pollution*, **2013**, *178*, 483.

15. R.P. Mofokeng and D. Glassom. Time Integrated Metal Accumulation on Pellets in an Industrial Harbour "Durban Harbour". *Microplastics*, **2021**, *1*, 3.

16. T.D. Moshood, et al. Sustainability of biodegradable plastics: New problem or solution to solve the global plastic pollution? *Current Research in Green and Sustainable Chemistry*, **2022**, *5*, 100273.

17. M. Padervand, et al. Removal of microplastics from the environment. A review. *Environmental Chemistry Letters*, **2020**, *18*, 807.

18. J. Lawrence, et al. Freshwater Lacustrine Zooplankton and Microplastic: An Issue to Be Still Explored. *Toxics*, **2023**, *11*, 1017.

19. L. Lei, et al. Microplastic particles cause intestinal damage and other adverse effects in zebrafish Danio rerio and nematode Caenorhabditis elegans. *Science of The Total Environment*, **2018**, *619*, 1.

20. R. Sussarellu, et al. Oyster reproduction is affected by exposure to polystyrene microplastics. *Proceedings of the National Academy of Sciences*, **2016**, *113*, 2430.

21. K.L. Law, et al. Distribution of Surface Plastic Debris in the Eastern Pacific Ocean from an 11-Year Data Set. *Environmental Science & Technology*, **2014**, *48*, 4732.

22. E. Milad, et al. Protective Nanocomposite Coating Based on Ginger Modified Clay and Polyurethane: Preparation, Characterization and Evaluation Anti-Corrosion and Mechanical Properties. *Polymer Science, Series B*, **2022**, *64*, 756.

23. E. Alinia-Ahandani, et al. Some effective medicinal plants on cardiovascular diseases in Iran - a review. *Journal of Global Trends in Pharmaceutical Sciences*, **2020**, *11*, 8021.

24. E. Alinia-Ahandani, Z. Alizadeh-Tarpoei, and M. Sheydaei. Some Pointed Medicinal Plants to Treat the Tick-Borne Disease. *Open Access Journal of Biogeneric Science and Research*, **2020**, *28*, 12.

25. C. Simoneau, L. Van den Eede, and S. Valzacchi. Identification and quantification of the migration of chemicals from plastic baby bottles used as substitutes for polycarbonate. *Food Additives & Contaminants: Part A*, **2011**, *29*, 469.

26. K.D. Cox, et al. Human Consumption of Microplastics. *Environmental Science & Technology*, **2019**, *53*, 7068.

27. O. Setälä, V. Fleming-Lehtinen, and M. Lehtiniemi. Ingestion and transfer of microplastics in the planktonic food web. *Environmental Pollution*, **2014**, *185*, 77.

28. J.-Q. Jiang. Occurrence of microplastics and its pollution in the environment: A review. *Sustainable Production and Consumption*, **2018**, *13*, 16.

29. H.G. Dam, et al. Plastic Pollution in the World's Oceans: More than 5 Trillion Plastic Pieces Weighing over 250,000 Tons Afloat at Sea. *PLoS ONE*, **2014**, *9*, e111913.

30. Z. Long, et al. Microplastic abundance, characteristics, and removal in wastewater treatment plants in a coastal city of China. *Water Research*, **2019**, *155*, 255.

31. J. Sun, et al. Microplastics in wastewater treatment plants: Detection, occurrence and removal. *Water Research*, **2019**, *152*, 21.

32. T.R. Walker. (Micro)plastics and the UN Sustainable Development Goals. *Current Opinion in Green and Sustainable Chemistry*, **2021**, *30*, 100497.

33. O. Bajt. From plastics to microplastics and organisms. *FEBS Open Bio*, **2021**, *11*, 954.

34. M.A. Browne, et al. Accumulation of Microplastic on Shorelines Woldwide: Sources and Sinks. *Environmental Science & Technology*, **2011**, *45*, 9175.

35. L. Nizzetto, M. Futter, and S. Langaas. Are Agricultural Soils Dumps for Microplastics of Urban Origin? *Environmental Science & Technology*, **2016**, *50*, 10777.

36. E. Huerta Lwanga, et al. Incorporation of microplastics from litter into burrows of Lumbricus terrestris. *Environmental Pollution*, **2017**, *220*, 523.

37. E.C. Hunter, et al. Quantification and Characterisation of Pre-Production Pellet Pollution in the Avon-Heathcote Estuary/Ihutai, Aotearoa-New Zealand. *Microplastics*, **2022**, *1*, 67.

38. P.L. Corcoran, et al. Hidden plastics of Lake Ontario, Canada and their potential preservation in the sediment record. *Environmental Pollution*, **2015**, *204*, 17.

39. A.A. Horton, et al. Microplastics in freshwater and terrestrial environments: Evaluating the current understanding to identify the knowledge gaps and future research priorities. *Science of The Total Environment*, **2017**, *586*, 127.

40. F. Lagarde, et al. Microplastic interactions with freshwater microalgae: Hetero-aggregation and changes in plastic density appear strongly dependent on polymer type. *Environmental Pollution*, **2016**, *215*, 331.

© 2025 The Authors. This article is licensed under a Creative Commons Attribution 4.0 International License.

41. M. Sheydaei. Breast Cancer and the Role of Polymer-Carriers in Treatment. *Biomedical Journal of Scientific & Technical Research*, **2021**, *34*, 27057.

42. M. Sheydaei and E. Alinia-Ahandani. Cancer and the Role of Polymeric-Carriers in Diagnosis and Treatment %J Journal of Advanced Biomedical Sciences. **2020**, *10*, 2408.

43. M. Edraki, et al. Characterization and antimicrobial properties of Matcha green tea %J Chemical Review and Letters. **2022**, *5*, 76.

44. S. Arossa, et al. Microplastic removal by Red Sea giant clam (Tridacna maxima). *Environmental Pollution*, **2019**, *252*, 1257.

45. M. Li, et al. Review of Techniques for the Detection, Removal, and Transformation of Environmental Microplastics and Nanoplastics. *ACS Applied Materials & Interfaces*, **2025**, *17*, 20560.

46. M.A.A. Amparán, et al. Review and future outlook for the removal of microplastics by physical, biological and chemical methods in water bodies and wastewaters. *Environmental Monitoring and Assessment*, **2025**, *197*, 429.

47. J. Lu, et al. Insights into the role of attapulgite clay on the efficient removal of microplastics by sand filters in various waters. *Chemical Engineering Journal*, **2025**, *504*, 159085.

48. H.K. McIlwraith, et al. Positive controls with representative materials are essential for the advancement of microplastics research. *Microplastics and Nanoplastics*, **2025**, *5*, 9.

49. T. Poerio, E. Piacentini, and R. Mazzei. Membrane Processes for Microplastic Removal. *Molecules*, **2019**, *24*, 4148.

50. F. Lotfigolsefidi, et al. Removal of microplastics by algal biomass from aqueous solutions: performance, optimization, and modeling. *Scientific Reports*, **2025**, *15*, 501.

51. M.M. Maw, et al. Microplastics in wastewater and sludge from centralized and decentralized wastewater treatment plants: Effects of treatment systems and microplastic characteristics. *Chemosphere*, **2024**, *361*, 142536.

52. G. Di Bella, et al. Occurrence of Microplastics in Waste Sludge of Wastewater Treatment Plants: Comparison between Membrane Bioreactor (MBR) and Conventional Activated Sludge (CAS) Technologies. *Membranes*, **2022**, *12*, 371.

53. N.N. Phuong, et al. Factors influencing the microplastic contamination of bivalves from the French Atlantic coast: Location, season and/or mode of life? *Marine Pollution Bulletin*, **2018**, *129*, 664.

54. I.L.N. Bråte, et al. Mytilus spp. as sentinels for monitoring microplastic pollution in Norwegian coastal waters: A qualitative and quantitative study. *Environmental Pollution*, **2018**, *243*, 383.

55. A. Gomiero, et al. First occurrence and composition assessment of microplastics in native mussels collected from coastal and offshore areas of the northern and central Adriatic Sea. *Environmental Science and Pollution Research*, **2019**, *26*, 24407.

56. K. Gedik and A.R. Eryaşar. Microplastic pollution profile of Mediterranean mussels (Mytilus galloprovincialis) collected along the Turkish coasts. *Chemosphere*, **2020**, *260*, 127570.

57. N. Digka, et al. Microplastics in mussels and fish from the Northern Ionian Sea. *Marine Pollution Bulletin*, **2018**, *135*, 30.

58. X. Qu, et al. Assessing the relationship between the abundance and properties of microplastics in water and in mussels. *Science of The Total Environment*, **2018**, *621*, 679.

59. M. Renzi, et al. Marine litter in stomach content of small pelagic fishes from the Adriatic Sea: sardines (Sardina pilchardus) and anchovies (Engraulis encrasicolus). *Environmental Science and Pollution Research*, **2018**, *26*, 2771.

60. C. Lefebvre, et al. Microplastics FTIR characterisation and distribution in the water column and digestive tracts of small pelagic fish in the Gulf of Lions. *Marine Pollution Bulletin*, **2019**, *142*, 510.

61. G. Pellini, et al. Characterization of microplastic litter in the gastrointestinal tract of Solea solea from the Adriatic Sea. *Environmental Pollution*, **2018**, *234*, 943.

62. C. Tsangaris, et al. Using Boops boops (osteichthyes) to assess microplastic ingestion in the Mediterranean Sea. *Marine Pollution Bulletin*, **2020**, *158*, 111397.

63. O. Garcia-Garin, et al. Boops boops as a bioindicator of microplastic pollution along the Spanish Catalan coast. *Marine Pollution Bulletin*, **2019**, *149*, 110648.

64. L. Cheung, C. Lui, and L. Fok. Microplastic Contamination of Wild and Captive Flathead Grey Mullet (Mugil cephalus). *International Journal of Environmental Research and Public Health*, **2018**, *15*, 597.

65. A. Abomohra and D. Hanelt. Recent Advances in Micro-/Nanoplastic (MNPs) Removal by Microalgae and Possible Integrated Routes of Energy Recovery. *Microorganisms*, **2022**, *10*, 2400.

© 2025 The Authors. This article is licensed under a Creative Commons Attribution 4.0 BY International License.

© 2025 The Authors. This article is licensed under a Creative Commons Attribution 4.0 International License.

Fluoride Adsorption Behavior in Cost-effective Plant-based Bio-sorbents

Malathi Visarapu, Anna Tanuja Safala B., Bharath Kumar Ch., Madhavi Vemula *

BVRIT HYDERABAD College of Engineering for Women, Hyderabad, India

Editor's note: The detrimental effects of excessive fluoride on the health of both humans and animals through drinking-water sources are evident, particularly regarding dental and skeletal fluorosis. This underscores the critical need for stringent control of fluoride concentration levels in drinking water. In their study, Visarapu et al. presented various plant-based biosorbents for fluoride removal, and their results demonstrated that Hibiscus leaves achieved a high fluoride removal efficiency with an impressively low dosage of just 1 g.

doi: 10.22034/jams.2025.210144

How to cite: M. Visarapu et al. *Journal of Applied Material Science*, **2025**, *1*, 210144.

JOURNAL OF
APPLIED
MATERIAL
SCIENCE
jams.hsu.ac.ir

© 2025 *J. Appl. Mater. Sci.* This material is licensed under a Creative Commons Attribution 4.0 International License.

Journal of Applied Material Science **2025**, *1*, 210144
How to cite: M. Visarapu et al., *Journal of Applied Material Science*, **2025**, *1*, 210144.
Journal homepage: **jams.hsu.ac.ir**

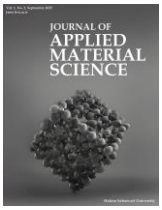

Communication

Fluoride Adsorption Behavior in Cost-effective Plant-based Bio-sorbents

Malathi Visarapu, Anna Tanuja Safala B., Bharath Kumar Ch., Madhavi Vemula *

BVRIT HYDERABAD College of Engineering for Women, Hyderabad, India

Abstract

Concerns regarding the effects of excessive fluoride in water sources on human health have been raised globally. Conventional fluoride remediation approaches generally involve chemical treatment or expensive filtration systems that can introduce additional pollutants, leading to environmental implications. The utilization of plant-based biosorbent materials for fluoride removal holds promise as a sustainable approach to tackle the issue of fluoride in water sources. Utilizing these materials can lead to significant environmental benefits, including reduced toxicity and improved human health outcomes, ultimately contributing to a greener and more sustainable future. This work explores the potential of various plant-based biosorbents for fluoride removal, presenting a sustainable and environmentally friendly approach. The biosorption tests were executed and measured the factors of initial fluoride concentration, contact time, pH levels, and biosorbent dose on fluoride removal bio-sorption efficiencies. At a fluoride concentration of 10 mg/L, all the leaf powder biosorbents demonstrated remarkable sorption efficiencies, achieving removal rates ranging from 90% to 100% at pH 6 and a contact time of 60 minutes. Notably, Hibiscus leaves achieved high fluoride removal efficiency with a remarkably low dose of just 1 g. This study highlights the benefits of exploring plant-based biosorbents as more environmentally sustainable solutions to removing fluoride and other contaminants, which will result in improving human health while also being more environmentally friendly.

Keywords: Fluoride adsorption; Plant-based biosorbents; Cost-effectiveness, Sorption efficiency; Sustainable approach.

1. Introduction

Fluoride is an essential trace element that plays a crucial role in maintaining dental health and preventing tooth decay. Excessive fluoride impacts on the health of humans and animals via drinking-water sources demonstrated negative health impacts, most particularly dental and skeletal fluorosis, underscoring the necessity for tight control of fluoride concentration levels in drinking-water sources [1].

Continuous access to excessive fluoride can lead to skeletal fluorosis, a severely debilitating condition characterized by abnormalities of bone and joints, reinforcing the importance of fluoride being removed from drinking water on a global scale [2-4]. While techniques of coagulation, precipitation, and ion

* Corresponding author.
Email address: madhuchem9@gmail.com (M. Vemula)

Received 23 June 2025
Revised 1 July 2025
Accepted 5 July 2025
Available online 7 July 2025

https://doi.org/10.22034/jams.2025.210144
© 2025 The Authors. This article is licensed under a Creative Commons Attribution 4.0 International License.

exchange can significantly reduce fluoride concentrations, these techniques employ chemicals and depict complicated techniques that are potentially costly and, more importantly, unsustainable from an environmental context, especially in environments with resource limitations [5, 6]. This highlights the urgent requirement for innovative, cost-effective, and eco-friendly fluoride removal strategies. Adsorption technology stands out due to its affordability, design simplicity, and ease of operation and maintenance. There are a number of factors that influence the efficiency of adsorption, which include contaminants and absorbent concentration, the surface characteristics of the adsorbent, pH of solution, and contact time [7].

In recent years, plant-based biosorbents have emerged as favorable candidates for fluoride remediation in water. Natural adsorbents, derived from various plant materials, agricultural waste, and naturally occurring minerals, possess inherent adsorption properties that make them attractive for water treatment applications [8, 9]. These adsorbents demonstrate notable selectivity, substantial adsorption capacities, and facile regenerability, rendering them viable candidates for efficient fluoride removal applications. Furthermore, these adsorbents are abundant, renewable, biodegradable, and present minimal risks to human health and the environment. Adsorption of fluoride ions on solid adsorbent occurs via diffusion of ions from solution across the boundary layer, followed by transfer of these ions to the internal surface for porous materials [10-15].

This manuscript aims for fluoride removal by plant-based biosorbents. It will explore the underlying mechanisms of fluoride adsorption onto these materials and highlight their potential advantages over traditional methods. Various plant-derived biosorbents, including tamarind leaves, custard apple leaves, betel leaves, orange peels, hibiscus leaves, mango leaves, curry leaves, moringa leaves, guava leaves, insulin leaves, grape tree leaves and rose petals have been explored for fluoride removal at pH 6, as reported in previous research [16]. Furthermore, this manuscript will comprehensively examine the key parameters that modulate the adsorption capacity and efficacy of these materials, including pH levels, contact duration, and adsorbent concentration.

The potential challenges and limitations associated with the implementation of plant-based biosorbents for large-scale fluoride removal will be addressed, along with strategies to overcome them. Additionally, the manuscript will shed light on the economic feasibility and sustainability aspects of utilizing these materials for water treatment purposes.

The insights provided in the study represent a key step forward in understanding fluoride removal technologies and provide an applicable reference for researchers, environmental engineers, and policy makers seeking effective, sustainable ways to remediate fluoride contamination of water sources and thereby provide access to safe drinking water on a global scale.

2. Experimental

2.1. Materials

Sodium Fluoride, SPADNS reagent, and Zirconyl Chloride were purchased from Merck. HCl, NaOH were purchased from Alfa Aesar. Naturally occurring and abundantly available low-cost materials such as Tamarind leaves, Custard apple leaves, betel leaves, orange peels, Hibiscus leaves, mango leaves, Curry leaves, Moringa leaves, Guava leaves, Insulin leaves, Grape tree leaves, rose petals were collected from the local market surrounding Hyderabad, India. All the leaf powders were dried until the water content was reduced to less than 5%. The dried leaf powders were then ground, and the powder smaller than 60 mesh was collected.

2.2. Fluoride stock preparation

A stock solution was made by dissolving 2.21 g of anhydrous sodium fluoride in 100 mL of double-distilled water and then diluting to 1000 mL. Fresh working solutions of 10 mg/L fluoride were prepared from the stock solution, as required. The pH was adjusted to 6 with 0.5 N HCl and 0.5 N NaOH solutions.

2.3. Batch biosorption studies

Biosorption investigations were performed by changing the biosorbent dosage to 1g, 2g, and 3g of 50 mL of 10 mg/L fluoride solutions with a contact time of 60 minutes at pH 6 and room temperature in a 100 mL Erlenmeyer flask under mixing conditions at 150 rpm on a rotary.

UV-vis spectrophotometric analysis of the fluoride ion in solution was carried out using the SPADNS reagent method. 958 mg of standard SPADNS reagent was prepared by dissolving the reagent in 500 mL of

© 2025 The Authors. This article is licensed under a Creative Commons Attribution 4.0 International License.

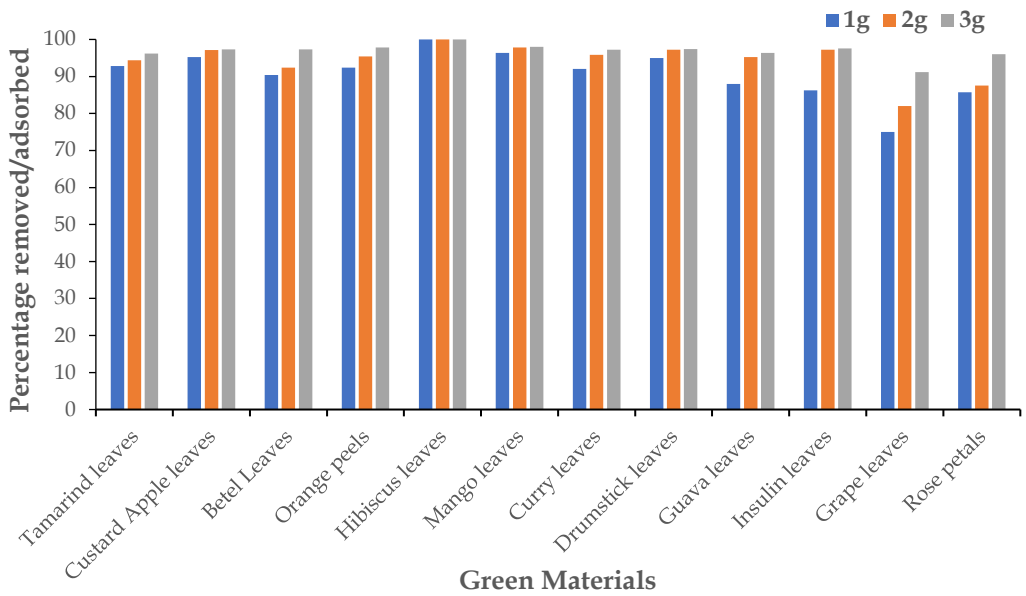

Figure 1. Percentage of fluoride removal/adsorption by various plant-based biosorbents determined by SPADNS method at 570 nm.

double-distilled water (DDW) and kept in the dark from sunlight. The zirconyl acid reagent was prepared by dissolving 133 mg of zirconium chloride in 25 mL of DDW and 350 mL of 1N HCl with distilled water made up to 500 mL. Then, equal volumes of the SPADNS reagent and the zirconyl acid reagent were combined to prepare a reference for the solution. Table 1 summarizes the operating conditions for Fluoride ion adsorption.

Table 1. Summary of operating conditions for Fluoride ion adsorption

Parameter	Operating condition
pH	6
Contact time	60 min
Biosorbent dosage	1g, 2g, 3g
Initial Fluoride ion concentration	10 mg/L

Biosorption tests were conducted in the manner of shaking 50 mL of fluoride solution with several biosorbent doses (1g, 2g, and 3g) in an orbital shaker for 60 minutes. The solids were then separated from the solution by filtration through Whatman 42 filter paper, and the solution adjusted to 20 mL. The fluoride concentration was determined using a UV-Visible Spectrophotometer (Shimadzu) utilizing acid-zirconyl SPADNS reagent at 570 nm. Fluoride removal percentage and adsorption efficiency were then calculated. Three replicates were conducted, and the average values are shown. Control experiments without biosorbent were conducted to ensure that good detection was exclusive to biosorbent. The percentage removal and adsorption efficiency of biosorbents for fluoride were calculated according to the equations.

$$Q_e = ((C_i - C_e))/m\,V \quad (1)$$

$$\text{Sorption efficiency (\%)} = ((C_i - C_e))/C_i \times 100 \quad (2)$$

where Q_e represents the amount of fluoride ions adsorbed at equilibrium (mg/g), C_i and C_e denote the initial and equilibrium fluoride concentrations (mg/L), m is the mass of the adsorbent (mg), and V is the volume of the solution (mL).

3. Results and discussion

The equilibrium sorption results were determined at pH 6, a contact time of 60 minutes, and a fluoride concentration of 10 mg/L and are shown in Figure 1. As the biosorbent dose increased (1g, 2g, and 3g), fluoride removal efficiency also increased, with the highest removal efficiency obtained at 3g of biosorbent dose. This indicates that at 3g, the biosorbent had enough active sites for efficient fluoride binding. The increased

© 2025 The Authors. This article is licensed under a Creative Commons Attribution 4.0 International License.

Table 2. Comparative Analysis of Fluoride Removal Percentages of Various Biosorbents

Biosorbent	Dose of Adsorbent (mg/L)	pH	Removal Percentage (%)	Reference
Lemon peel	20	5	48.36	[17]
H-modified tea biochar	500	2	93.31	[18]
Moringa oleifera seed powder	10	6.5	97.2	[19]
Grape pomace	10	3	96.13	[20]
Bivalve shell	3	5.5	97.26	[21]
Terminalia Chebula	4	7	98	[22]
Insulin leaves	10	6	97.6	Present work
Orange peels	10	6	97.8	Present work
Mango leaves	10	6	97.98	Present work
Hibiscus leaves	10	6	100	Present work

biosorption efficiency at higher biosorbent dosages may be attributed to less flocking and increased availability of pores, surface area, and active binding sites, resulting in more fluoride ions binding. Table 2 provides a comparative summary of fluoride removal percentages for different biosorbents.

These different leaf powders exhibit varying levels of removal performance when used for Fluoride removal at 10mg/L. The range of removal performance depends on the chemical constituents, properties, and characteristics of materials and the contaminant being targeted as well [23-25]. The results showed that all biosorbents used in the experiments have a good to high affinity for adsorbing/removal of Fluoride onto their surfaces. The results indicate that hibiscus leaves are highly effective for fluoride removal, with a remarkable 100% removal rate achieved at a low dose of 1g. The minimum removal performance was observed with 75% of grape tree leaves at 1g. The range of performance, i.e., low (85-90%), medium (90-95%), and high (95-100%), by these biosorbents was also presented here in Figure 2.

This study assessed the effectiveness of different plant-derived biosorbents for fluoride removal using UV-Vis spectrophotometry (SPADNS method) at 570 nm. There was a noticeable increase in removal efficiency; first with increasing biosorbent dosage (1g to 2g and 2g to 3g); second, in that 9 materials had a minimal increase (0-5%) in removal efficiency for each subsequent dosage level, and 2 materials had a moderate increase (5-10%). The comparison of the lowest and highest dosage level (1g-3g) highlighted differences: 5 materials had increases in removal efficiency in the range of 5-10%, 4 materials with 10-15%, and 2 materials in the range of 15-20%. Grape tree leaves had the highest

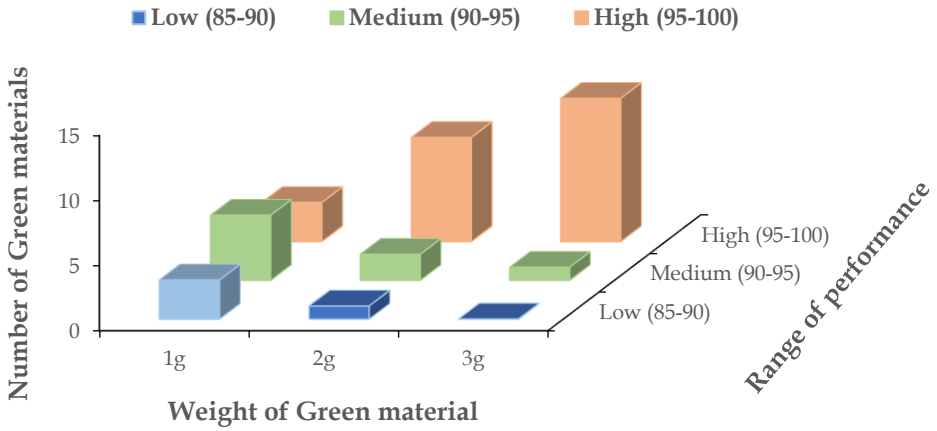

Figure 2. The range of performance, i.e., low (85-90%), medium (95-100%), and high (95-100%) by weight 1g, 2g, 3g of various leaf powders, with dose determined by SPADNS method with UV-Vis spectrophotometry at 570nm.

© 2025 The Authors. This article is licensed under a Creative Commons Attribution 4.0 International License.

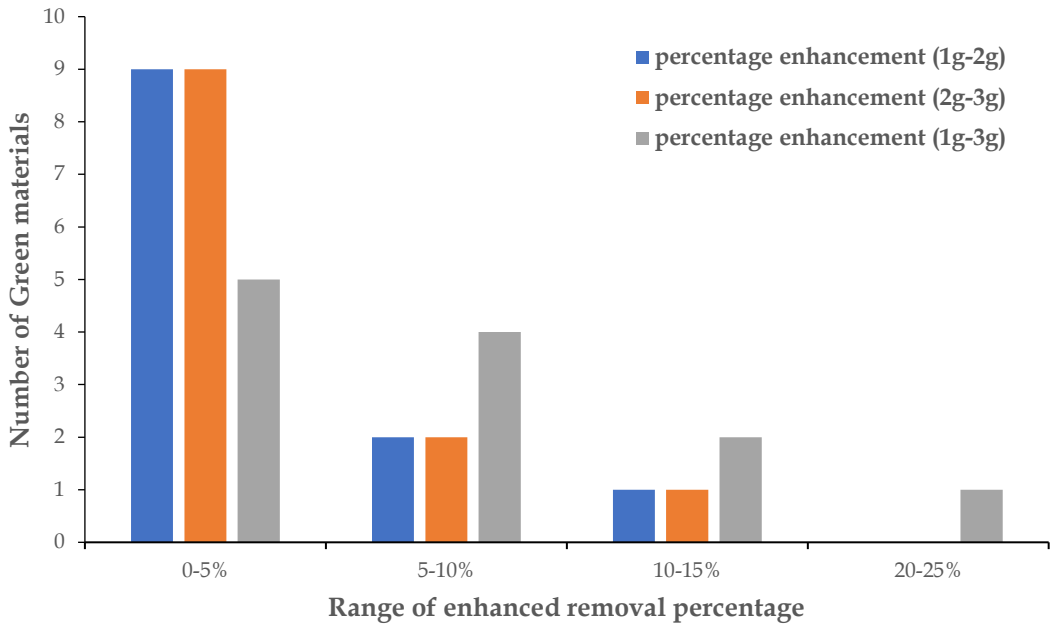

Figure 3. Enhancement in removal percentage from 1g-2g, 2g-3g, 1g-3g of fluoride ion by various leaf powder materials determined by SPADNS method with UV-Vis spectrophotometry at 570nm.

increase in removal efficiency, having a 22% increase in removal efficiency (75%-97%) from the increase of dosage of 1g to 3g; demonstrating the importance of biosorbent dosage on fluoride removal (Figure 3).

4. Conclusions

Batch experiments were conducted to explore the biosorption of fluoride ions using 12 distinct plant-based biosorbent materials, examining the effects of key operating parameters such as pH, contact time, adsorbate concentration, and biosorbent dosage. The studies evaluated the potential of diverse biosorbent materials in removing fluoride ions from water. This study has shown that biosorption is significantly affected by biosorbent dose. The data suggested that the optimum removal of fluoride ions was at pH 6, and a concentration of 10 mg/L of fluoride was achieved in 60 minutes of contact time. Nevertheless, hibiscus leaves displayed high removal efficiency at only 1 g biosorbent dose. Most of the plant-based biosorbent materials exhibited good to excellent removal efficiency, and some of them showed an up to 100% adsorption efficiency. The biosorbents were environmentally friendly, practical, and inexpensive, thereby presenting an efficient option for removing fluoride ions from water.

Acknowledgments

The authors acknowledge BVRIT Hyderabad College of Engineering for Women, Hyderabad, for providing a laboratory to conduct experiments.

Conflict of Interest

The authors declare no conflict of interest.

References

1. S. Nizam, H.S. Virk, and I.S. Sen. High levels of fluoride in groundwater from Northern parts of Indo-Gangetic plains reveals detrimental fluorosis health risks. *Environmental Advances*, 2022, *8*, 100200.

2. C.F.Z. Lacson, M.-C. Lu, and Y.-H. Huang. Fluoride-containing water: A global perspective and a pursuit to sustainable water defluoridation management -An overview. *Journal of Cleaner Production*, **2021**, *280*, 124236.

3. J. He, et al. Review of fluoride removal from water environment by adsorption. *Journal of Environmental Chemical Engineering*, **2020**, *8*, 104516.

© 2025 The Authors. This article is licensed under a Creative Commons Attribution 4.0 International License.

4. S. Ahmad, et al. Fluoride contamination, consequences and removal techniques in water: a review. *Environmental Science: Advances*, **2022**, *1*, 620.

5. R. Garg, et al. Water remediation using biosorbent obtained from agricultural and fruit waste. *Materials Today: Proceedings*, **2021**, *46*, 6669.

6. H.V.R. dos Santos, et al. Fluoride Removal from Aqueous Medium Using Biochar Produced from Coffee Ground. *Resources*, **2023**, *12*, 84.

7. T.s. Algarni and A.M. Al-Mohaimeed. Water purification by adsorption of pigments or pollutants via metaloxide. *Journal of King Saud University - Science*, **2022**, *34*, 102339.

8. A.I. Osman, et al. Methods to prepare biosorbents and magnetic sorbents for water treatment: a review. *Environmental Chemistry Letters*, **2023**, *21*, 2337.

9. A.N.M.A. Haque, et al. Sustainable Adsorbents from Plant-Derived Agricultural Wastes for Anionic Dye Removal: A Review. *Sustainability*, **2022**, *14*, 11098.

10. T. Turki, A. Hamdouni, and A. Enesca. Fluoride Adsorption from Aqueous Solution by Modified Zeolite—Kinetic and Isotherm Studies. *Molecules*, **2023**, *28*, 4076.

11. B. Xiang, et al. Preparation of aluminium-hydroxide-modified diatomite and its fluoride adsorption mechanism. *Scientific Reports*, **2023**, *13*, 3871.

12. V.J. Inglezakis, M. Balsamo, and F. Montagnaro. Liquid–Solid Mass Transfer in Adsorption Systems—An Overlooked Resistance? *Industrial & Engineering Chemistry Research*, **2020**, *59*, 22007.

13. L. Huang, et al. Experimental and modeling studies for adsorbing different species of fluoride using lanthanum-aluminum perovskite. *Chemosphere*, **2021**, *263*, 128089.

14. J. Chen, et al. Removal of fluoride from water using aluminum hydroxide-loaded zeolite synthesized from coal fly ash. *Journal of Hazardous Materials*, **2022**, *421*, 126817.

15. U. Kumari, et al. Facile method to synthesize efficient adsorbent from alumina by nitric acid activation: Batch scale defluoridation, kinetics, isotherm studies and implementation on industrial wastewater treatment. *Journal of Hazardous Materials*, **2020**, *381*, 120917.

16. S. Guo, et al. Enhanced fluoride removal from drinking water by activated carbon supported Ce–Al oxides: performance and mechanism. *RSC Advances*, **2025**, *15*, 14363.

17. S. Ramasamy, et al. Fluoride removal from contaminated water using natural bio-adsorbents: A numerical and experimental investigation. *Desalination and Water Treatment*, **2025**, *321*, 100984.

18. Y.I.E. Aboulsoud. Biosorptive removal of fluoride from wastewater using tea domestic waste biochar. *Environment, Development and Sustainability*, **2024**. https://doi.org/10.1007/s10668-024-04598-2.

19. B. Vani, et al. Effective removal of fluoride and arsenic from groundwater via integrated biosorption and membrane ultrafiltration. *Water Science and Engineering*, **2025**, *18*, 30.

20. Y. Zhang and K. Huang. Grape pomace as a biosorbent for fluoride removal from groundwater. *RSC Advances*, **2019**, *9*, 7767.

21. M. Hashemkhani, et al. Fluoride removal from aqueous solution via environmentally friendly adsorbent derived from seashell. *Scientific Reports*, **2022**, *12*, 9655.

22. J. Sumathi, et al. Adsorption isotherms and kinetic studies for the defluoridation from aqueous solution using eco-friendly natural adsorbent like Terminalia Chebula. *Sustainable Chemistry for Climate Action*, **2024**, *4*, 100040.

23. B.S. Rathi and P.S. Kumar. Application of adsorption process for effective removal of emerging contaminants from water and wastewater. *Environmental Pollution*, **2021**, *280*, 116995.

24. M. Qiu, et al. Biochar for the removal of contaminants from soil and water: a review. *Biochar*, **2022**, *4*, 19.

25. A.A. Ahmad, et al. Gasification char residues management: Assessing the characteristics for adsorption application. *Arabian Journal of Chemistry*, **2023**, *16*, 104993.

© 2025 The Authors. This article is licensed under a Creative Commons Attribution 4.0 BY International License.

© 2025 The Authors. This article is licensed under a Creative Commons Attribution 4.0 International License.

A Theoretical and Experimental Analysis of the Complexation Process Between Progesterone and Cyclodextrin Nanosponge

Mehrdad Hadadian *, Behnam Mahdavi, Esmail Rezaei-Seresht

Department of Chemistry, Faculty of Science, Hakim Sabzevari University, Sabzevar, Iran

Editor's note: Cyclodextrin nanosponges are polymeric porous nanostructures that are widely utilized in encapsulation-based drug delivery systems. These nanosponges exhibit exceptional properties for encapsulating drugs such as progesterone. In this study, Hadadian et al. synthesized cyclodextrin nanosponges using hexamethylene diisocyanate as the crosslinker and investigated the complexation of progesterone within the nanosponge structure of these carriers. Their experimental and theoretical findings suggest the formation of a 1:2 (drug:host) molar ratio complex, indicating that hydrogen bonding is the primary driving force behind this phenomenon.

doi: 10.22034/jams.2025.210145

How to cite: M. Hadadian et al., *Journal of Applied Material Science*, **2025**, *1*, 210145.

JOURNAL OF
APPLIED
MATERIAL
SCIENCE
jams.hsu.ac.ir

© 2025 *J. Appl. Mater. Sci.* This material is licensed under a Creative Commons Attribution 4.0 International License.

Journal of Applied Material Science **2025**, *1*, 210145
How to cite: M. Hadadian et al., *Journal of Applied Material Science*, **2025**, *1*, 210145.
Journal homepage: **jams.hsu.ac.ir**

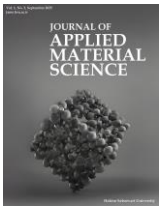

Original Research

A Theoretical and Experimental Analysis of the Complexation Process Between Progesterone and Cyclodextrin Nanosponge

Mehrdad Hadadian *, Behnam Mahdavi, Esmail Rezaei-Seresht

Department of Chemistry, Faculty of Science, Hakim Sabzevari University, Sabzevar, Iran

Abstract

Progesterone, a widely used steroid drug for the treatment of luteal phase deficiency, has very low water solubility and bioavailability. Cyclodextrin nanosponges are polymer-like materials used to enhance the aqueous solubility and bioavailability of lipophilic drugs. In this study, cyclodextrin nanosponges were synthesized using β-cyclodextrin and hexamethylene diisocyanate as a crosslinker; meanwhile, the complexation of progesterone within the nanosponge was investigated using Fourier transform infrared spectroscopy and X-ray diffraction analyses. Furthermore, the encapsulation efficiency and phase solubility of progesterone were assessed by UV-visible spectroscopy. Characterization techniques confirm the successful formation of the complex. The nanosponge was found to be able to encapsulate 70% of the drug and increase its aqueous solubility approximately 45 times. Moreover, phase solubility studies suggest the formation of a 1:2 (drug:host) molar ratio complex. Moreover, molecular docking simulation confirms the obtained experimental data and ensures the formation of a 1:2 complex by visualizing a hydrogen bond between the drug and host molecules.

Keywords: Drug delivery; Molecular docking; Phase solubility; Nanosponge; Cyclodextrin.

1. Introduction

Cyclodextrin nanosponges (CNS) are nanostructured polymers made up of hyperlinked cyclodextrins (CD) with unique superior properties [1]. These multifunctional materials, with their high porosity features, can encapsulate various organic and inorganic compounds while floating on aqueous media. In this regard, they are ideal candidates for biomedical applications by making inclusion or non-inclusion complexes with medications or for water filtration by removing pollutants from contaminated water [1]. Nanosponges take advantage of the beneficial features of pristine cyclodextrins, like increasing the water solubility of lipophilic substances, stabilizing degradable guests, conserving volatile ingredients, and prolonging drug release [2]; meanwhile, they show the efficacious properties of polymer-based materials, such as high thermal stability up to 300˚C [3]. Moreover, CNS is widely recognized as a safe material for drug delivery purposes, especially for steroidal drugs, as they could increase their water solubility [4].

Many approaches have been made to increase the water solubility of lipophilic drugs, and cyclodextrins are one of the most efficacious carriers for this purpose

* Corresponding author.
Email address: hadadianmehrdad@gmail.com (M. Hadadian)

Received 7 June 2025
Revised 4 July 2025
Accepted 9 July 2025
Available online 11 July 2025

https://doi.org/10.22034/jams.2025.210145
© 2025 The Authors. This article is licensed under a Creative Commons Attribution 4.0 International License.

[5, 6]. In this way, it is assumed that cyclodextrin-based nanosponges could show superior properties in encapsulating hydrophobic drugs, like higher encapsulation efficiency, biodegradability, thermal stability, and bioavailability.

Progesterone (Pro), a sex hormone of women, is produced by the adrenal gland to prepare the uterus for embryo implantation and sexual behavior or by the corpus luteum through the luteal phase (Scheme 1). Luteal phase deficiency (LPD) is when the level of progesterone in patients decreases below a sufficient level, resulting in an abnormal menstrual cycle, embryogenesis, and pregnancy [7]. It is suggested that a level of 10-20 ng/ml of progesterone is needed to suppress the LDP consequences. For this purpose, progesterone is commercialized to help patients in the reproductive technology cycle, with anovulatory bleeding, with secondary amenorrhea, and to prevent recurrent pregnancy loss. However, its low water solubility (11.9 μg/mL) hindered its transportation to the body organisms, resulting in limited absorption *via* the gastrointestinal tract and low oral bioavailability [8]. To confront this problem, many steroids are formulated as hydrogels using ethanol or microemulsions with the means of detergents [2]. For specific progesterone, it is formulated as a suspension in peanut oil, which could improve the intestinal absorption of the drug [8]. These formulations with their benefits have some drawbacks, including skin irritations, variable oral absorption, and hence, showing less impact on the treatment [2, 8].

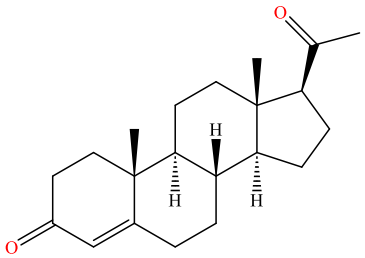

Scheme 1. Molecular structure of progesterone.

Many researchers have been making multiple efforts to increase the water solubility of lipophilic drugs using various methods, such as solid dispersion, salt formation, supercritical-fluid processing, micellar solubilization, hydrotrophy, solubilizers, and cyclodextrins [8, 9]. In recent years, cyclodextrins have found substantial interest because of their unusual physicochemical properties, especially when making an inclusion complex with drugs, increasing their bioavailability, solubility, and stability [10]. Meanwhile, CNSs have become of interest because of their capacity for delivering drugs to specific organs and increasing the effects of drugs. For example, several previous studies have declared that CNS could increase the stability, anti-inflammatory, anti-cancer, and anti-viral activity of active pharmaceutical forms [4, 5]. CNS could make inclusion complex with steroid drugs by encapsulating them within their nanocavities, similar to CDs, and non-inclusion complex in the tiny mesh-like spaces that have been formed after crosslinking [5]. For instance, the encapsulation of dexamethasone by CNS has been investigated, and the obtained results showed that the drug is entrapped within the nanocavities of CDs, as well as the porous matrix of CNS [11]. In addition, the encapsulation of curcumin within the CNS has been studied, which represents superior water solubility for curcumin, favoring its entry into the CNS [4]. Until recently, the complexation of progesterone within β-cyclodextrin (β-CD) has been widely studied, which has demonstrated the potential of β-CD to encapsulate this lipophilic drug for drug delivery and water purification applications [6, 12]. However, there is a huge gap in utilizing β-CD nanosponge for these purposes, except for a study by Matencio et al. that suggested a non-covalent nanosponge using the ball mill method [13].

This study aimed to fabricate a covalently crosslinked cyclodextrin nanosponge using hexamethylene diisocyanate (HMDI) as a crosslinker to increase the water solubility of progesterone by encapsulation. For the characterization, the FT-IR and XRD techniques have been used. The phase water solubility and drug loading studies were conducted spectroscopically. Moreover, the binding affinity of progesterone with cyclodextrin in 1:1 and 1:2 molar ratios has been assessed using molecular docking.

2. Experimental

2.1. Materials

Progesterone (Pro, purity >98%, $C_{21}H_{30}O_2$, MW: 314.46 g/mol) was purchased from Sigma-Aldrich. β-Cyclodextrin (β-CD, purity > 98%, $C_{42}H_{70}O_{35}$, MW: 1134.98 g/mol), dimethyl sulfoxide (DMSO), hexamethylene diisocyanate (HMDI, ≥ 99.0%), methanol (≥ 96.0%), and acetone (≥ 99.5%) were purchased from Merck (Germany). All other reagents and chemicals

© 2025 The Authors. This article is licensed under a Creative Commons Attribution 4.0 International License.

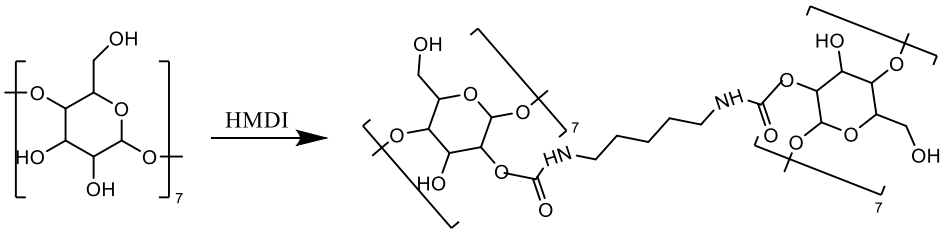

Scheme 2. The synthesis route of cyclodextrin nanosponge.

used were of analytical grade and without additional purification.

2.2. Synthesis of β-Cyclodextrin Nanosponge (CNS)

Cyclodextrin nanosponge was prepared according to the literature with some modifications [14]. Firstly, 3.34 mmol of β-CD was dissolved in 16 mL of DMSO. Then, the temperature of the solution was increased to 40˚C, and 27.5 mmol of HMDI was added to the solution. For a further 4 hours, the reaction temperature was kept at 70˚C to form a gel-like CNS. Finally, the unreacted reagents were removed using Soxhlet extraction with acetone. Scheme 2 represents the synthesis route of NS.

A methanolic solution of progesterone (25 mg in 3 mL) was added to an aqueous dispersion of CNS (32 mg in 2 mL). Then, the mixture was put in an ultrasonic bath for 30 min at RT. Afterward, the mixture was permitted to stir under the same conditions. After 24 hours, the mixture was allowed to settle at 4 °C for 12 hours. Finally, the solid residue was separated using a centrifuge and washed three times with a mixture of deionized water and methanol to remove unreacted progesterone [2].

2.3. Measurements

FT-IR spectra of β-cyclodextrin, CNS, Pro, and Pro/CNS were obtained using a Shimadzu 8400 with KBr disc from 440 to 4000 cm^{-1}. The XRD patterns of β-CD, CNS, Pro, and Pro/CNS were obtained with a diffraction angle of 6° to 90° at a rate of 2°/min, and Cu Kα radiation at 45 kV and 40 mA, using the STOE PW2773.00 device. The spectroscopic method was utilized using a Jena Speko L2000 spectrophotometer at 200-800 nm.

Determination of the encapsulation efficiency (EE%): The encapsulation efficiency of the Pro/CNS complex was assessed using the spectroscopic method due to its cost-effectiveness, accessibility, simplicity, and high accuracy [15]. For this purpose, 30 mg of CNS was suspended in 2 mL of deionized water, and a 3 mL methanolic solution of Pro (20 mg) was added to the suspension, followed by the procedure mentioned in section 2.2.2. The residue was filtered using a nylon Cameo filter syringe (0.45 µm). The concentration of unloaded Pro was assessed spectrophotometrically at the maximum wavelength of Pro (258 nm) and compared with its calibration curve. The EE% was examined according to equation 1.

$$EE\% = \frac{amount\ of\ unloaded\ drug\ (mg)}{amount\ of\ feed\ drug\ (mg)} * 100 \qquad (1)$$

Phase solubility studies: The phase solubility of progesterone in aqueous media was assessed using the Higuchi-Connors method [2]. For this purpose, an excessive amount of progesterone was added to the vials containing various concentrations of CNS (0-10 mM), and the vials were shaken for 24 hours at 25 °C to reach an equilibrium. Then, the suspensions were passed through a nylon Cameo filter syringe (0.45 µm), and the concentration of unloaded drugs was calculated using a spectroscopic method at the maximum wavelength of 258 nm. The suspensions were diluted with methanol.

2.4. Molecular docking simulation

A molecular docking study is beneficial in rationalizing the experimental data. For this purpose, the PDB files of β-CD and progesterone were obtained from: https://pubchem.ncbi.nlm.nih.gov/. The energy of molecules was minimized using Gaussian 0.9W at the Hartree–Fock energy minimization at the 3-21G level. The energy minimization was performed in the gas phase, as it is recommended for organic molecules, while reducing computational complexity and retaining structural accuracy. Then, the minimized molecules

© 2025 The Authors. This article is licensed under a Creative Commons Attribution 4.0 International License.

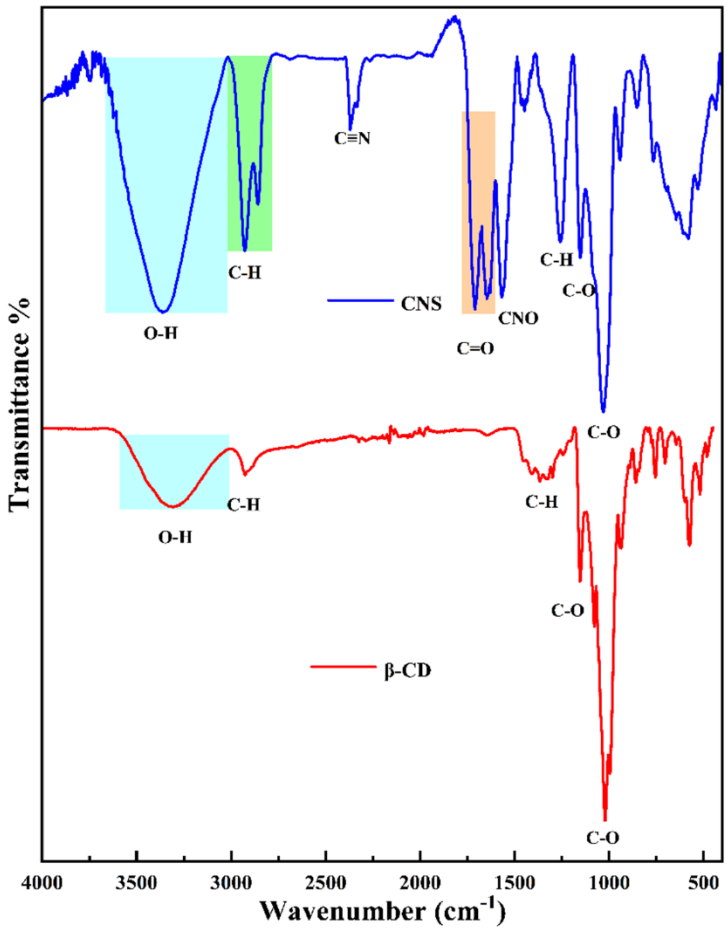

Figure 1. FT-IR spectra of β-CD and CNS.

were saved as an output file and converted to PDB format using GaussView 5.0. Cyclodextrin was assumed as the receptor and progesterone as the ligand in the Autodock Tools-1.5.7. The obtained data was visualized using Schrodinger PyMOL 3.1.1 software. For studying 1:2 drug/host complexation, the extracted β-CD was modeled into two β-CD in PyMOL, and its energy was minimized using Gaussian 0.9W.

For a 1:1 complex, β-CD was placed in the center of a grid box with dimensions of 40 Å × 40 Å × 40 Å with a grid spacing of 0.374 Å. For a 1:2 complex, a grid map with dimensions of 54Å×40Å×40Å and grid spacing of 0.374Å was provided. The molecular docking for both complexes was performed by LGA algorithms, and the number of runs was set to 150 with a population size of 150. These settings followed standard protocols to ensure the reproducibility and accuracy of docking.

3. Results and discussion

3.1. Physicochemical characterization of the prepared products

3.1.1. FT-IR analysis

Infrared spectroscopy is a reliable technique for assessing the stepwise formation of products by monitoring the spectra. Usually, the peak's presence, position, and shape can change after the formation of the host/guest complex, which is a key reason for the importance of FT-IR analysis in recognizing the final products [16]. The FT-IR spectra of β-CD and CNS are presented in Figure 1, and Pro and Pro/CNS in Figure 2. The spectrum of β-CD shows two characteristic peaks at 1023 and 1152 cm^{-1}, which are attributed to the C-O bonds. The peaks at 1345 and 2921 cm^{-1} are related to the

© 2025 The Authors. This article is licensed under a Creative Commons Attribution 4.0 International License.

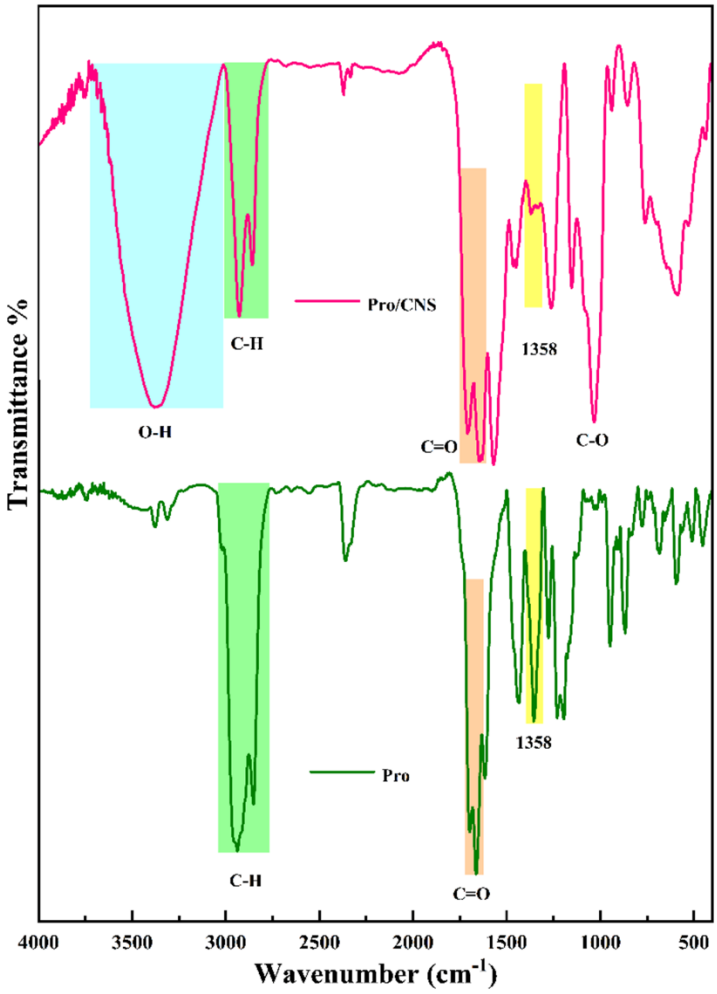

Figure 2. FT-IR spectra of Pro and Pro/CNS.

C-H bonds. Moreover, a broad peak at 3307 cm^{-1} relates to the abundant hydroxyl groups.

The peak at 938 cm^{-1} is assigned to the C-H stretching vibrational bands of the CD ring. The spectrum of CNS shows all the characteristic peaks of β-CD with some alteration in their positions (OH = 3362 cm^{-1}, C-O = 1032 cm^{-1}, C-H = 1259 cm^{-1}), along with two sharp peaks at 1647 and 1711 cm^{-1}, which are associated with the C=O groups variations, and a distinct peak of the CNO group at 1568 cm^{-1}. Besides, there is a sharp peak at 2370 cm^{-1} related to the nitrile group, indicating the presence of hexamethylene diisocyanate groups with one unreacted head, which could resonate and change from N=C=O group to the N≡C-O^- group. In addition, the peaks between 700-1000 cm^{-1} relate to the deformation vibration bands of glucopyranose units [17].

Figure 2 represents the FT-IR spectrum of Pro, including two sharp peaks at 1664 and 1695 cm^{-1} associated with the C=O groups and a peak at 2927 related to the C-H groups. Moreover, the complexation of Pro with CNS modified the peaks' position, which confirmed the successful formation of the final product. In this regard, the peak at 1360 cm^{-1} recurred in both Pro and Pro/CNS; meanwhile, the C=O peaks are observable at 1711 and 1641 cm^{-1}, the C-H group at 2928 cm^{-1}, and the O-H group at 3362 cm^{-1}.

3.1.2. XRD analysis

The X-ray diffraction method provides additional evidence for the confirmation of the drug/host complex through peak disappearance, emergence, or reduction in the intensity of the peak. Figures 3 and 4 represent the

© 2025 The Authors. This article is licensed under a Creative Commons Attribution 4.0 International License.

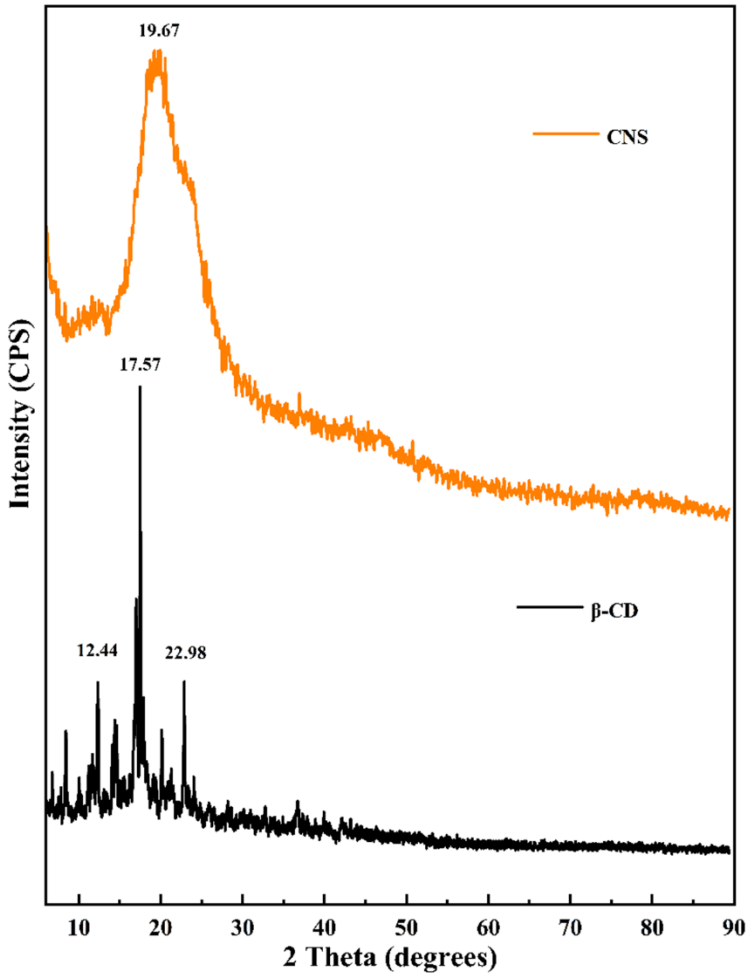

Figure 3. XRD patterns of β-CD and CNS.

XRD patterns of β-CD, CNS, Pro, and Pro/CNS. As can be seen in the diffractogram of β-CD, it has a crystalline structure with distinctive peaks at values of 2θ ~ 12.44°, 17.57°, and 22.98°. The XRD pattern of CNS shows a broad peak at the maximum intensity at 2θ ~ 19.67. It seems that the well-ordered crystalline structure of β-CD, which is evident by the sharp and intense peaks, was ameliorated upon polymerization, leading to an amorphous nanosponge. The polymerization process affects the XRD pattern by the disappearance or broadening of the sharp peaks of the ingredient and the appearance the broad humps, indicating the formation of an amorphous phase in the product. Similar observations are reported in previous research [18, 19]. Moreover, the X-ray spectrum of Pro recorded three sharp peaks at the values of 2θ ~ 11.48°, 15.92°, and 21.72°, indicating the crystalline structure. The XRD pattern of Pro/CNS shows the disappearance of Pro peaks and the appearance of some new peaks and peaks` modifications, which confirms the successful formation of the final product [4].

3.1.3. Drug loading study

To delve into the capability of the prepared CNS to encapsulate a hydrophobic drug, the co-loading study was run. For this purpose, the initial weight and the remaining amount of Pro were assessed using the UV-visible method and compared with the Pro calibration curve. According to equation 1, the EE% for Pro/CNS was calculated to be 70%. This noteworthy encapsulation efficiency for CNS could be attributed to various reasons, including entrapment of Pro into the pores of CNS with its high porosity features, hydrophobic interactions between the drug and

© 2025 The Authors. This article is licensed under a Creative Commons Attribution 4.0 International License.

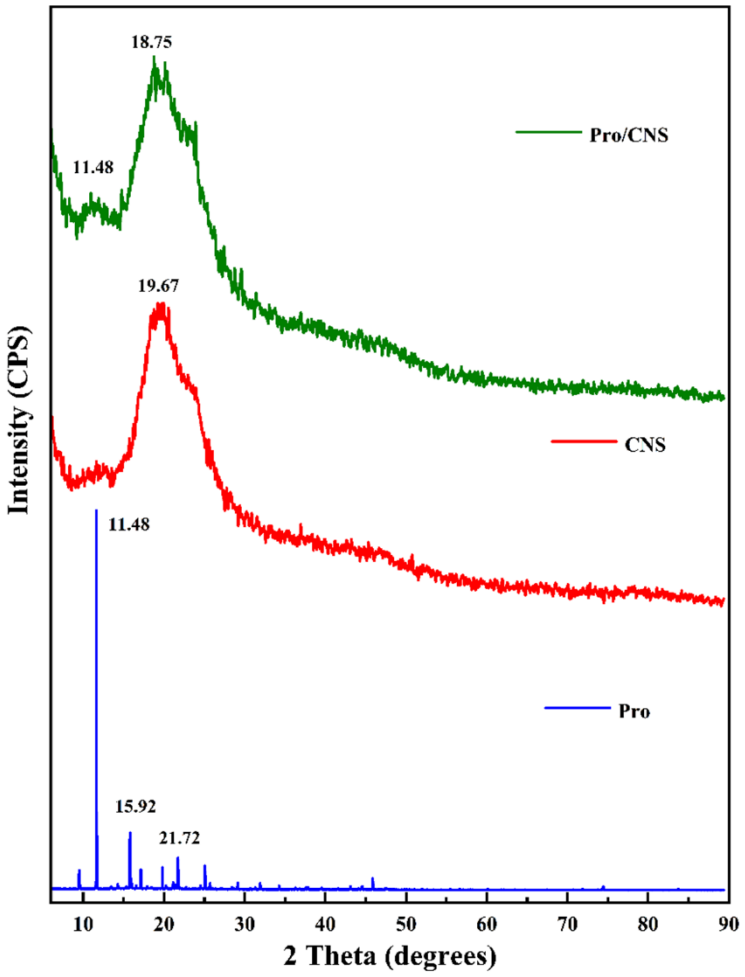

Figure 4. XRD patterns of Pro, CNS, and Pro/CNS.

cyclodextrin pores, and hydrogen bonding between the carbonyl groups of Pro and hydroxyl groups of CNS. Moreover, the gonane structure of Pro can fit perfectly into the cavity of cyclodextrin [16]. The prepared nanosponge showed higher encapsulation efficiency for progesterone compared to other carriers suggested for its delivery. For example, a microparticle of chitosan and tripolyphosphate showed an EE% of roundly 62% [20]. A magnetic nanoaggregate comprising Pluronic F-68 and β-cyclodextrin depicted a mean encapsulation efficiency of 49.68% for progesterone [21].

3.1.4. Phase solubility studies

The phase solubility of Pro/CNS was evaluated at RT and neutral pH. According to the Higuchi method, the phase solubility diagram is classified into two categories: A and B types, indicating complexes with high solubility and low solubility, respectively. Moreover, type-B diagrams can be subdivided into two categories, including Bs (limited solubility) and B_I (negligible solubility). On the other hand, three subtypes are derived from A-type diagrams. When the drug solubility increases in a linear slope as a function of the enhancement of CNS concentration, the related diagram is A_L. On the contrary, the A_P diagram exhibits diagrams with positive deviations and A_N for negative deviations. The phase solubility studies are so beneficial in optimizing CNS for the encapsulation of drugs to increase their solubility and designing drug delivery systems [16]. Figure 5 represents the phase solubility diagram of Pro/CNS in water. It seems that the aqueous solubility of Pro followed a linear increase as a function of CNS concentration, with a determination coefficient (R^2) of 0.868.

© 2025 The Authors. This article is licensed under a Creative Commons Attribution 4.0 International License.

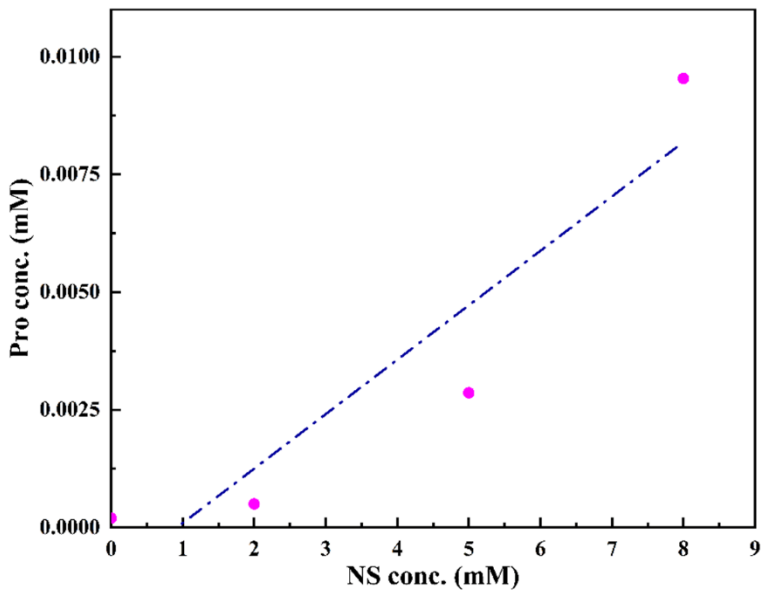

Figure 5. The phase solubility diagram of Pro/CNS in water and RT.

The phase solubility diagram of Pro/CNS depicts an A_P-type, indicating the formation of a complex in a molar ratio of 1:2 (Pro:CNS). This subtype suggests that abundant hydrogen bonding is formed between the host molecule and the solvent, and more water molecules are available to participate in the solute-solvent interactions, leading to positive deviation. In another way, this phenomenon can be interpreted by the observation that one drug molecule is surrounded by two CD molecules, which provide more oxygen and hydroxyl groups to make hydrogen bonds with the hydrogen of water [22]. In addition, the encapsulation of Pro within the CNS substantially increases the water solubility of this lipophilic drug. While the intrinsic aqueous solubility of Pro was calculated to be 0.2×10^{-3} mM, it increased to 9.5×10^{-3} mM with a CNS concentration of 8 mM. Table 1 compares the solubility of progesterone within different formulations that are reported in other literature and CNS, indicating better results for the Pro/CNS formulation.

3.2. *Molecular docking study*

Molecular docking simulation, by comparing the bond strength between molecules, provides deeper insight into the orientation and interaction of the drug with the cavity of cyclodextrins and also complements experimental data [25]. In this regard, the conformation with the lowest binding energy (ΔG) was chosen as the best conformation.

As the phase solubility studies suggest a 1:2 (drug/host) molar ratio complexation between drug and NS, we compared the 1:1 and 1:2 complexation to ensure the consistency of the obtained experimental data. The obtained result indicates that progesterone and NS make a complex in a 1:1 molar ratio with a binding energy of -

Table 1. Electrochemical parameters obtained from the polarization test on samples immersed in the saline solution

Delivery system	Carrier type	Preparation method	Route of administration	Solubility	Encapsulation efficiency (%)	Reference
Micelle	Brij®35	solvent evaporation	vaginal	20-fold	15%	[23]
Polymer	Polyvinylpyrrolidone	solvent evaporation	oral	1.4-fold	-	[24]
Polymer	Cyclodextrin-nanospone	Co-precipitation method	oral	45-fold	70%	This work

© 2025 The Authors. This article is licensed under a Creative Commons Attribution 4.0 International License.

7.46 kcal/mol. Meanwhile, this value for the 1:2 complex was calculated to be -8.05 kcal/mol. These data reveal that the 1:2 complex is the stable product by recording a lower binding energy, which confirms the phase solubility studies` finding. The lower binding energy for the 1:2 complex is rooted in the interaction between the drug and host molecules.

Figure 6 represents the orientations and interactions between the Pro and cyclodextrins in 1:1 and 1:2 states. As can be seen, there is a hydrogen bond (blue dots) between the oxygen atom of pro and the hydroxyl group of cyclodextrin in the 1:2 complex, which is the main driving force for the formation of this complex. Moreover, this complexation could explain the high phase solubility of pro after encapsulation in CNS, as the whole of the pro molecule is entrapped within the two CD molecules, which are abundant in hydrogen and oxygen atoms, enabling them to make hydrogen bonds with water molecules. Apart from hydrogen bonds, various non-covalent interactions play a key role in the formation of the drug/host complexes, including dipole-dipole, electrostatic, and hydrophobic effects [26]. While the inner cavity of cyclodextrins is hydrophobic, the pro molecule could reside in this moiety due to the favorable enthalpy. Moreover, the pro with the negative dipole moment makes an electrostatic interaction with the positive dipole moment of cyclodextrin. These interactions are similar in both complexes, while hydrogen bonding makes the differences between them.

4. Conclusions

In this study, a complexation between progesterone and a nanosponge based on β-cyclodextrin has been prepared. The nanosponge was made using β-CD and HMDI as a crosslinker, where FT-IR and XRD analyses confirmed its formation. Moreover, similar characterization methods were used to ensure the preparation of the Pro/CNS complex. The encapsulation efficiency of Pro/CNS was found to be 70%. The phase

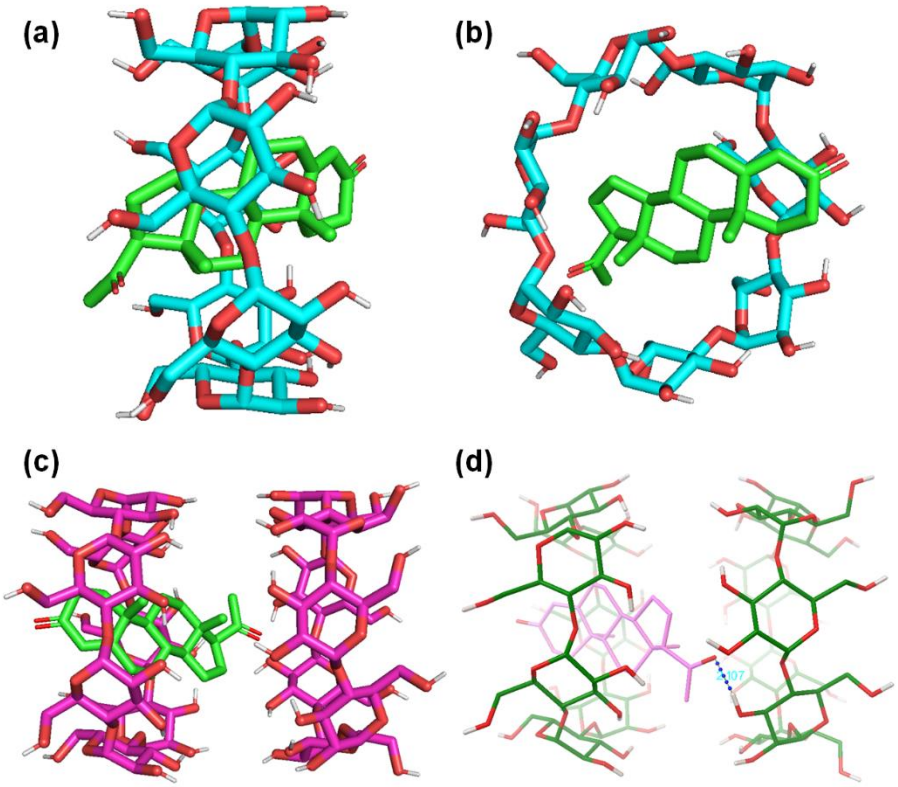

Figure 6. The 3D structures of (a and b) Pro/CNS (1:1) and (c and d) Pro/CNS (1:2) (hydrogen bonding in blue dots).

© 2025 The Authors. This article is licensed under a Creative Commons Attribution 4.0 International License.

solubility findings indicated that a CNS concentration of 8 mM could increase the hydrophobicity of Pro roughly 45 times after the encapsulation process. Moreover, it suggested the formation of a 1:2 (Pro/CNS) complex, which was confirmed by molecular docking studies, indicating that hydrogen bonding is the key driving force for this phenomenon. The encapsulation of progesterone within cyclodextrin-nanosponge seems to be a promising strategy for increasing the hydrophobicity, bioavailability, and effectiveness of this drug, which is prescribed for multiple purposes. However, an *in vitro* drug release study should be conducted to check the behavior of this formulation in a physiological environment. Furthermore, an *in vivo* study is favored to assess the cytotoxicity of this formulation.

Conflict of Interest

The authors declare no conflict of interest.

References

1. B. Mognetti, et al. In vitro enhancement of anticancer activity of paclitaxel by a Cremophor free cyclodextrin-based nanosponge formulation. *Journal of Inclusion Phenomena and Macrocyclic Chemistry*, 2012, *74*, 201.

2. M. Hadadian, B. Mahdavi, and E. Rezaei-Seresht. Exploring modified cyclodextrins for enhanced encapsulation and release of ethinyl estradiol: Physicochemical characterization and kinetic modeling. *Journal of Science: Advanced Materials and Devices*, **2025**, *10*, 100837.

3. A. Moin, et al. Design and formulation of polymeric nanosponge tablets with enhanced solubility for combination therapy. *RSC advances*, **2020**, *10*, 34869.

4. H. Mashaqbeh, R. Obaidat, and N. Al-Shar'i. Evaluation and characterization of curcumin-β-cyclodextrin and cyclodextrin-based nanosponge inclusion complexation. *Polymers*, **2021**, *13*, 4073.

5. S. Abou Taleb, et al. Quercitrin loaded cyclodextrin based nanosponge as a promising approach for management of lung cancer and COVID-19. *Journal of Drug Delivery Science and Technology*, **2022**, *77*, 103921.

6. M. Hadadian, R. Allahyari, and B. Mahdavi. A New Approach for Improving the Water Solubility of Progesterone by Encapsulation with Carboxymethyl-β-CD. *Organic Chemistry Research*, **2023**, *9*, 35.

7. T.B. Mesen and S.L. Young. Progesterone and the luteal phase: a requisite to reproduction. *Obstetrics and gynecology clinics of North America*, **2015**, *42*, 135.

8. V.K. Shankar, et al. Optimization of sulfobutyl-ether-β-cyclodextrin levels in oral formulations to enhance progesterone bioavailability. *International Journal of Pharmaceutics*, **2021**, *596*, 120212.

9. M. Hadadian, et al. Design, characterization, and in vitro evaluation of magnetic carboxymethylated β-cyclodextrin as a pH-sensitive carrier system for amantadine delivery: a novel approach for targeted drug delivery. *RSC advances*, **2025**, *15*, 446.

10. M. Hadadian, et al. Optoelectronic properties of β-Cyclodextrin compound and doped with Na: Comparative study by experimental and DFT approaches. *Journal of Molecular Structure*, **2024**, *1316*, 138862.

11. S. Swaminathan, et al. Structural evidence of differential forms of nanosponges of beta-cyclodextrin and its effect on solubilization of a model drug. *Journal of inclusion phenomena and macrocyclic chemistry*, **2013**, *76*, 201.

12. J.T. Hołaj-Krzak. Assessment of the usefulness of β-cyclodextrin in the removal of progesterone from the environment. *Science of The Total Environment*, **2024**, *950*, 174908.

13. A. Matencio, et al. Study of progesterone complexation in cyclodextrins and cyclodextrin-based nanosponges as an example of solvent-free complexation. *Journal of Drug Delivery Science and Technology*, **2024**, *98*, 105893.

14. P. Shende, et al. Acute and repeated dose toxicity studies of different β-cyclodextrin-based nanosponge formulations. *Journal of pharmaceutical sciences*, **2015**, *104*, 1856.

15. Y. Hanqi, et al. Development of a magnetic Carboxymethyl-β-Cyclodextrin nanocarrier for targeted sitagliptin delivery. *Journal of Molecular Liquids*, **2025**, *433*, 127872.

16. M. Hadadian, et al. Comparative study of β-cyclodextrin and carboxymethyl-β-cyclodextrin as effective drug delivery systems for oxymetholone: Design, preparation, characterization, phase solubility and in vitro drug release studies. *Journal of Science: Advanced Materials and Devices*, **2024**, *9*, 100751.

17. L. Nikolić, et al. The formulation of curcumin: 2-hydroxypropyl-β-cyclodextrin complex with smart hydrogel for prolonged release of curcumin. *Pharmaceutics*, **2023**, *15*, 382.

18. M. Ramirez-Ambrosi, et al. Encapsulation of apple polyphenols in β-CD nanosponges. *Journal of Inclusion Phenomena and Macrocyclic Chemistry*, **2014**, *80*, 85.

19. J. Chen, et al. Characterization of curcumin/cyclodextrin polymer inclusion complex and investigation on its antioxidant and antiproliferative activities. *Molecules*, **2018**, *23*, 1179.

© 2025 The Authors. This article is licensed under a Creative Commons Attribution 4.0 International License.

20. I.M. Helbling, et al. Preparation of TPP-crosslinked chitosan microparticles by spray drying for the controlled delivery of progesterone intended for estrus synchronization in cattle. *Pharmaceutical Research*, **2018**, *35*, 1.

21. D.M. Ragab, S. Rohani, and S. Consta. Controlled release of 5-fluorouracil and progesterone from magnetic nanoaggregates. *International journal of nanomedicine*, **2012**, *7*, 3167.

22. H.D. Williams, et al. Strategies to address low drug solubility in discovery and development. *Pharmacological reviews*, **2013**, *65*, 315.

23. A.S. Hassan, et al. Solubilization and enhancement of ex vivo vaginal delivery of progesterone using solid dispersions, inclusion complexes and micellar solubilization. *Current drug delivery*, **2018**, *15*, 110.

24. X. Chen, et al. Solubility improvement of progesterone from solid dispersions prepared by solvent evaporation and co-milling. *Polymers*, **2020**, *12*, 854.

25. F.M. Mady and U. Farghaly Aly. Experimental, molecular docking investigations and bioavailability study on the inclusion complexes of finasteride and cyclodextrins. *Drug design, development and therapy*, **2017**, *11*, 1681.

26. S.R. Arsad, et al. Theoretical and Molecular Docking Study of Ketoconazole on Heptakis (2, 3, 6-tri-O-methyl)-β-cyclodextrin as Chiral Selector. *Chirality*, **2016**, *28*, 209.

© 2025 The Authors. This article is licensed under a Creative Commons Attribution 4.0 BY International License.

© 2025 The Authors. This article is licensed under a Creative Commons Attribution 4.0 International License.

Antibacterial/Magnetic Iron Oxide Nanoparticles: A Comprehensive Review of Synthesis Methods, Doping Effects, Antibacterial Properties, and Applications in Medical and Food Industries

Hamid Hosseinzadeh *

Advanced Materials Research Center of Fanavaran Sanat Novin Garsha Co., Science and Technology Park of Khorasan Razavi, Growth and Technology Center of Sabzevar, Sabzevar 9618676115, Iran

Editor's note: Magnetic nanoparticles are gaining attention as effective solutions to the growing problem of multidrug-resistant bacteria. In this systematic review, Hosseinzadeh provided a detailed overview of recent studies on the effects of various dopants on the antibacterial mechanisms of magnetic nanoparticles. These dopants boosted the antibacterial activity of these nanoparticles for a variety of applications in clinical, food, and environmental fields, such as drug delivery systems, coatings for implants, wound healing, and antimicrobial packaging.

doi: 10.22034/jams.2025.210146

How to cite: H. Hosseinzadeh. *Journal of Applied Material Science*, **2025**, *1*, 210146.

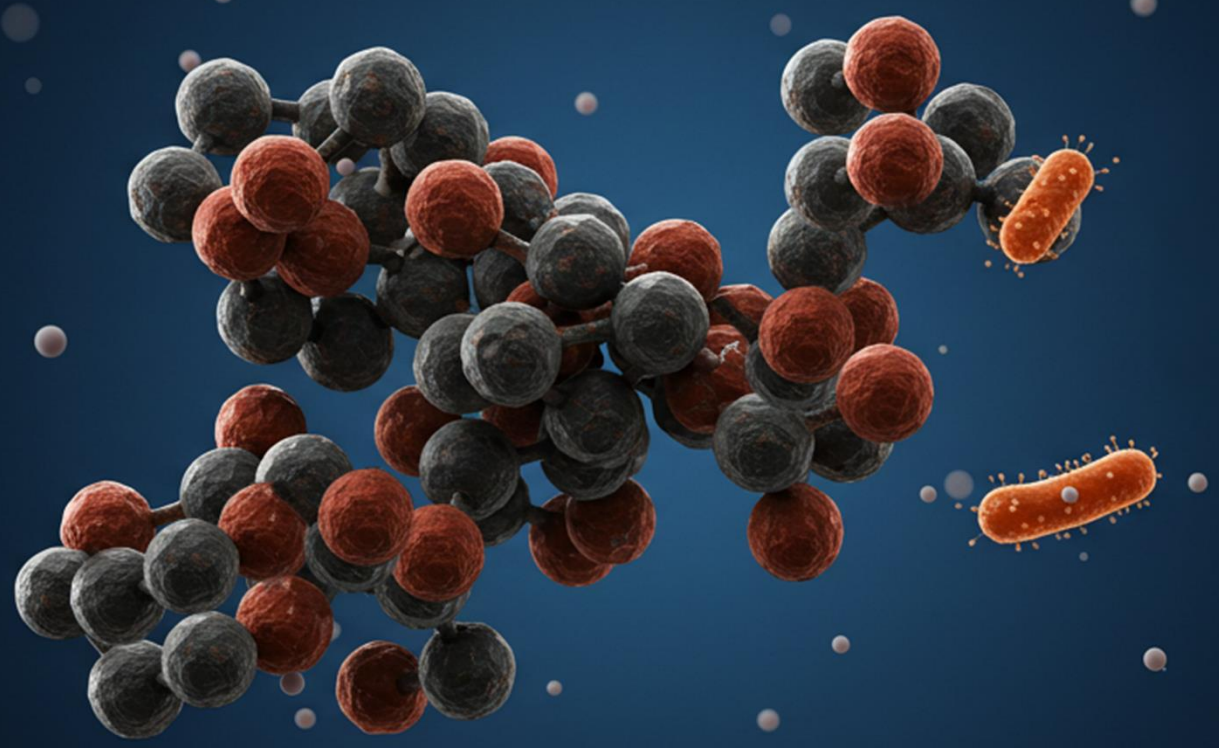

JOURNAL OF
APPLIED
MATERIAL
SCIENCE
jams.hsu.ac.ir

© 2025 *J. Appl. Mater. Sci.* This material is licensed under a Creative Commons Attribution 4.0 International License.

Journal of Applied Material Science **2025**, *1*, 210146
How to cite: H. Hosseinzadeh, *Journal of Applied Material Science*, **2025**, *1*, 210146.
Journal homepage: **jams.hsu.ac.ir**

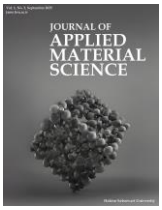

Review

Antibacterial/Magnetic Iron Oxide Nanoparticles: A Comprehensive Review of Synthesis Methods, Doping Effects, Antibacterial Properties, and Applications in Medical and Food Industries

Hamid Hosseinzadeh *

Advanced Materials Research Center of Fanavaran Sanat Novin Garsha Co., Science and Technology Park of Khorasan Razavi, Growth and Technology Center of Sabzevar, Sabzevar 9618676115, Iran

Abstract

The alarming rise of multidrug-resistant (MDR) bacteria has necessitated the development of innovative antimicrobial strategies beyond traditional antibiotics. Magnetic nanoparticles (MNPs) have emerged as promising candidates due to their unique physicochemical properties, including high surface area, superparamagnetism, and facile surface modification. This review explores the multi-faceted antibacterial mechanisms of MNPs, including membrane disruption, reactive oxygen species (ROS) generation, metal ion release, biofilm penetration, intracellular uptake, and hyperthermia-induced bacterial eradication. These mechanisms operate synergistically, allowing MNPs to combat a broad spectrum of bacterial pathogens, including biofilm-associated and drug-resistant strains. The incorporation of antibacterial dopants such as silver (Ag^+), zinc (Zn^{2+}), copper (Cu^{2+}), cobalt (Co^{2+}), and manganese (Mn^{2+}) into MNPs further enhances their antimicrobial activity by promoting ROS generation, enzymatic inhibition, and DNA damage, while also improving magnetic and catalytic performance. Surface functionalization further enables targeted delivery, biocompatibility, and multi-functionality for therapeutic and diagnostic applications. MNPs hold significant promise in clinical, food safety, and environmental contexts, particularly for applications such as drug delivery, implant coatings, wound healing, and antimicrobial packaging. Their ability to combine physical, chemical, and biological antibacterial mechanisms positions MNPs as a versatile platform for next-generation antimicrobial technologies aimed at overcoming the global antibiotic resistance crisis.

Keywords: Magnetic nanoparticles; Antibacterial dopants; Antibacterial mechanisms; Medical applications; Food industry.

1. Introduction

The rapid and widespread emergence of antibiotic-resistant microorganisms has become a critical global health concern, threatening the effectiveness of conventional antimicrobial therapies and posing serious challenges to the management of infectious diseases. The overuse and misuse of antibiotics in clinical, agricultural, and industrial settings have accelerated the

* Corresponding author.
Email addresses: h.hosseinzadeh13638@gmail.com (H. Hosseinzadeh)

Received 9 July 2025
Revised 3 August 2025
Accepted 3 August 2025
Available online 6 August 2025

https://doi.org/10.22034/jams.2025.210146
© 2025 The Authors. This article is licensed under a Creative Commons Attribution 4.0 International License.

evolution of multidrug-resistant (MDR) bacterial strains, leading to increased morbidity, mortality, and healthcare costs worldwide [1, 2]. This alarming situation necessitates the urgent development of novel antimicrobial agents and alternative strategies that can effectively overcome bacterial mechanisms of resistance while minimizing adverse effects on human health and the environment [3, 4].

Nanotechnology has emerged as a transformative field offering innovative solutions to this problem, with magnetic nanoparticles standing out as up-and-coming candidates due to their unique and tunable physicochemical properties. Characterized by their nanoscale dimensions, including a high surface area-to-volume ratio, superparamagnetic behavior, and facile surface modification, MNPs offer a multifunctional platform for targeted antimicrobial interventions [5, 6]. Their nanoscale size enables intimate interaction with microbial cells, allowing for enhanced adhesion, penetration, and disruption of bacterial membranes [7]. Furthermore, the intrinsic magnetic properties of these nanoparticles facilitate their manipulation by external magnetic fields, enabling targeted delivery, controlled localization, and stimulus-responsive activation, critical features for precision antimicrobial therapies [8, 9].

The antibacterial activity of MNPs arises from a combination of physicochemical and biochemical mechanisms. These include the generation of reactive oxygen species (ROS), which induce oxidative stress and damage vital cellular components such as lipids, proteins, and nucleic acids, direct disruption of the bacterial cell membrane integrity leading to leakage of intracellular contents, release of metal ions that interfere with enzymatic functions and genetic material, and intracellular uptake that disrupts metabolic pathways and gene expression [10-13]. This multifaceted mode of action not only enhances antimicrobial potency but also reduces the risk of resistance development, making MNPs effective against a broad spectrum of bacterial pathogens, including drug-resistant strains and biofilm-forming communities.

Beyond their antimicrobial efficacy, MNPs exhibit remarkable versatility, extending their utility across various biomedical and industrial applications [14-17]. In the medical field, they have been extensively studied as vectors for targeted drug delivery, enhancing the therapeutic index of antibiotics and other antimicrobial agents by localizing treatment to infected tissues while sparing healthy cells [18]. Additionally, MNPs serve as contrast agents in magnetic resonance imaging (MRI), improving diagnostic accuracy [19]. Their ability to generate localized heat under alternating magnetic fields, known as magnetic hyperthermia, provides a non-invasive approach to eradicate infections and tumors [20]. Moreover, MNPs are incorporated into advanced wound dressings and tissue engineering scaffolds to promote healing and prevent infection simultaneously, addressing two critical aspects of wound management [21, 22].

In the food industry, MNPs are gaining traction as active components in packaging materials designed to inhibit microbial contamination and extend the shelf life of perishable products. They are employed in preservation technologies and incorporated into nanosensors capable of detecting microbial spoilage and contamination in real time, thereby enhancing food safety and quality control. The magnetic properties of MNPs also enable their recovery and reuse, offering sustainable solutions for food processing and packaging [23, 24]. An exciting emerging application of MNPs lies in their capacity to serve as carriers and stabilizers for enzymes. The immobilization of enzymes on the surface of magnetic nanoparticles enhances their enzymatic stability, activity, and reusability, which is highly advantageous for industrial biocatalysis, environmental remediation, and biosensing applications [25]. This multi-functionality positions MNPs not only as antimicrobial agents but also as integral components in biotechnological and environmental innovations.

Given their broad spectrum of functions and potential impact, magnetic nanoparticles represent a dynamic and rapidly evolving area of research at the intersection of nanotechnology, microbiology, medicine, and food science. This review aims to provide a comprehensive overview of the current state-of-the-art in the synthesis, surface functionalization, antibacterial mechanisms, and practical applications of MNPs in medical and food sectors. By highlighting recent advancements and identifying existing challenges and future perspectives, we seek to underscore the critical role of magnetic nanoparticles as multifunctional tools in addressing microbial threats and enhancing human health and food security in the era of escalating antimicrobial resistance.

2. Synthesis methods of antibacterial magnetic nanoparticles

The synthesis of magnetic nanoparticles (MNPs) with effective antibacterial properties is a fundamental and decisive step in their development, as it directly

© 2025 The Authors. This article is licensed under a Creative Commons Attribution 4.0 International License.

influences critical attributes such as particle size, shape (morphology), magnetic characteristics, surface chemistry, stability, and ultimately their interaction with biological systems [26, 27]. These physicochemical properties govern not only the antimicrobial efficacy of MNPs but also their biocompatibility, toxicity profile, and functionality in complex environments such as human tissues or food matrices [28].

Over the years, researchers have developed and optimized a wide range of synthesis techniques aimed at producing MNPs with tailored properties to meet the demands of specific biomedical, pharmaceutical, and food-related applications (Table 1). These synthesis methods are generally classified into three main categories: physical, chemical, and biological approaches. Each category offers distinct advantages and limitations concerning control over nanoparticle characteristics, scalability, cost-effectiveness, environmental impact, and the ability to incorporate functional elements such as antibacterial dopants or surface coatings.

Physical methods encompass top-down approaches such as ball milling, laser ablation, and physical vapour deposition, which typically involve the mechanical or physical breakdown of bulk materials into nano-sized particles. These methods allow for the production of MNPs without the use of chemical reagents, reducing contamination risks. However, they often yield particles with broad size distributions and irregular shapes, which can affect reproducibility and biological activity [29].

Chemical methods are among the most widely employed techniques due to their ability to control nanoparticle size, composition, and surface properties precisely [27]. These methods include co-precipitation, thermal decomposition, hydrothermal/solvothermal synthesis, microemulsion, and sol-gel processes. The co-precipitation method is favored for its simplicity and scalability, where iron salts are chemically precipitated in alkaline media to form iron oxide nanoparticles. Thermal decomposition provides highly uniform and crystalline MNPs by decomposing organometallic precursors at elevated temperatures in organic solvents. Chemical methods also facilitate the doping of MNPs with antibacterial metal ions (e.g., silver, copper, zinc) and the functionalization of nanoparticle surfaces with polymers, ligands, or antimicrobial agents to enhance stability, biocompatibility, and targeted action.

Table 1. Comparison of magnetic nanoparticle synthesis methods

Synthesis method	Common materials/precursors	Advantages	Disadvantages	Particle control	Antibacterial enhancement
Co-precipitation	$FeCl_2$, $FeCl_3$, NH_4OH or NaOH	Simple, low-cost, scalable	Poor size control, possible agglomeration	Moderate	Can be doped with Ag^+, Cu^{2+}, Zn^{2+}
Thermal decomposition	Iron oleate, $Fe(acac)_3$ in organic solvents	High monodispersity, good crystallinity	Expensive, toxic solvents, not eco-friendly	Excellent	Precise shape and surface control
Hydrothermal/solvothermal	$FeCl_3$, organic solvents, surfactants	Good control over shape and crystallinity, high purity	Requires high temperature/pressure equipment	Good	Suitable for doping and surface functionalization
Green-synthesis	Fe salts + plant extracts, bacteria, fungi	Eco-friendly, biocompatible, cost-effective	Less control over size/shape, slower reactions	Low to moderate	Natural capping agents enhance antibacterial activity
Microemulsion	Fe salts + surfactants in oil/water emulsions	Produces uniform particles, tunable size	Complex system, low yield	Good	Allows for multi-metallic compositions
Sol–gel	Metal alkoxides (e.g., TEOS, $Fe(NO_3)_3$)	High purity, good chemical homogeneity	Time-consuming, requires calcination	Moderate	Easily combined with silica or antibacterial agents

© 2025 The Authors. This article is licensed under a Creative Commons Attribution 4.0 International License.

Biological synthesis methods have recently gained traction as environmentally friendly and sustainable alternatives. These green-synthesis approaches utilize biological entities such as bacteria, fungi, plant extracts, and enzymes to mediate the reduction and stabilization of metal ions into magnetic nanoparticles [30]. Biological methods often produce biocompatible MNPs with intrinsic surface functional groups that can enhance interaction with microbial cells and reduce toxicity. Moreover, they avoid the use of hazardous chemicals and high energy inputs, aligning with green chemistry principles [31]. However, challenges remain regarding the control of particle uniformity and large-scale production [32].

The choice of synthesis method is closely linked to the intended application of the MNPs. For biomedical uses such as targeted drug delivery, imaging, or hyperthermia, strict control over particle size and surface chemistry is essential to ensure biocompatibility and functional performance [33]. In food-related applications, synthesis routes that prioritize safety, non-toxicity, and environmental sustainability are especially desirable. Therefore, the diverse synthesis methodologies available for magnetic nanoparticles provide a versatile toolbox for designing MNPs with optimized antibacterial properties and tailored functionalities.

Continuous advancements in synthesis techniques, including hybrid methods that combine physical, chemical, and biological processes, are expanding the potential of MNPs in combating microbial threats across the medical and food industries. In this section, we will review several widely utilized chemical synthesis methods for magnetic nanostructures, critically evaluating and comparing their respective advantages and limitations.

2.1. Co-precipitation

Among the various chemical synthesis methods for magnetic nanoparticles, co-precipitation is one of the most commonly employed techniques due to its inherent simplicity, cost-effectiveness, and scalability for large-scale production. This method involves the simultaneous precipitation of divalent and trivalent metal ions, typically iron (II) (Fe^{2+}) and iron (III) (Fe^{3+}) salts, from aqueous solutions in the presence of a base, commonly sodium hydroxide (NaOH) or ammonium hydroxide (NH_4OH). Under controlled alkaline conditions, these ions react to form magnetite (Fe_3O_4) or, through subsequent oxidation, maghemite (γ-Fe_2O_3) nanoparticles.

The co-precipitation process offers several advantages. First, it allows for relatively straightforward control over nanoparticle size and composition by adjusting parameters such as pH, temperature, ionic strength, and the Fe^{2+}/Fe^{3+} molar ratio. These factors influence nucleation and growth kinetics, enabling the synthesis of nanoparticles typically ranging from 5 to 20 nanometers in diameter. Second, the aqueous nature of the process makes it environmentally friendly and compatible with a broad range of functionalization strategies post-synthesis.

Despite these benefits, co-precipitation has some inherent limitations. The nanoparticles produced often tend to aggregate due to their high surface energy and magnetic dipole interactions. This aggregation can reduce colloidal stability and limit their effective surface area, which is critical for antibacterial activity and other biomedical functions. Moreover, controlling the phase purity and oxidation state of the nanoparticles can be challenging, as incomplete oxidation or over-oxidation may lead to mixed phases that affect magnetic properties and biological performance. Careful optimization of reaction conditions and use of inert atmospheres during synthesis can mitigate these issues.

The co-precipitation method remains a versatile and practical method for producing magnetic nanoparticles with antibacterial properties, particularly when followed by appropriate surface engineering. Its ease of operation and adaptability make it a preferred choice for both research and industrial-scale production of MNPs tailored for medical and food-related applications [34, 35].

2.2. Thermal decomposition

Thermal decomposition is a widely utilized chemical synthesis method that provides superior control over the size uniformity, crystallinity, and morphology of magnetic nanoparticles. This approach involves the high-temperature decomposition of metal-organic precursors, such as metal acetylacetonates or metal carbonyls, in the presence of organic solvents and surfactants or stabilizing agents. The elevated

© 2025 The Authors. This article is licensed under a Creative Commons Attribution 4.0 International License.

temperatures, typically ranging from 200 ˚C to 350 ˚C, facilitate the controlled nucleation and growth of nanoparticles, resulting in highly monodisperse and crystalline structures with narrow size distributions.

Compared to simpler aqueous-based methods like co-precipitation, thermal decomposition offers enhanced precision in tuning nanoparticle properties, including size, shape, and magnetic behavior, by carefully adjusting reaction parameters such as temperature, precursor concentration, and surfactant type. This level of control is particularly important for biomedical applications where consistency in nanoparticle characteristics directly influences their performance and safety profile. For instance, in targeted drug delivery, uniform particle size ensures predictable biodistribution and cellular uptake, while in magnetic resonance imaging (MRI), high crystallinity and size uniformity enhance contrast efficiency.

Despite these advantages, thermal decomposition is inherently more complex, requiring specialized equipment, organic solvents, and inert atmospheric conditions to prevent premature oxidation or contamination. Moreover, the process tends to be more costly and less environmentally friendly due to the use of organic solvents and high energy input. Nevertheless, the high-quality nanoparticles produced via thermal decomposition are highly sought after in advanced biomedical research and clinical applications, where their reproducibility and functional performance are critical [36, 37].

2.3. *Hydrothermal and solvothermal synthesis*

Hydrothermal and solvothermal synthesis are versatile chemical methods that utilize reactions conducted in sealed autoclaves under elevated temperatures and pressures to produce magnetic nanoparticles with controlled size, crystallinity, and morphology. In hydrothermal synthesis, aqueous solvents are employed, whereas solvothermal methods use non-aqueous organic solvents, allowing a broader range of reaction conditions and product characteristics. These high-pressure, high-temperature environments facilitate enhanced solubility and reactivity of precursors, promoting the formation of highly crystalline nanoparticles with uniform size distributions.

By carefully adjusting key synthesis parameters such as temperature, reaction duration, solvent type and composition, and precursor concentration, researchers can precisely tailor the physicochemical properties of magnetic nanoparticles to meet specific application requirements. One of the significant advantages of hydrothermal and solvothermal methods is their ability to synthesize nanoparticles with diverse morphologies, including spheres, rods, plates, and phase purity, which directly influence magnetic properties and antibacterial efficacy. Additionally, these methods often yield nanoparticles with superior crystallinity compared to conventional co-precipitation, resulting in enhanced magnetic behavior desirable for biomedical imaging, drug delivery, and hyperthermia treatments. However, the requirement for specialized high-pressure equipment and longer reaction times can limit the scalability and increase production costs. Despite these challenges, hydrothermal and solvothermal syntheses remain valuable tools in producing high-quality magnetic nanoparticles for both medical and food industry applications, where precise control over nanoparticle characteristics is essential [38, 39].

2.4. *Green-synthesis methods*

Green-synthesis methods have emerged as a sustainable and environmentally friendly alternative for producing MNPs, avoiding the use of toxic chemicals and harsh reaction conditions typically associated with conventional chemical techniques. These approaches harness biological entities such as plant extracts, bacteria, fungi, or algae, which act simultaneously as reducing, capping, and stabilizing agents during the synthesis process. The biomolecules present in these natural sources, such as polyphenols, flavonoids, terpenoids, proteins, and enzymes, not only facilitate the reduction of metal ions but also impart surface functional groups that can enhance the biological activity and biocompatibility of the resulting nanoparticles. Plant-mediated synthesis is particularly attractive due to its simplicity, scalability, and the wide availability of plant resources.

Extracts from leaves, roots, or fruits can efficiently mediate nanoparticle formation under mild conditions, eliminating the need for high temperatures, pressures, or toxic solvents. Microbial synthesis using bacteria or fungi offers another promising route, providing precise

© 2025 The Authors. This article is licensed under a Creative Commons Attribution 4.0 International License.

control over nanoparticle nucleation and growth through enzymatic and metabolic pathways. One of the most noteworthy features of green-synthesized MNPs is their surface bio-functionalization. The natural capping agents not only stabilize the nanoparticles but can also enhance their antibacterial activity by facilitating better interaction with microbial cell membranes or promoting ROS generation. Moreover, the improved biocompatibility of these particles makes them suitable candidates for various biomedical applications, including wound healing, targeted drug delivery, and biosensing.

In the food industry, green-synthesized MNPs have shown potential in the development of biodegradable antimicrobial packaging, active food coatings, and nano-sensors for spoilage detection. Their non-toxic nature and natural origin make them particularly suited for applications requiring human or environmental safety. Despite their advantages, green-synthesis methods may face challenges such as batch-to-batch variability, lower reaction yields, and limited control over particle size and morphology. Nevertheless, persistent research is focused on optimizing these parameters to expand the applicability of green-synthesized MNPs in both medical and food-related domains [40-42].

3. Antibacterial mechanisms of magnetic nanoparticles

Magnetic nanoparticles, particularly those doped with antibacterial ions or functionalized with bioactive agents, exhibit potent antimicrobial activity through multiple synergistic mechanisms [43]. These mechanisms operate at the molecular and cellular levels and vary depending on the nanoparticle's chemical composition, size, surface functionalization, and the type of bacterial strain (i.e., gram-positive vs. gram-negative). The following is a detailed overview of the principal antibacterial mechanisms by which magnetic nanoparticles inactivate or destroy bacterial cells.

3.1. Disruption of bacterial cell membrane integrity

One of the most prominent and direct antibacterial mechanisms of magnetic nanoparticles involves the disruption of the bacterial cell membrane, a critical structural component essential for maintaining cellular integrity and homeostasis. Owing to their nanoscale dimensions and high surface-area-to-volume ratio, MNPs exhibit unique physicochemical properties that facilitate close interaction with bacterial cells. Notably, their surface charge enables strong electrostatic interactions with the negatively charged components of bacterial cell walls, such as lipopolysaccharides in Gram-negative bacteria and teichoic acids in Gram-positive species.

Upon approaching the bacterial surface, MNPs can adsorb and penetrate the outer structures of the cell envelope. This interaction is often driven by electrostatic attraction and can result in the insertion of nanoparticles into the lipid bilayer. Such insertion disrupts the membrane's structural integrity, leading to several downstream effects: destabilization of the lipid matrix, formation of nanoscale pores, and leakage of vital intracellular components, including proteins, ions, and nucleic acids. These events compromise membrane function and induce increased permeability, creating an osmotic imbalance that ultimately culminates in bacterial cell lysis. Furthermore, the antibacterial efficacy of MNPs can be significantly enhanced through surface modification or doping with antimicrobial metal ions such as silver (Ag^+) or copper (Cu^{2+}). These dopants facilitate additional modes of action, including the generation of ROS, catalytic oxidative stress, and direct interactions with membrane proteins and phospholipids, further weakening the cell envelope. Collectively, these synergistic effects make MNPs, particularly when functionalized, highly effective agents against a broad spectrum of bacterial pathogens [44-46].

3.2. Generation of reactive oxygen species (ROS)

A central antibacterial mechanism of magnetic nanoparticles is the induction of oxidative stress through the generation of ROS. These include highly reactive molecules such as hydroxyl radicals ($OH^{\bullet}$), superoxide anions ($O_2^{\bullet-}$), and hydrogen peroxide (H_2O_2), which can interact destructively with essential biomolecules within bacterial cells, leading to structural and functional damage. ROS generation by MNPs occurs primarily through Fenton and Fenton-like reactions, in which ferrous (Fe^{2+}) and ferric (Fe^{3+}) ions catalyze the decomposition of hydrogen peroxide into reactive radicals. The presence of redox-active dopants such as copper (Cu^{2+}) or manganese (Mn^{2+}) can further enhance

© 2025 The Authors. This article is licensed under a Creative Commons Attribution 4.0 International License.

this process by facilitating electron transfer reactions that intensify ROS production. Additionally, in certain composite or semiconductor-modified MNPs, exposure to ultraviolet or visible light induces photo-activation, resulting in the formation of electron-hole pairs. These photo-induced charges subsequently react with molecular oxygen and water to generate ROS through a series of redox reactions. Once formed, these reactive species readily diffuse into bacterial cells, where they initiate a cascade of oxidative damage.

Lipid peroxidation compromises the integrity and fluidity of the cell membrane, leading to increased permeability, disruption of ion gradients, and eventual cell lysis. Proteins are also targeted, undergoing oxidative modifications that result in loss of enzymatic activity and breakdown of metabolic pathways. Furthermore, ROS can cause significant genotoxic effects by introducing strand breaks, base modifications, and oxidative lesions in DNA, thereby impairing replication and transcription processes. This oxidative mechanism is particularly effective under aerobic conditions, where sufficient oxygen is available to sustain the redox cycles involved in ROS generation. As a result, MNP-induced oxidative stress contributes to a broad-spectrum antibacterial effect that is non-specific, making it highly effective against diverse classes of bacterial pathogens. Moreover, this mode of action often works synergistically with other antibacterial mechanisms of MNPs, such as membrane disruption and metal ion toxicity, thereby enhancing their overall antimicrobial efficacy [47, 48].

3.3. Metal ion release and intracellular toxicity

Another important antibacterial mechanism of magnetic nanoparticles, particularly those doped with biologically active metal ions such as silver (Ag^+), zinc (Zn^{2+}), or copper (Cu^{2+}), is their ability to act as reservoirs for controlled and sustained ion release. When these doped MNPs come into contact with aqueous environments or bacterial cells, the embedded metal ions are gradually released into the surrounding medium. This release is often facilitated by factors such as local pH, redox conditions, or the presence of cellular metabolites, allowing for a regulated exposure that enhances antimicrobial efficacy while minimizing off-target toxicity. Once liberated, these metal ions can readily penetrate bacterial membranes and accumulate within the intracellular environment, where they exert toxic effects through multiple molecular pathways. A key mode of action involves the binding of metal ions to thiol (-SH) groups in bacterial proteins and enzymes. This interaction leads to conformational changes or inactivation of critical metabolic enzymes, disrupting processes such as nutrient metabolism, redox homeostasis, and stress response systems. Furthermore, metal ions can directly interfere with genetic processes by interacting with nucleic acids, thereby impairing DNA replication, transcription, and protein synthesis. These interactions not only hinder bacterial proliferation but may also induce genotoxic stress and mutagenesis.

In addition to enzymatic and genetic disruption, metal ions are known to interfere with cellular energy production. They can impair the function of membrane-bound proteins involved in the electron transport chain, leading to a collapse in proton motive force and a significant reduction in ATP synthesis. This energy depletion compromises the cell's ability to maintain homeostasis and repair damage, ultimately contributing to cellular dysfunction and death. This ion-mediated toxicity is particularly valuable in combating antibiotic-resistant bacterial strains, as it operates through mechanisms distinct from those targeted by conventional antibiotics. By supplementing the physical effects of membrane disruption and the oxidative stress induced by reactive oxygen species, metal ion release provides a multifaceted antibacterial strategy that enhances the overall potency of MNP-based antimicrobial systems [49-51].

3.4. Biofilm penetration and inhibition

Bacterial biofilms represent a significant challenge in antimicrobial therapy due to their highly structured, multicellular architecture and protective extracellular polymeric matrix, which confer enhanced resistance to conventional antibiotics and host immune responses. These biofilms, commonly found on implanted medical devices, chronic wound surfaces, and mucosal tissues, create a physical and chemical barrier that limits the diffusion of antimicrobial agents and promotes the persistence of bacterial infections.

Magnetic nanoparticles, owing to their unique physicochemical properties and external controllability, offer a promising strategy for biofilm disruption and eradication. One of the most distinctive advantages of

© 2025 The Authors. This article is licensed under a Creative Commons Attribution 4.0 International License.

MNPs is their responsiveness to external magnetic fields, which enables their targeted and magnetically guided transport deep into dense biofilm structures. This targeted penetration allows MNPs to overcome diffusion limitations that typically hinder conventional treatments. Once within the biofilm, MNPs can be engineered to generate ROS in situ, particularly upon exposure to light or in the presence of catalytic metal ions.

The localized production of ROS within the biofilm microenvironment facilitates the oxidative degradation of the extracellular polymeric substances (EPS) that form the scaffold of the biofilm matrix. This degradation weakens the physical integrity of the biofilm and increases its permeability, rendering the embedded bacterial cells more susceptible to antimicrobial action. Furthermore, MNPs can be functionalized to carry or co-deliver biofilm-disrupting agents, such as dispersin B, DNase, or surfactants, which enzymatically or chemically break down matrix components like extracellular DNA, polysaccharides, and proteins. This multifunctional approach not only enhances the penetration and dispersion of biofilms but also aids in the prevention of biofilm reformation. By combining physical penetration, chemical degradation, and potential therapeutic delivery, MNPs provide a versatile and effective platform for targeting biofilm-associated infections. Their applicability is particularly relevant in the management of chronic infections related to indwelling medical devices and poorly healing wounds, where traditional antibiotics often fail to achieve sufficient therapeutic outcomes [44, 52, 53].

3.5. Intracellular uptake and metabolic interference

Beyond their extracellular actions, magnetic nanoparticles also exert potent intracellular effects following their uptake by bacterial cells. Although bacteria lack the classical endocytic machinery found in eukaryotic cells, various studies suggest that MNPs can enter bacterial cytoplasm through mechanisms resembling endocytosis or via direct penetration facilitated by membrane disruption, especially in the presence of nanoparticle surface modifications that enhance cellular adhesion and translocation. Once internalized, MNPs interact with key intracellular components, initiating a cascade of cytotoxic events that compromise bacterial viability.

A primary mode of intracellular toxicity involves the disturbance of redox homeostasis. Internalized MNPs can catalyze the generation of ROS within the cytosol, intensifying oxidative stress beyond the cell's capacity for detoxification.

This intracellular ROS accumulation leads to widespread damage to nucleic acids, proteins, and membrane structures from within the cell itself. In addition to oxidative stress, MNPs can interfere directly with ribosomal function, disrupting the process of protein translation. By hindering the synthesis of essential enzymes and structural proteins, MNPs severely limit the bacteria's ability to grow, replicate, and respond to environmental stressors. Moreover, exposure to internalized nanoparticles has been shown to alter gene expression profiles and modulate the activity of critical metabolic enzymes. Such interference with the regulation of genes involved in cell division, repair mechanisms, and energy metabolism can push bacterial cells into a state of metabolic arrest or apoptosis-like death.

The cytosolic presence of MNPs, therefore, introduces a multilayered form of metabolic interference that complements their extracellular actions. This intracellular mechanism becomes particularly powerful when MNPs are used as carriers for antibiotics or bioactive polymers. By delivering therapeutic agents directly into the bacterial cytoplasm, MNPs bypass external resistance mechanisms and maximize the intracellular drug concentration, thereby enhancing overall antibacterial efficacy. This integrated strategy makes MNPs valuable tools in combating resistant bacterial strains and persistent infections [48, 54].

3.6. Photo-thermal and magnetic hyperthermia effects

In addition to their intrinsic chemical and biological activities, MNPs can be engineered to respond to external physical stimuli, enabling localized thermal therapy as an auxiliary antibacterial strategy. Specifically, when exposed to alternating magnetic fields (AMFs), certain MNPs undergo magnetic relaxation processes that result in the generation of localized heat, a phenomenon known as magnetic hyperthermia.

Similarly, MNPs modified with photo-thermal agents or possessing intrinsic optical absorption capabilities can convert near-infrared (NIR) light or laser irradiation into

© 2025 The Authors. This article is licensed under a Creative Commons Attribution 4.0 International License.

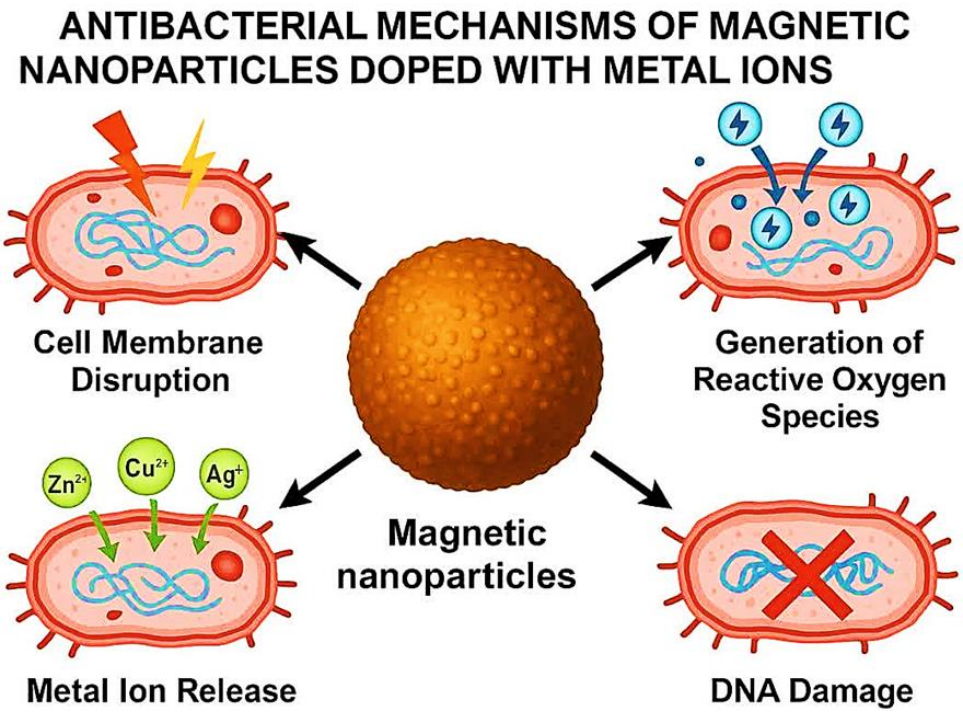

Figure 1. Schematic representation of the antibacterial mechanisms of magnetic nanoparticles.

heat through non-radiative decay, producing a photo-thermal effect. The mild, localized elevation of temperature in the range of approximately 42–50 ˚C, while not damaging to surrounding healthy tissue, is sufficient to exert bactericidal effects. This thermal energy can denature bacterial proteins, destabilize cellular membranes, and impair essential enzymatic functions, leading to irreversible damage and cell death. Moreover, hyperthermia has been shown to enhance the efficacy of other antibacterial mechanisms, such as ROS-mediated oxidative stress and antibiotic action.

By increasing bacterial membrane permeability and disrupting repair pathways, heat treatment can facilitate the intracellular uptake of drugs and potentiate their effects, thereby overcoming common resistance mechanisms. The capacity for spatially controlled activation through external stimuli makes this approach particularly attractive for non-invasive and site-specific antibacterial therapies. This is especially valuable in the treatment of deep-seated infections or biofilm-associated infections on implanted medical devices, where conventional systemic antibiotics often fail to achieve therapeutic concentrations. Thus, photo-thermal and magnetic hyperthermia strategies represent a promising extension of MNP functionality, contributing to the development of responsive, multimodal, and highly effective antimicrobial platforms [55-57].

In conclusion, the antibacterial activity of magnetic nanoparticles arises from a combination of physical, chemical, and biochemical interactions. Their multi-target action makes them effective even against multidrug-resistant (MDR) bacterial strains. By tuning the particle design through doping, surface modification, or external activation, MNPs can be adapted to specific medical or food-related antibacterial challenges. These diverse mechanisms make MNPs one of the most promising candidates for next-generation antimicrobial technologies. Figure 1 illustrates a schematic representation of the antibacterial mechanisms exhibited by magnetic nanoparticles.

4. Antibacterial dopants in magnetic nanoparticles: Properties and applications

To enhance antibacterial efficacy and tune magnetic features, researchers have focused on incorporating other functional metal ions into the iron oxide lattice.

© 2025 The Authors. This article is licensed under a Creative Commons Attribution 4.0 International License.

The substitution of iron ions with metals such as silver (Ag^+), zinc (Zn^{2+}), copper (Cu^{2+}), cobalt (Co^{2+}), or manganese (Mn^{2+}) can significantly alter the surface reactivity, redox potential, and ion release profile of the nanoparticles. These dopant ions not only increase the oxidative stress generated upon interaction with microbial cells but also disrupt key cellular processes such as membrane integrity, enzyme activity, and DNA replication [58, 59].

The modified particles thus exhibit multifaceted antimicrobial actions that are often more potent than their undoped counterparts. For instance, Ag-doped Fe_3O_4 nanoparticles have been shown to possess synergistic antimicrobial capabilities, whereby silver ions confer strong bactericidal effects while the iron oxide core maintains magnetic properties necessary for targeted delivery and post-use recovery. Beyond bulk composition, the surface chemistry of MNPs plays a crucial role in their colloidal stability, interaction with bacterial membranes, and compatibility with biological environments [18].

Surface functionalization, often performed post-synthesis, enables the introduction of stabilizing or bioactive agents such as polymers, surfactants, biopolymers, or small molecules. These modifications serve to improve dispersion in aqueous or biological media, prevent nanoparticle agglomeration, and increase specificity toward microbial targets [60]. Moreover, tailored surface coatings can facilitate the loading of therapeutic agents, enzymes, or fluorescent markers, thus transforming MNPs into multifunctional platforms capable of simultaneous bacterial eradication, diagnostics, and therapeutic delivery. In medical applications and food safety, the ability to fine-tune the chemical composition and surface characteristics of MNPs is of paramount importance. In clinical contexts, such engineered nanoparticles are being explored for use in targeted drug delivery, wound healing, implant coatings, and theranostic systems that combine antimicrobial activity with imaging functionalities.

In the food sector, compositionally optimized MNPs are being integrated into smart packaging materials, active coatings, and biosensors for contamination monitoring [61]. Ultimately, the convergence of compositional engineering and surface functionalization allows for the rational design of advanced MNPs with enhanced antibacterial efficiency, improved safety profiles, and increased versatility across diverse application domains.

Doped-magnetic nanoparticles, particularly iron oxides, with antibacterial metal ions are a common strategy to enhance their antimicrobial efficacy while preserving or tuning their magnetic properties. These dopants not only contribute directly to bacterial cell disruption but also modulate surface reactivity, oxidative stress generation, and biocompatibility. The following is a detailed overview of the most prominent antibacterial dopants, their roles, and application relevance in medical and food-related fields.

4.1. Silver (Ag^+)

Silver ions (Ag^+), as a functional dopant in magnetic nanoparticles, are recognized as one of the most potent and broad-spectrum antimicrobial agents, with mechanisms of action that include disruption of bacterial membranes, interference with DNA replication, and the induction of oxidative stress through ROS generation [62, 63].

In the context of magnetic nanoparticles, Ag^+ is often doped onto or incorporated into iron oxide cores such as Fe_3O_4 (magnetite) or γ-Fe_2O_3 (maghemite), effectively combining the intrinsic magnetic responsiveness of these cores with the potent antibacterial properties of silver. This integration enables the design of multifunctional nanostructures capable of both diagnostic and therapeutic applications. From a biomedical standpoint, silver-doped MNPs have shown great promise in a range of clinical applications. They are widely employed as antimicrobial coatings on medical implants, catheters, and surgical tools to prevent bacterial colonization and biofilm formation.

In wound management, Ag^+-functionalized MNPs are incorporated into hydrogels and advanced wound dressings to accelerate healing while providing localized antibacterial protection. Additionally, their ability to serve as both imaging agents (e.g., magnetic resonance imaging contrast enhancers) and therapeutic agents positions them as effective components in theranostic platforms aimed at simultaneously detecting and treating localized infections [64-66].

In the field of food safety, silver-doped MNPs have also demonstrated utility as active components in antimicrobial packaging materials, which inhibit

© 2025 The Authors. This article is licensed under a Creative Commons Attribution 4.0 International License.

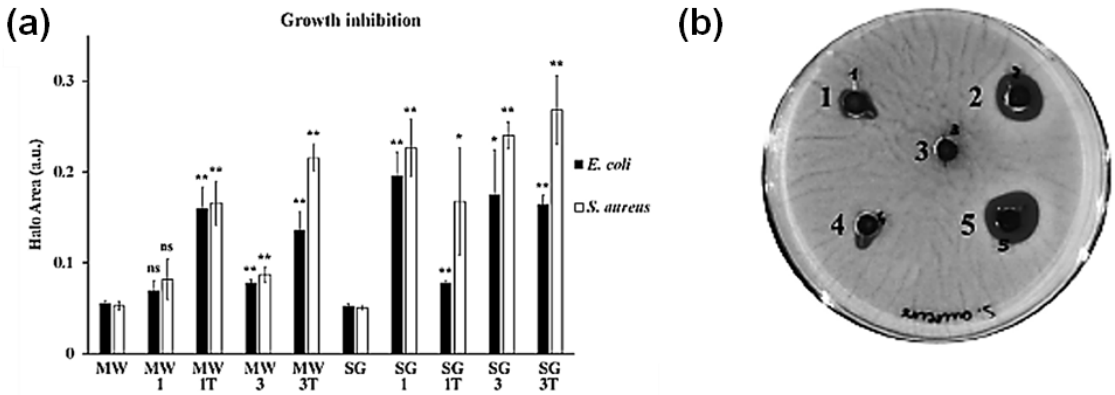

Figure 2. Investigation of the silver dopant effect on the antibacterial activity (a) of $MgFe_2O_4$ nanoparticles against *S. aureus* and *E. coli* bacteria and growth inhibition properties (b) against *S. aureus*. Reprinted/adapted with permission from Ref. [69]. 2021, MDPI.

microbial growth and extend shelf life. Moreover, they are applied as surface disinfectants and antimicrobial coatings in food processing environments, where microbial contamination poses a serious threat to public health [67, 68].

While silver doping may lead to a slight reduction in the overall magnetic saturation of iron oxide nanoparticles, this trade-off is generally acceptable given the substantial enhancement in antimicrobial efficacy. Notably, even at relatively low silver concentrations, these nanocomposites exhibit significant bactericidal activity, making them a cost-effective and efficient option for diverse antibacterial applications.

Fantozzy et al. [69] investigated the effect of silver doping on the antibacterial performance of $MgFe_2O_4$ nanoparticles. The results (Figure 2) demonstrated that the incorporation of silver ions into the structure led to a significant enhancement in the antibacterial properties. Also, with increasing silver dopant levels, an increase in antibacterial properties was observed.

Rabbi and colleagues [70] synthesized the magnetic iron oxide/silver (IO/Ag) nanocomposites via a co-precipitation method, where bare iron oxide nanoparticles were stabilized using green-synthesized silver nanoparticles.

The catalytic reduction performance of the IO/Ag nanocomposite was evaluated using $NaBH_4$ as a reducing agent, demonstrating effective degradation of the anionic azo dye Congo Red (CR). Complete degradation of 20 mL of 0.1 mM CR solution was achieved within 2 minutes when 40 µg/mL of IO/Ag particles were applied. The nanocomposite also exhibited moderate antibacterial activity against four pathogenic bacterial strains, including both Gram-positive (*Staphylococcus aureus*) and Gram-negative bacteria (*Escherichia coli*, *Shigella dysenteriae*, and *Shigella boydii*). Antibacterial activity was found to increase with particle concentration, with inhibition zones ranging from 7 to 12.5 mm, reaching a maximum inhibition zone of 12.5 mm against *S. aureus* at a concentration of 105 µg/disc. Notably, the bare IO nanoparticles did not exhibit any antibacterial effect, indicating that the observed antimicrobial performance is attributable to the presence of silver nanoparticles in the composite.

Regarding the mechanisms of antibacterial action, two primary pathways are suggested, which are the release of silver ions (Ag^+) from the nanoparticles, which penetrate bacterial membranes and disrupt vital cellular processes such as respiration and osmotic balance, and direct contact-based bacterial membrane disruption via anchored AgNPs on the nanocomposite surface. In addition to their antibacterial capabilities, the IO/Ag nanocomposite particles demonstrated significant antioxidant activity, with 94% DPPH free radical scavenging observed at a particle concentration of 100 µg/mL.

Overall, these biocompatible and relatively low-toxicity IO/Ag nanocomposites show promise as bioactive materials for a wide range of applications in biomedicine and health-related consumer products, particularly due to their recoverability from application

© 2025 The Authors. This article is licensed under a Creative Commons Attribution 4.0 International License.

media, which minimizes potential environmental and health risks.

In a related study, Güneş et al. [71] successfully synthesized magnetic iron oxide nanoparticles (MIONPs) via a chemical co-precipitation method. To improve their surface functionality, activated carbon (AC) derived from Hibiscus esculentus (HE) fruit was utilized to coat the nanoparticles, yielding MIONPs/HEAC nanocomposites. Subsequently, to enhance the antimicrobial performance of the system, silver ions were chemically reduced and deposited onto the MIONPs/HEAC surfaces, forming MIONPs/HEAC@Ag nanocomposites. Antibacterial evaluations revealed that both MIONPs/HEAC and MIONPs/HEAC@Ag exhibited inhibitory effects against *Staphylococcus aureus* and *Escherichia coli*. Notably, the MIONPs/HEAC@Ag nanocomposite demonstrated superior antimicrobial efficacy, which is attributed to the synergistic interplay between the intrinsic magnetic properties of iron oxide and the potent bactericidal activity of silver nanoparticles (Figure 3).

4.2. Zinc (Zn^{2+})

Zinc ions (Zn^{2+}), as a biocompatible antibacterial dopant in magnetic nanoparticles, possess moderate but effective antibacterial activity, making them particularly attractive for biomedical applications where antimicrobial efficacy must be balanced with biocompatibility [72]. As an essential trace element in human physiology, zinc participates in numerous enzymatic and regulatory pathways, and its incorporation into antibacterial materials is generally well tolerated by biological systems. The antibacterial mechanism of Zn^{2+} primarily involves the inhibition of critical bacterial enzymes, disruption of membrane integrity, and induction of oxidative stress through the generation of reactive oxygen species [73]. Zn^{2+} is typically doped with iron oxide matrices such as Fe_3O_4 or γ-Fe_2O_3. This doping not only imparts antimicrobial functionality but also enhances the overall biological safety and colloidal stability of the nanomaterial. Zinc-doped MNPs have demonstrated particular effectiveness against Gram-positive bacterial strains, which are often

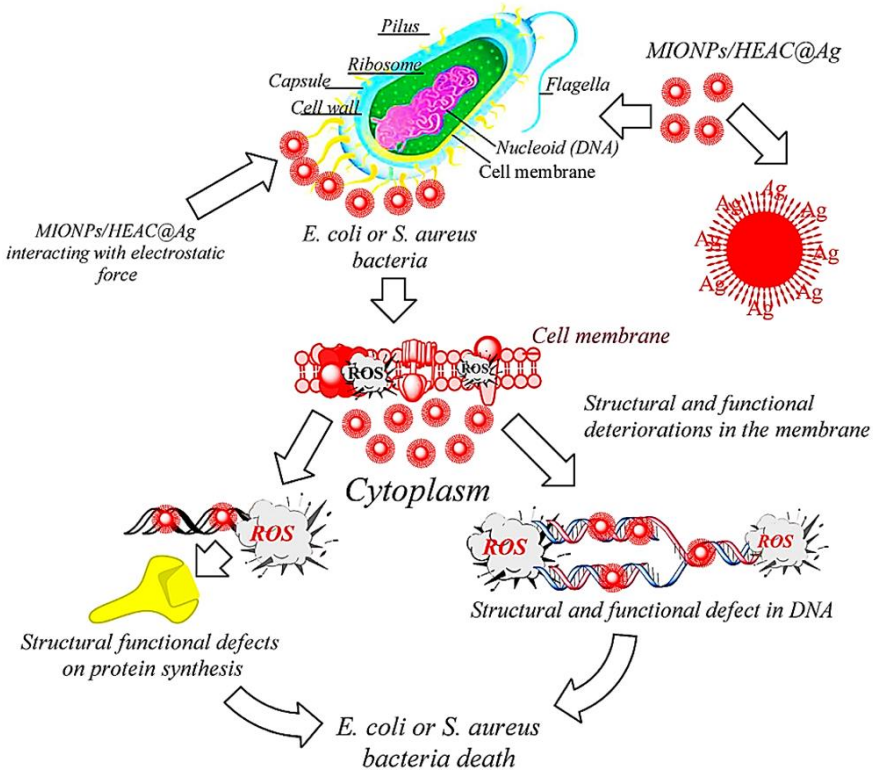

Figure 3. The scheme of antimicrobial mechanisms of MIONPs/HEAC@Ag nanocomposites. Reprinted/adapted with permission from Ref. [71]. 2025, MDPI.

© 2025 The Authors. This article is licensed under a Creative Commons Attribution 4.0 International License.

more resilient to conventional treatments due to their thick peptidoglycan layers. Additionally, Zn-doping has been shown to improve the chemical stability and reduce the cytotoxicity of the nanoparticles, making them especially suitable for applications requiring prolonged or repeated exposure [74-76].

In the medical field, zinc-functionalized MNPs are widely explored as components of bone cements, scaffold materials, and other bioactive platforms intended for orthopedic applications. Their antimicrobial properties help prevent post-surgical infections, while their biocompatibility supports tissue integration and healing [77, 78]. Zinc's application also extends to the food industry, where it serves as a safe and effective antimicrobial active material and additive in various food packaging systems. Zn-doped MNPs are incorporated into edible coatings and biodegradable films used to preserve perishable goods such as fresh fruits, vegetables, and meats. These films not only inhibit microbial growth but also contribute greatly to the extended shelf life of products and reduced spoilage under storage conditions [79-81].

Hosseinzadeh et al. [82] investigated the effects of zinc doping and surface coating with various morphologies of zinc oxide on the Zn^{2+} ion release rate, antibacterial activity, and biological properties of Fe_3O_4 nanoparticles. Their findings revealed that the lowest zinc ion release rate was observed in structures incorporating zinc as a dopant, while the highest release rate corresponded to nanoparticles coated with mesoporous zinc oxide. This increased release rate was directly correlated with the surface area exposed to the reaction medium. Moreover, as the zinc ion release rate increased, there was a marked enhancement in both the inhibition of bacterial growth and bactericidal activities of the compounds. These results suggest a direct relationship between the release of zinc ions and the antibacterial efficacy of the nanoparticles.

Yusof et al. [83] investigated the antibacterial activity of biologically synthesized ZnO NPs against poultry-associated foodborne pathogens, *Salmonella spp.*, *E. coli*, and *S. aureus* (Figure 4). The Zn^{2+} dissolution study revealed that ZnO NPs dissolved more ions than their bulkier counterparts, implying that the release of high Zn^{2+} was responsible for the antibacterial activity. Based on the agar well diffusion assay, MIC and MBC, time-kill assay, and antibiofilm activity tests, the ZnO NPs exhibited effective antibacterial actions against poultry-associated foodborne pathogens, with *S. aureus* as the most susceptible to ZnO NPs. The ROS formation, cellular leakage, and SEM study revealed that the underlying antibacterial mechanisms of ZnO NPs include the generation of ROS, oxidative stress on the bacterial cell membrane leading to membrane damage, and cellular material leakage, which ultimately leads to cell death.

Overall, the incorporation of zinc into magnetic nanoparticles enhances their antimicrobial spectrum while maintaining a favorable safety profile. Its multi-functionality and compatibility with both biomedical and food-grade applications make Zn^{2+} a valuable dopant for the development of next-generation antimicrobial nanomaterials.

4.3. Copper (Cu^{2+})

Copper ions (Cu^{2+}), as a potent antibacterial dopant in magnetic nanoparticles, are well recognized for their strong antibacterial activity, particularly against gram-negative bacteria, which are often more challenging to treat due to their complex outer membrane structures. The antimicrobial efficacy of Cu^{2+} arises from its ability to generate ROS, leading to oxidative damage of vital microbial components such as proteins and nucleic acids. This oxidative stress results in compromised cellular functions and eventual bacterial death [84].

When incorporated into magnetic nanoparticles, copper ions enhance the oxidative stress-inducing capacity of the nanomaterial, amplifying its bactericidal potential. Additionally, copper doping may synergize with other metal ions like silver and iron, resulting in multi-modal antibacterial activity that targets bacteria through complementary mechanisms. In medical applications, Cu^{2+}-doped MNPs have been utilized as topical antimicrobial agents for treating skin infections, leveraging their potent bactericidal effects while minimizing systemic toxicity [85]. Furthermore, copper-functionalized nanoparticles are increasingly investigated as coatings for orthopedic implants and surgical devices to prevent post-operative infections, a major concern in clinical settings [86].

By inhibiting bacterial colonization and biofilm formation, these coatings contribute to improved patient outcomes and implant longevity. In the food industry,

© 2025 The Authors. This article is licensed under a Creative Commons Attribution 4.0 International License.

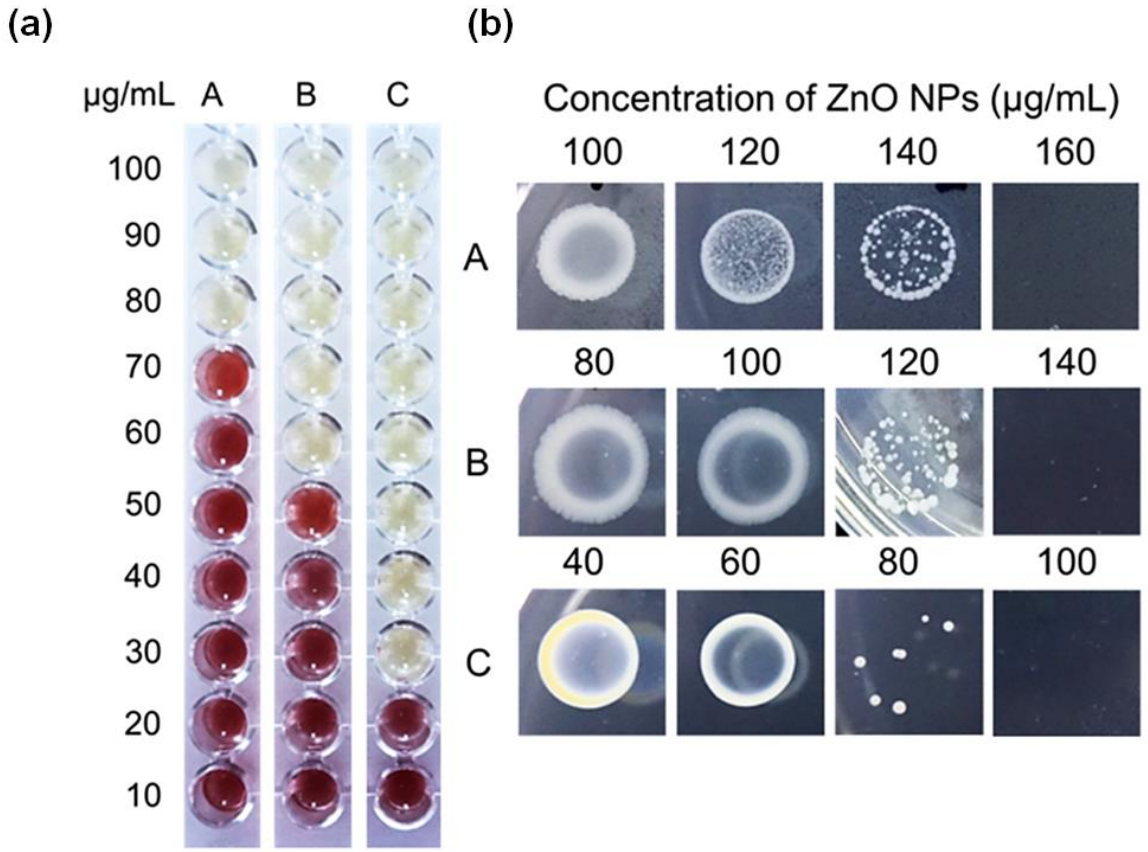

Figure 4. Minimum inhibitory concentration (MIC) (a) and minimum bactericidal concentration (MBC) (b) of biosynthesized ZnO NPs against *Salmonella* spp. (A), *E. coli* (B), and *S. aureus* (C). Reprinted/adapted with permission from Ref. [83]. 2016, MDPI.

copper-based MNPs are incorporated into nano-sanitizers and disinfectants designed for the effective decontamination of processing tools and surfaces, thereby reducing the risk of foodborne pathogens. Additionally, copper-doped nanomaterials are integrated into recyclable antimicrobial films, which serve as active packaging to inhibit microbial growth and prolong the shelf life of food products [87].

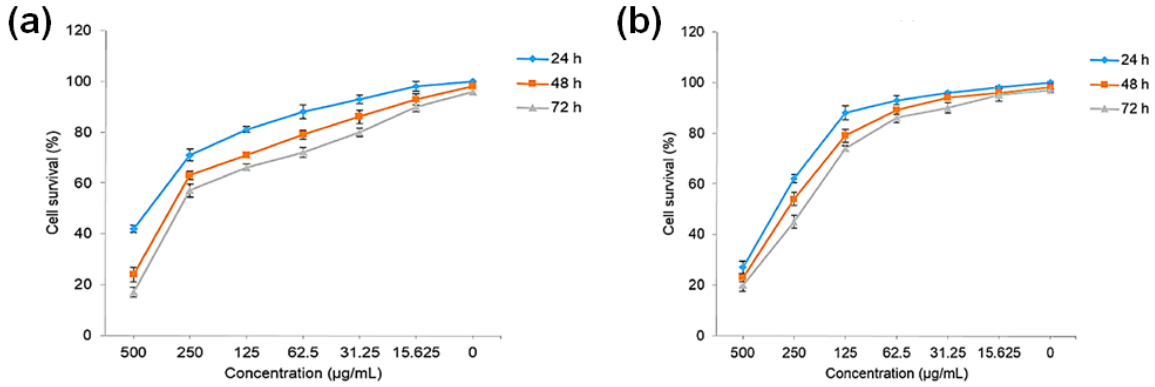

Figure 5. The cytotoxic effect of $CuFe_2O_4$ (a) and $ZnFe_2O_4$ (b) nanoparticles on MCF-7 cell-lines. Reprinted/adapted with permission from Ref. [89]. 2016, MDPI.

© 2025 The Authors. This article is licensed under a Creative Commons Attribution 4.0 International License.

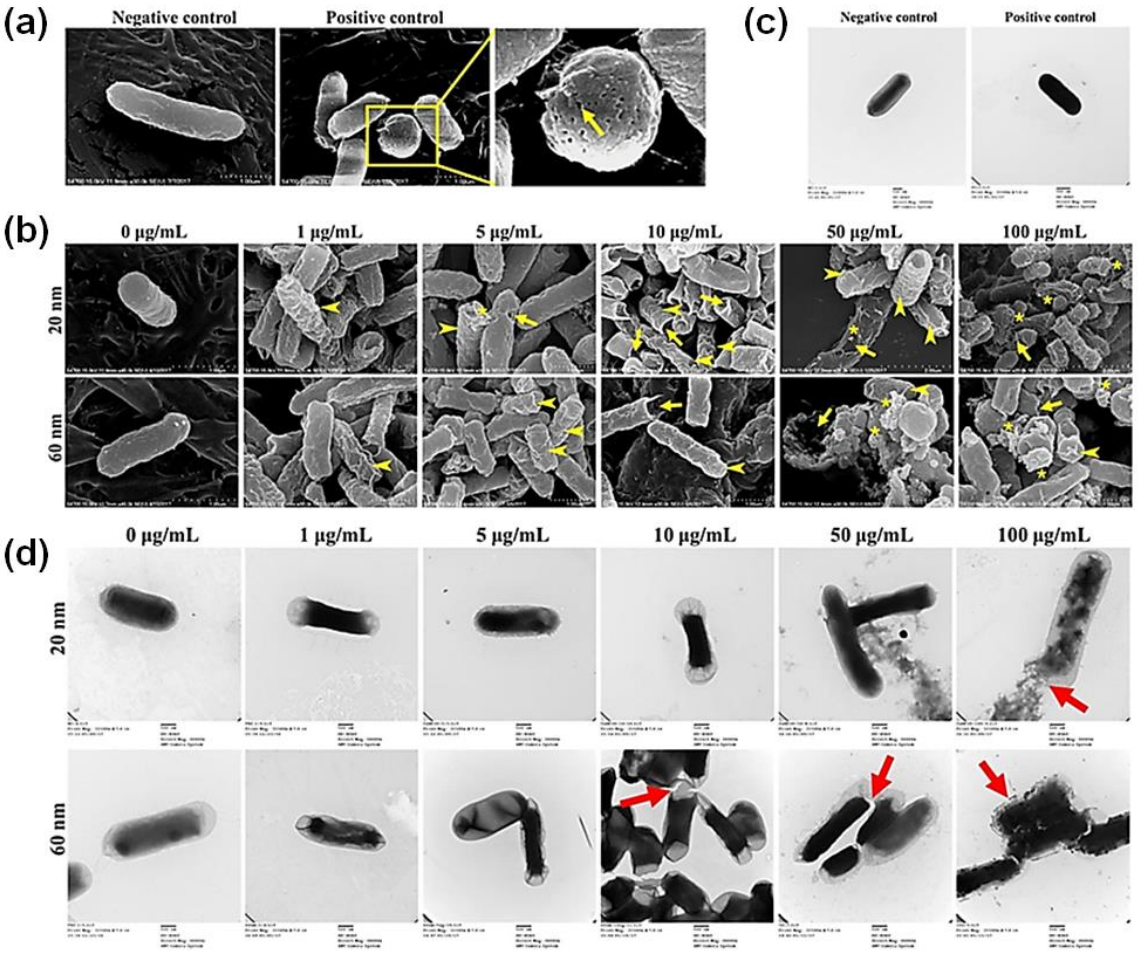

Figure 6. Electron microscopy images of *E. coli* treated with two sizes of CuNPs in different concentrations. Live or dead cells observed via SEM (a,b) and Live or dead cells observed via TEM (c,d). Reprinted/adapted with permission from Ref. [90]. 2022, MDPI.

Despite its potent antimicrobial properties, the high ROS generation associated with copper ions necessitates careful surface modification of MNPs to control potential cytotoxicity and ensure biocompatibility, especially for applications involving direct human contact [88]. These modifications can optimize the balance between efficacy and safety, broadening the practical utility of copper-doped MNPs in diverse antibacterial applications. In a study, Kanagesan et al. [89] investigated the cytotoxicity induced by copper and zinc doping in magnetite nanoparticles. The results (Figure 5) showed that the cytotoxic effect of copper ions on MCF-7 cells was greater than that of zinc ions.

Lai et al. [90] investigated the effects of copper oxide nanoparticles' size and concentration on their antibacterial properties through multiple mechanisms. The obtained results (Figure 6) demonstrated that both 20 nm and 60 nm CuNPs exhibited effective antimicrobial activity with minimal cytotoxicity toward normal human skin cells. ROS assays showed that both particle sizes increased intracellular ROS levels in *E. coli*, but only at low concentrations (1 and 5 µg/mL) did the 20 nm CuNPs generate significantly higher ROS compared to the 60 nm particles. Notably, no clear dose-dependent trend was observed in ROS production across increasing concentrations, consistent with the bactericidal analysis. Further evaluations, including DNA gel electrophoresis, annexin V-PI staining, and modulator rescue experiments, confirmed that the bactericidal effects of CuNPs were size and concentration-dependent, acting through multiple mechanisms.

© 2025 The Authors. This article is licensed under a Creative Commons Attribution 4.0 International License.

Figure 7 provides a comprehensive schematic of the main toxicity pathways associated with copper oxide-based nanoparticles, as well as the surface contact-mediated antibacterial mechanisms operating under both wet and dry conditions. In wet environments, CuO NPs can release Cu^{2+} ions and induce oxidative stress through the generation of reactive oxygen species (ROS), leading to damage to bacterial membranes, proteins, and nucleic acids. Additionally, direct interaction with the bacterial cell surface can disrupt membrane integrity, resulting in leakage of intracellular contents.

Under dry conditions, the antibacterial effect is predominantly governed by physical contact between nanoparticles and bacterial surfaces, which may cause mechanical disruption and localized oxidative stress. Together, these mechanisms highlight the multifaceted nature of CuO NP-induced antimicrobial activity, influenced by both environmental conditions and nanoparticle properties.

4.4. Cobalt (Co^{2+})

Cobalt ions (Co^{2+}), as a multifunctional dopant in magnetic nanoparticles, are widely employed as dopants in magnetic nanoparticles primarily to modulate their magnetic and catalytic properties rather than to provide direct, strong antibacterial effects. While cobalt exhibits mild to moderate antibacterial activity, its main contribution lies in enhancing the physicochemical characteristics of MNPs, including improved thermal stability, increased coercivity, and elevated surface energy. These modifications are critical for optimizing nanoparticle performance in applications such as magnetic hyperthermia and magnetically controlled drug delivery [92-94].

When combined with more potent antibacterial ions like silver or copper, cobalt contributes to the development of multifunctional nanoplatforms that simultaneously offer enhanced magnetic responsiveness and broad-spectrum antimicrobial activity [95, 96]. In biomedical contexts, cobalt-doped MNPs are particularly valued for their role in specialized imaging techniques and magnetic hyperthermia therapies, where their enhanced magnetic anisotropy improves diagnostic resolution and therapeutic efficacy [97, 98]. Furthermore, cobalt's influence on nanoparticle stability and magnetic behavior facilitates precise magnetically guided drug release, offering controlled and targeted treatment options with added antibacterial protection.

Although cobalt's use in food-related applications remains limited due to concerns about potential toxicity, it is being explored in sensor technologies aimed at detecting microbial contamination, leveraging its magnetic properties for sensitive and rapid diagnostics [99, 100]. Overall, cobalt doping enhances the functional versatility of magnetic nanoparticles, making them

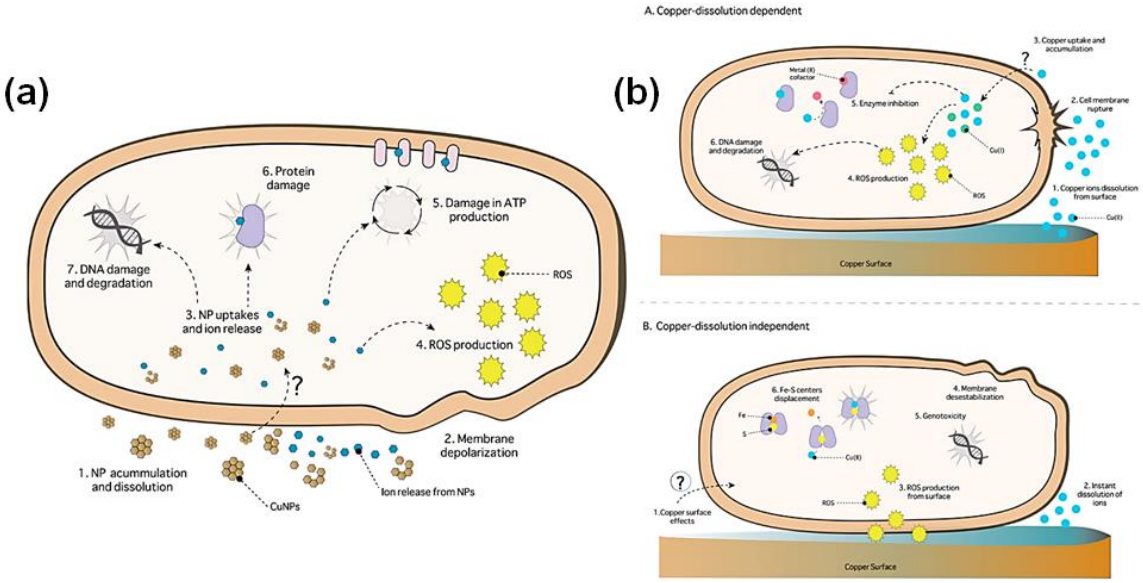

Figure 7. Schematic representation of the general toxicity mechanisms of copper oxide-based nanoparticles (a) and the surface contact-mediated antibacterial mechanisms under both wet and dry conditions (b). Reprinted/adapted with permission from Ref. [91]. 2023, MDPI.

© 2025 The Authors. This article is licensed under a Creative Commons Attribution 4.0 International License.

valuable components in advanced biomedical devices and diagnostic tools, albeit with careful consideration of biocompatibility and safety profiles.

Kajani and coworkers [101] synthesized chitosan-coated mesoporous cobalt–iron nanoparticles (CoFeCH NPs) using a facile one-step hydrothermal method. The incorporation of chitosan (CH) significantly improved the biocompatibility of the nanoparticles on human cells in vitro, while simultaneously enhancing their antibacterial activity against both *Staphylococcus aureus* and *Escherichia coli*. Notably, CoFeCH NPs exhibited antibacterial efficacy comparable to, and in some cases exceeding, that of standard antibiotics. After 18 hours of incubation with 25 µg of the nanoparticles, inhibition zone diameters of 25.8 ± 1.4 mm (CoFe NPs) and 30.1 ± 1.9 mm (CoFeCH NPs) were recorded against *S. aureus*, whereas amoxicillin produced only a 13.1 ± 1.2 mm zone under the same conditions.

For *E. coli*, CoFeCH NPs also showed a significant increase in inhibition zone size (22.7 ± 2.9 mm) compared to uncoated CoFe NPs (17.6 ± 1.3 mm) and gentamicin (27.1 ± 1.6 mm). Control experiments using chitosan alone demonstrated only mild activity against *S. aureus* and no inhibition of *E. coli*, further emphasizing the synergistic antibacterial enhancement from CH coating. In addition to their antibacterial effects, both CoFe and CoFeCH NPs were evaluated as MRI contrast agents. CoFeCH NPs exhibited a transverse relaxivity (R_2) value of 91.3 mM^{-1} s^{-1}, slightly lower than that of bare CoFe NPs (97.4 mM^{-1} s^{-1}), due to the polymer coating. These

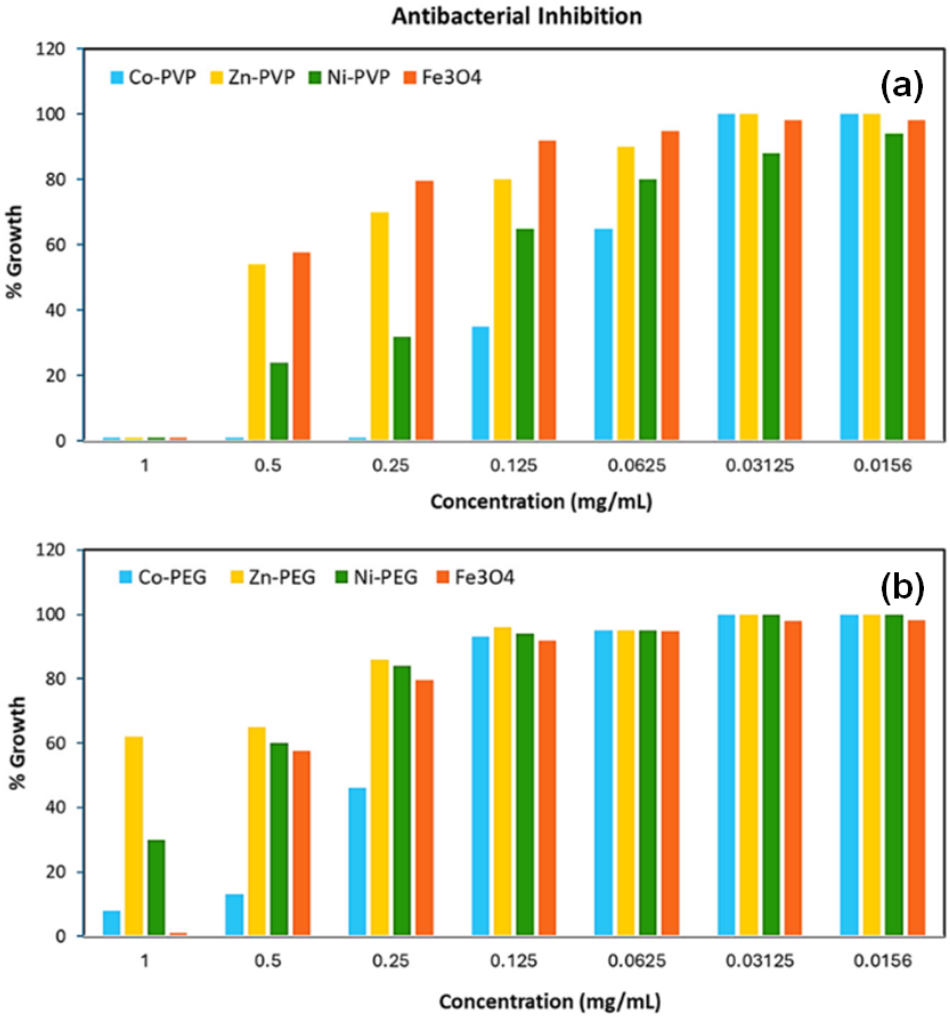

Figure 8. The evaluation of the inhibitory effects of the divalent metal-doped ferrite nanoparticles on the antibacterial properties of PVP (a) and PEG (b) ferrite nanoparticles against the Gram-negative *E. coli* bacteria. Reprinted/adapted with permission from Ref. [102]. 2025, MDPI.

© 2025 The Authors. This article is licensed under a Creative Commons Attribution 4.0 International License.

findings suggest that CoFeCH NPs offer a promising multifunctional platform, combining enhanced antibacterial performance, improved biocompatibility, and effective MRI imaging capability.

AlMatri et al. [102] investigated the antibacterial properties of polymerized divalent metal-doped ferrite nanoparticles ($PMFe_2O_4$ NPs), where the divalent metal ions (M) included Ni, Zn, and Co (Figure 8). The study focused on evaluating their inhibitory effects against the Gram-negative bacterium *Escherichia coli*. Among the tested dopants, cobalt- and nickel-substituted ferrites exhibited the most pronounced antibacterial activity, resulting in significant inactivation of bacterial cells. These findings underscore the unique antimicrobial potential of biocompatible, metal-doped ferrites and highlight their applicability as effective antibacterial agents. Potential applications include water purification, biomedical device coatings, and other antimicrobial surface treatments.

4.5. Manganese (Mn^{2+})

Manganese ions (Mn^{2+}), as a functional dopant in magnetic nanoparticles, play a significant role in redox reactions and are known to enhance the production of ROS, thereby contributing to antimicrobial activity through oxidative stress mechanisms [58]. In magnetic nanoparticles, manganese is commonly incorporated within spinel ferrite structures such as $MnFe_2O_4$, where it imparts tunable magnetic properties alongside enhanced bactericidal effects.

The antimicrobial efficacy of manganese-doped nanoparticles can be further improved through surface engineering techniques that optimize nanoparticle interactions with bacterial cells. In medical applications, manganese-doped nanoparticles are utilized as dual-modality imaging agents, combining magnetic resonance imaging (MRI) capabilities with fluorescence properties for improved diagnostic precision [103]. Additionally, Mn^{2+}-functionalized MNPs serve as components of biodegradable drug delivery systems, where their antimicrobial surfaces help prevent infection while delivering therapeutic payloads. These features make manganese-doped nanomaterials highly attractive for integrated theranostic platforms [104, 105].

Though still in experimental stages, manganese-based MNPs are also being explored within the food industry for smart packaging applications and nanosensors designed to monitor food spoilage, leveraging their magnetic responsiveness and catalytic activity for real-time quality control [80, 106]. Furthermore, manganese doping enhances the control over nanoparticle magnetization and improves the biodegradability of the nanoparticle matrix, contributing to the development of environmentally friendly antimicrobial materials.

Dou et al. [107] investigated the antibacterial properties of manganese dioxide (MnO_2) nanosheets through mechanisms mediated by ROS generation and disruption of bacterial membrane integrity. The results showed that MnO_2 nanosheets possess potent antibacterial activity against *Salmonella* (Figure 9).

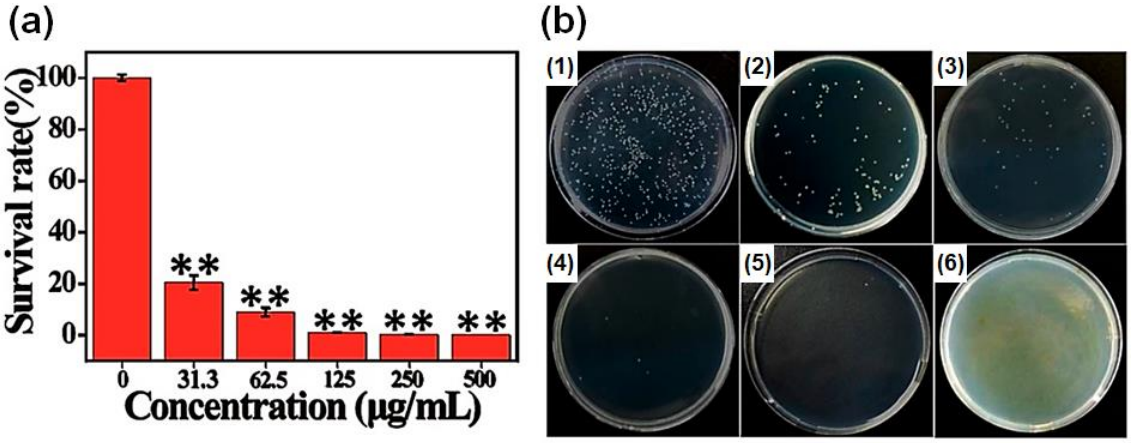

Figure 9. In vitro antibacterial activity of MnO_2 nanosheets against *Salmonella* pathogen: (a) Cell survival rates and (b) agar plates at different concentrations (0–500 μg/mL) with $p < 0.01$. Reprinted/adapted with permission from Ref. [107]. 2020, MDPI.

© 2025 The Authors. This article is licensed under a Creative Commons Attribution 4.0 International License.

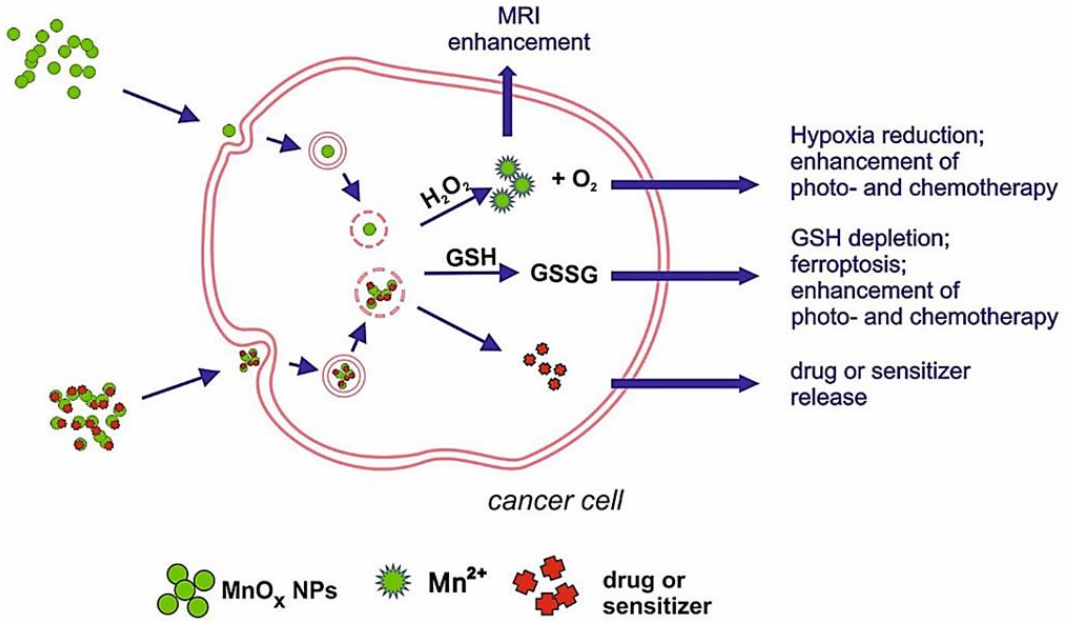

Figure 10. Schematic illustration of the main mechanisms involved in manganese oxide medical applications. Reprinted/adapted with permission from Ref. [108]. 2021, MDPI.

Growth curve analysis and colony-forming unit (CFU) assays revealed that a concentration of 125 µg/mL MnO_2 nanosheets could eliminate 99.2% of Salmonella cells.

These results were further confirmed by fluorescence-based live/dead staining. Furthermore, mechanistic studies showed that treatment with MnO_2 nanosheets significantly induced ROS production, enhanced ATPase activity, and led to leakage of intracellular electrolytes and protein content, ultimately resulting in bacterial cell death. Figure 10 schematically illustrates the key functional mechanisms of manganese oxide in medical applications. A summary of different dopants and their characteristics is presented in Table 2.

5. Applications of antibacterial magnetic nanoparticles in medical and food sectors

Magnetic nanoparticles with antibacterial properties have garnered significant attention as next-generation multifunctional nanomaterials, offering innovative solutions to persistent challenges in healthcare and food safety. Their distinctive physicochemical characteristics, including superparamagnetism, high specific surface area, customizable surface functionalities, and intrinsic or dopant-enhanced antimicrobial activity, render them highly versatile for a broad spectrum of biomedical and industrial applications.

Table 2. Dopants and their characteristics

Dopant	Antibacterial strength	Magnetic effect	Key applications	Toxicity/Biocompatibility
Ag^+	Very high	Slightly reduces magnetism	Medical coatings, packaging, wound care	Moderate (dose-dependent)
Zn^{2+}	Moderate	Slightly reduces magnetism	Bone scaffolds, food films, oral hygiene	High biocompatibility
Cu^{2+}	High	Slightly reduces magnetism	Disinfectants, orthopedic coatings, packaging	Moderate (requires surface control)
Co^{2+}	Mild to moderate	Enhances coercivity	Theranostics, drug delivery, sensors	Lower biocompatibility (caution needed)
Mn^{2+}	Moderate	Enhances magnetization	Imaging agents, smart food materials	Generally biocompatible at low doses

© 2025 The Authors. This article is licensed under a Creative Commons Attribution 4.0 International License.

In the medical domain, these nanoparticles can be engineered for targeted antimicrobial therapy, biofilm disruption, controlled drug delivery, and theranostic systems, integrating both diagnostic and therapeutic functions. Their magnetic responsiveness enables remote manipulation using external magnetic fields, allowing for site-specific accumulation and minimally invasive treatments, particularly in localized infections or implant-associated complications.

Within the food industry, MNPs offer promising strategies for pathogen detection, active food packaging, and antibacterial surface coatings, contributing to extended shelf-life, reduced spoilage, and enhanced microbial safety [9, 109]. Additionally, their potential for magnetic separation and recycling makes them attractive candidates for sustainable and scalable antimicrobial interventions [110].

The following sections present a comprehensive overview of the principal applications of antibacterial MNPs across medical and food-related sectors, with an emphasis on their mechanistic roles, formulation strategies, and translational potential in real-world environments. Figure 11 highlights the potential and functional capabilities of magnetic/antibacterial nanoparticles for applications in the medical field.

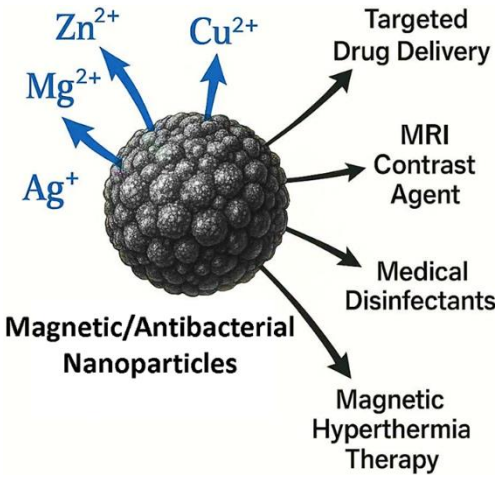

Figure 11. The potential and functional capabilities of magnetic/antibacterial nanoparticles for medical applications.

5.1. Medical applications

5.1.1. Targeted drug delivery: Antibacterial/magnetic nanoparticles have emerged as a promising platform for targeted antimicrobial drug delivery, offering precise spatial control over therapeutic agent localization through the application of external magnetic fields. This capability allows for the concentration of drug-loaded MNPs at specific infection sites, significantly enhancing therapeutic efficacy while reducing systemic drug exposure and associated toxicity, especially important in treating infections near vital or sensitive tissues.

The magnetic core, typically composed of biocompatible iron oxide nanoparticles (such as Fe_3O_4 or γ-Fe_2O_3), enables magnetic field-guided navigation and retention at the target site. Beyond their magnetic responsiveness, these nanoparticles can be surface-functionalized with a variety of antimicrobial agents, including broad-spectrum antibiotics, antimicrobial peptides (AMPs), or plant-derived bioactives, offering a flexible delivery vehicle adaptable to diverse clinical contexts [111, 112].

Surface modification plays a critical role in optimizing their biological performance. Coatings such as polyethylene glycol (PEG), chitosan, polylactic-co-glycolic acid (PLGA), or dextran serve multiple functions such as improving colloidal stability, preventing rapid clearance by the mononuclear phagocyte system (MPS), enhancing biocompatibility, and providing functional groups for further conjugation with targeting ligands or stimuli-responsive linkers [113, 114]. In addition, MNP-based systems can be engineered for controlled or stimuli-responsive drug release, enabling site-specific activation in response to local environmental cues such as acidic pH, bacterial enzymes, or oxidative stress, which are often present at infection or inflammation sites.

This precise delivery not only ensures high local drug concentration, improving bacterial eradication, but also helps in limiting the development of antimicrobial resistance, a growing concern in conventional systemic antibiotic therapies. Furthermore, the magnetic properties of the core can be exploited for real-time imaging via magnetic resonance imaging (MRI), facilitating simultaneous diagnosis and therapy (theranostics). This dual functionality is especially useful for monitoring treatment response in deep tissue infections or chronic biofilm-related diseases.

In summary, magnetic nanoparticle-based targeted drug delivery systems represent a cutting-edge approach in modern antimicrobial therapy, combining precision targeting, controlled release, reduced systemic toxicity, and enhanced therapeutic outcomes, making

© 2025 The Authors. This article is licensed under a Creative Commons Attribution 4.0 International License.

them candidates for translation into clinical applications in infectious disease management [26, 115, 116].

5.1.2. Magnetic hyperthermia for infection control: Magnetic hyperthermia therapy (MHT) represents an innovative, non-invasive strategy for infection control, particularly suited to addressing chronic infections, biofilm-associated microbial colonization, and antibiotic-resistant bacterial strains. In this approach, MNPs are delivered to the site of infection, either through systemic administration or localized injection, and then exposed to an alternating magnetic field (AMF).

Upon stimulation, the MNPs convert magnetic energy into localized thermal energy, typically raising the temperature of the surrounding microenvironment to 42–50 °C. This localized hyperthermia exerts a dual therapeutic effect. Firstly, the elevated temperature induces thermal stress in bacterial cells, leading to membrane destabilization, protein denaturation, and ultimately cell death, without causing damage to adjacent healthy tissues when precisely controlled.

Secondly, the generated heat has been shown to disrupt extracellular polymeric substances (EPS) in bacterial biofilms, facilitating biofilm dispersion and improving the penetration of antimicrobial agents into previously protected microbial communities.

The efficacy of magnetic hyperthermia is significantly enhanced when used in combination with antibiotics, as hyperthermic conditions increase membrane permeability, reduce efflux pump activity, and promote passive diffusion of drugs into bacterial cells. This synergistic effect allows for lower antibiotic doses, which can reduce toxicity and the risk of resistance development [117, 118]. Moreover, hyperthermia has been observed to sensitize multidrug-resistant (MDR) pathogens, including methicillin-resistant *Staphylococcus aureus* (MRSA), by impairing their stress-response pathways and virulence mechanisms.

Another advantage of this method lies in its spatial precision [117]. By using externally controlled magnetic fields, clinicians can achieve site-specific heating, allowing treatment of localized infections, such as orthopedic implants, catheters, and chronic wounds, while minimizing collateral damage to surrounding healthy cells and tissues. Furthermore, the integration of theranostic capabilities, via MRI-visible magnetic cores, allows for simultaneous imaging, tracking, and treatment of infected areas [119, 120].

Advanced designs also incorporate temperature-sensitive polymers or drug-loaded coatings, enabling thermo-responsive drug release synchronized with the hyperthermic stimulus, thus providing dual-mode antimicrobial activity [121]. In conclusion, magnetic hyperthermia represents a powerful adjunct or alternative to traditional antimicrobial strategies. Its ability to bypass conventional resistance mechanisms, penetrate biofilms, and synergize with antimicrobial agents positions it as a highly promising modality for managing persistent or device-related infections in clinical settings.

5.1.3. Wound healing and antibacterial coatings: Magnetic/antibacterial nanoparticles have demonstrated considerable potential in the field of wound management, particularly when incorporated into advanced wound dressings, hydrogels, or nanocomposite scaffolds. Their dual functionality, combining antibacterial activity with magnetic responsiveness, positions them as powerful tools for enhancing wound healing outcomes, especially in cases complicated by microbial contamination or chronic infection.

In wound care applications, MNPs are typically embedded within biocompatible matrices such as alginate, gelatin, chitosan, or polyethylene glycol-based hydrogels. These materials serve as controlled-release platforms, allowing for sustained and localized antimicrobial action at the wound site [122].

The antibacterial properties of MNPs help prevent the colonization and proliferation of pathogenic microorganisms, thereby reducing the risk of infection, a major impediment to effective tissue regeneration. Additionally, the magnetic properties of these nanoparticles open avenues for external control or real-time monitoring. For instance, the application of an external magnetic field can be used to manipulate the distribution of MNPs, enhance their retention in the wound area, or trigger the release of co-loaded therapeutic agents such as antibiotics or growth factors. This magnetically assisted therapy modulation adds a layer of precision to traditional wound treatments [43, 123].

Doping MNPs with antimicrobial metal ions such as silver (Ag^+) or zinc (Zn^{2+}) has been shown to significantly enhance their antibacterial efficacy. Silver-

© 2025 The Authors. This article is licensed under a Creative Commons Attribution 4.0 International License.

doped MNPs exert strong bactericidal effects by inducing oxidative stress, disrupting cell membranes, and interfering with DNA replication [124]. Similarly, zinc-doped MNPs contribute both antimicrobial activity and tissue repair modulation, as zinc plays a critical role in enzyme function, cellular proliferation, and immune regulation during wound healing [125].

Preclinical studies have demonstrated that wound dressings incorporating Ag or Zn-doped MNPs can accelerate wound closure, promote angiogenesis, reduce microbial burden, and minimize inflammatory responses [126]. Furthermore, their nanoscale dimensions facilitate intimate interaction with cellular structures, enhancing cellular uptake and integration within the wound bed. In summary, MNP-based wound healing systems offer a multifunctional platform for infection control and tissue regeneration. Their tunable surface chemistry, biocompatibility, and ability to synergize with magnetic guidance and bioactive dopants make them promising candidates for next-generation wound care technologies, particularly in the management of chronic wounds, burns, and diabetic ulcers.

5.1.4. Imaging and theranostics: Iron oxide magnetic nanoparticles, owing to their superparamagnetic properties, have been extensively utilized as contrast agents in magnetic resonance imaging (MRI). Their superparamagnetism significantly enhances MRI sensitivity and spatial resolution, enabling more accurate visualization of biological tissues and pathological abnormalities [127]. When combined with antimicrobial agents, these nanoparticles offer a multifunctional platform that integrates both diagnostic and therapeutic capabilities, a strategy commonly referred to as theranostics.

Theranostic systems based on iron oxide MNPs facilitate simultaneous infection detection and treatment, which is particularly advantageous for managing infections in challenging sites such as deep tissues or implanted medical devices, where conventional diagnostic and therapeutic methods often fail [128]. In these systems, iron oxide MNPs serve as drug carriers that enable targeted delivery of antimicrobial compounds directly to the infection site, thereby improving therapeutic efficacy and minimizing systemic side effects. Moreover, the magnetic properties of these nanoparticles allow for external magnetic guidance and localization, further enhancing the concentration of therapeutic agents at the target site.

Concurrently, the intrinsic MRI contrast ability of iron oxide MNPs enables real-time monitoring of the treatment progress, offering valuable feedback for personalized medical interventions. Consequently, iron oxide-based theranostic platforms represent a promising and innovative approach to overcoming the limitations of traditional infection management strategies and have become a significant focus of ongoing research in nanomedicine and drug delivery technologies. The following table summarizes recent developments in the use of antibacterial metal dopants in magnetic nanoparticles across medical applications, highlighting the materials used, mechanisms of action, and key research findings. Table 3 summarizes recent developments in antibacterial metal-doped magnetic nanoparticles in medical applications.

5.2. Food industry applications

Nowadays, due to the high volume of food production and consumption, as well as the diversity of products and the need to implement measures related to storage, increasing shelf life, quality control, and preventing spoilage, the feasibility and use of magnetic/antibacterial nanoparticles is increasing [139]. Figure 12 represented the potential and functional capabilities of magnetic/antibacterial nanoparticles for applications in the food industry.

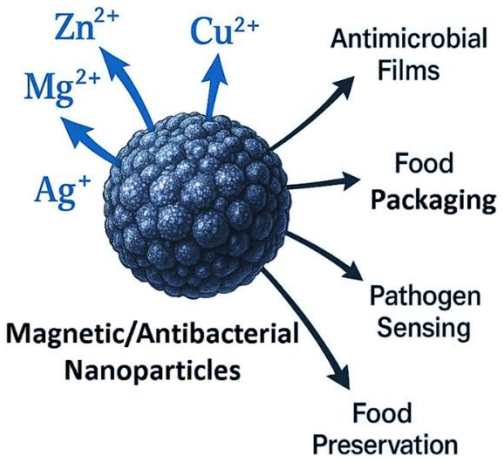

Figure 12. The potential and functional capabilities of magnetic/antibacterial nanoparticles in food industry.

© 2025 The Authors. This article is licensed under a Creative Commons Attribution 4.0 International License.

Table 3. Recent developments in antibacterial metal-doped magnetic nanoparticles in medicine

Dopant/Coating	Magnetic NP system	Antibacterial application	Mechanism & key findings	Reference
Ag (Silver)	Superparamagnetic iron oxide-AgO core-shell; $AgFe_2O_4$	Wound dressings, infection therapy, biofilm prevention	Released Ag^+ + ROS; magnetic hyperthermia synergy; effective vs antibiotic-resistant strains	[129, 130]
Zn (Zinc)	ZnO-coated Fe_3O_4 nanocomposite; $ZnFe_2O_4$	Drug delivery + antimicrobial + anticancer	ZnO-SPION improved antibacterial, ROS generation, and membrane disruption	[131, 132]
Co (Cobalt)	$CoFe_2O_4$, Co@ferrite nanocrystals	Implant coatings, antibacterial surfaces	Co-doped ferrite showed zones of inhibition against E. coli, S. aureus, and ROS-mediated	[133]
Cu (Copper)	$CuO@Fe_3O_4$; $CuFe_2O_4$	Surface sterilization, antibacterial materials	Strong inhibition vs Gram (–/+) (e.g., *B. cereus*); Cu ions + ferrite matrix effect	[134-136]
Mg (Magnesium)	$MgFe_2O_4$; $MgO-Fe_3O_4$ nanocomposite	Broad-spectrum antibacterial coatings	$MgFe_2O_4$ showed enhanced activity vs. pure ferrite	[137, 138]

5.2.1. Antimicrobial food packaging: Incorporating antibacterial/magnetic nanoparticles into biodegradable films or coatings has emerged as a promising strategy to enhance the shelf life and safety of food products by inhibiting microbial growth. These nanocomposite materials function as active packaging systems, capable of releasing antimicrobial agents in a controlled manner in response to specific environmental stimuli such as changes in moisture levels or temperature. This responsive release mechanism helps to maintain an antimicrobial environment within the packaging, effectively reducing the risk of spoilage and contamination [139, 140].

Among the various types of MNPs, those doped with silver and zinc have gained particular attention due to their broad-spectrum antimicrobial properties against a wide range of bacteria, fungi, and other pathogens. The incorporation of silver and zinc ions enhances the antimicrobial efficacy of the nanocomposites through mechanisms such as disruption of microbial cell membranes, generation of reactive oxygen species, and interference with cellular metabolism. Furthermore, the use of biodegradable polymer matrices as carriers for MNPs aligns with the increasing demand for sustainable packaging solutions, addressing environmental concerns related to plastic waste.

The integration of MNPs within these eco-friendly materials not only improves food preservation but also contributes to reducing the ecological footprint of packaging materials [141, 142]. Overall, the development of antimicrobial food packaging incorporating MNPs represents an innovative and effective approach to ensuring food quality and safety, with significant potential for application in the food industry.

5.2.2. Food preservation and storage: Antibacterial/magnetic nanoparticles have shown significant potential as preservatives when dispersed directly into liquid or semi-solid food matrices at safe and controlled concentrations. These nanoparticles exhibit effective antimicrobial activity against common spoilage and pathogenic microorganisms, including *Escherichia coli*, *Listeria monocytogenes*, and *Salmonella* species, which are major contributors to foodborne illnesses and spoilage [143].

By inhibiting the growth and proliferation of these microorganisms, MNPs help to extend the shelf life of food products and maintain their sensory and nutritional quality during storage. An important advantage of using MNPs in food preservation lies in their intrinsic magnetic properties, which enable facile separation and removal of the nanoparticles from the food matrix after the preservation process, if necessary [139]. This magnetic recoverability not only facilitates recycling and reuse of the nanoparticles but also ensures that residual nanoparticle concentrations in the final

© 2025 The Authors. This article is licensed under a Creative Commons Attribution 4.0 International License.

food product remain within safe limits, thereby preserving food safety and regulatory compliance. Furthermore, the ability to control the dispersion and dosage of MNPs within different food systems allows for customizable preservation strategies tailored to specific food types and storage conditions [144].

This approach offers a promising alternative to traditional chemical preservatives, which often face consumer resistance due to concerns about toxicity and synthetic additives. Overall, the application of antibacterial/magnetic nanoparticles in food preservation and storage represents an innovative and versatile technology with the potential to improve food safety, reduce spoilage, and meet growing consumer demand for safer and more sustainable food preservation methods.

5.2.3. Biosensing and contaminant detection: Functionalized magnetic nanoparticles have emerged as highly effective tools for the selective detection of bacterial cells and toxins in food products. By doping the antibacterial ions or attaching specific recognition molecules, such as antibodies or peptides, to the surface of MNPs, these nanomaterials can selectively bind to target microbial contaminants with high affinity and specificity. This functionalization enables the precise identification and isolation of pathogens or harmful substances from complex food matrices.

The magnetic properties of these nanoparticles facilitate rapid and efficient separation of bound contaminants from the sample through magnetic separation techniques, significantly reducing detection time compared to conventional methods [145, 146]. Additionally, MNPs can be integrated with optical or electrochemical sensors, thereby enhancing sensitivity and enabling real-time monitoring of microbial contamination. Such biosensing platforms enable early detection of foodborne pathogens, improving food safety by allowing timely interventions within the supply chain [147]. This capability to rapidly and accurately identify contaminants at low concentrations contributes to minimizing the risk of foodborne illnesses, reducing economic losses due to spoilage, and ensuring compliance with regulatory standards.

Consequently, MNP-based biosensing technologies represent a promising advancement in food safety monitoring, combining the advantages of nanotechnology with efficient diagnostic approaches.

5.2.4. Water disinfection: Antibacterial/magnetic nanoparticles have been increasingly utilized in water treatment applications due to their ability to effectively remove or inactivate bacterial pathogens. Their high surface reactivity enables strong antimicrobial effects through mechanisms such as the disruption of microbial cell walls, the generation of reactive oxygen species, and the catalytic degradation of contaminants. This makes MNPs particularly suitable for the disinfection of water used in food processing environments, ensuring microbiological safety. Moreover, the magnetic properties of MNPs allow for their facile recovery and reuse through magnetic separation techniques, which enhances the sustainability and cost-effectiveness of disinfection processes.

This recoverability reduces the environmental impact typically associated with chemical disinfectants and supports the development of eco-friendly sanitation protocols [148, 149]. By integrating MNP-based disinfection strategies, food production facilities can achieve higher standards of hygiene and safety, contributing to improved product quality and consumer health. Overall, the use of antibacterial/magnetic nanoparticles in water and surface disinfection represents a promising approach that combines high antimicrobial efficacy with environmental sustainability, addressing critical challenges in food safety management.

Table 4 provides an overview of recent progress in utilizing antibacterial metal dopants in magnetic nanoparticles for food packaging, emphasizing the employed materials, antibacterial mechanisms, and significant experimental findings.

6. Conclusions, challenges, and prospects

The unique multifunctional properties of antibacterial/magnetic nanoparticles have enabled their versatile application across diverse fields, particularly in the medical and food industries. Their ability to serve simultaneously as diagnostic and therapeutic agents has advanced precision medicine and non-invasive imaging techniques, improving the detection and treatment of infections.

In parallel, the integration of MNPs into food systems has introduced innovative solutions such as antimicrobial

© 2025 The Authors. This article is licensed under a Creative Commons Attribution 4.0 International License.

Table 4. Metal-doped magnetic nanostructures in antimicrobial food packaging

Dopant/Coating	Magnetic NP system	Food packaging application	Mechanism & key findings	Reference
Ag (Silver)	$AgO@Fe_3O_4$ core–shell; $AgFe_2O_4$	Coating on paper packaging, PE film, NR/PE blends	Sustained Ag^+ release + ROS; improved mechanical/barrier properties; MIC ~3–5 µg/mL; extended shelf life of fruits and sausages; inhibited *E. coli*, *S. aureus*, *Salmonella*	[150]
Zn (Zinc)	ZnO embedded/magnetic composite; $ZnFe_2O_4$	Bio-starch/chitosan/ZnO films & coatings on PLA, gelatin, cellulose	Zn^{2+} release + ROS under light; good barrier, UV resistance; extended shelf life of poultry/meat; full inactivation of *E. coli*, *S. enterica*, *S. aureus*	[151]
Cu (Copper)	Cu-doped -magnetic nanoparticles ($CuFe_2O_4$)	Antibacterial films/paper/cardboard	Cu^+ ions + ROS; strong inhibition but toxic concerns; used by coating or pulp mixing	[152]
Co (Cobalt)	$CoFe_2O_4$NPs	Rarely in food-related applications; composite film with $CoFe_2O_4$/MXene/chitosan	Similar antibacterial properties to Cu and Zn, but toxicity concerns; further investigation needed	[153]

packaging, enhanced preservation, rapid contaminant detection, and effective disinfection methods, all of which contribute to improving food safety and extending shelf life.

Despite these promising developments, the successful translation of MNP-based technologies from research settings to practical, real-world use depends heavily on continued investigation into their biocompatibility, long-term biosafety, and functional optimization. Furthermore, addressing regulatory challenges and ensuring compliance with safety standards are essential to gain public trust and facilitate widespread adoption.

Overall, antibacterial/ magnetic nanoparticles offer a powerful and flexible platform with significant potential to enhance both human health and food security, paving the way for next-generation applications in nanomedicine and food technology.

Challenges and future perspectives of antibacterial/ magnetic nanoparticles in biomedical and food applications: Antibacterial magnetic nanoparticles hold considerable promise across biomedical and food sectors due to their unique physical properties and versatile antibacterial mechanisms. However, addressing the existence challenges, particularly those related to biosafety, regulatory compliance, and functional stability, will be crucial for their successful integration into real-world applications. Future efforts should prioritize the development of environmentally friendly, biocompatible, and multifunctional antibacterial/magnetic composites and nanocomposites with tailored performance to meet the specific demands of clinical and industrial settings.

Key challenges:

Biocompatibility and cytotoxicity: The release of metal ions (e.g., Ag^+, Cu^{2+}, Co^{2+}) from doped magnetic nanoparticles can lead to unintended cytotoxic effects, inflammation, or tissue damage. Long-term safety data and a comprehensive understanding of nanoparticle–cell interactions are still lacking.

Controlled ion and drug release: Achieving site-specific, controlled, and sustained release of therapeutic agents or metal ions remains a technical barrier, particularly in dynamic physiological or food-related environments.

Stability in biological and food matrices: Magnetic nanoparticles may undergo aggregation, surface modification, or loss of function when exposed to complex biological fluids or food components, compromising their antibacterial efficacy.

Regulatory and safety barriers: The lack of well-defined regulatory frameworks and standardized safety evaluations limits the approval and commercialization of antibacterial/magnetic nanocomposites-based products, especially in the food and healthcare sectors.

Future perspectives:

Design of multifunctional smart nanoparticles: Future research should focus on the development of AMNPs capable of integrating diagnostic, therapeutic, and

© 2025 The Authors. This article is licensed under a Creative Commons Attribution 4.0 International License.

targeting functions within a single platform, enabling more effective and personalized treatment strategies.

Stimuli-responsive systems: Stimuli-sensitive nanoparticles that respond to pH, temperature, magnetic fields, or enzymatic activity could offer controlled activation of antibacterial mechanisms only in infected tissues, minimizing off-target effects.

Surface engineering for enhanced selectivity: Advanced surface functionalization with biocompatible polymers, ligands, or targeting moieties can improve cellular uptake, reduce toxicity, and enhance specificity toward bacterial cells over host tissues.

Conflict of Interest

The authors declare no conflict of interest.

References

1. M.A. Salam, et al. Antimicrobial Resistance: A Growing Serious Threat for Global Public Health. *Healthcare*, **2023**, *11*, 1946.

2. V.B. Kilari and T. Oroszi. The Misuse of Antibiotics and the Rise of Bacterial Resistance: A Global Concern. *Pharmacology & Pharmacy*, **2024**, *15*, 508.

3. T. Li, et al. Bacterial resistance to antibacterial agents: Mechanisms, control strategies, and implications for global health. *Science of The Total Environment*, **2023**, *860*, 160461.

4. S.K. Ahmed, et al. Antimicrobial resistance: Impacts, challenges, and future prospects. *Journal of Medicine, Surgery, and Public Health*, **2024**, *2*, 100081.

5. B. Rezaei, et al. Magnetic Nanoparticles: A Review on Synthesis, Characterization, Functionalization, and Biomedical Applications. *Small*, **2023**, *20*, 2304848.

6. C. Comanescu. Recent Advances in Surface Functionalization of Magnetic Nanoparticles. *Coatings*, **2023**, *13*, 1772.

7. H. Hemeg. Nanomaterials for alternative antibacterial therapy. *International Journal of Nanomedicine*, **2017**, *Volume 12*, 8211.

8. L.d.A.S. de Toledo, H.C. Rosseto, and M.L. Bruschi. Iron oxide magnetic nanoparticles as antimicrobials for therapeutics. *Pharmaceutical Development and Technology*, **2017**, *23*, 316.

9. G.R. Rodrigues, et al. Antimicrobial magnetic nanoparticles based-therapies for controlling infectious diseases. *International Journal of Pharmaceutics*, **2019**, *555*, 356.

10. M. Alavi and M. Rai. Recent advances in antibacterial applications of metal nanoparticles (MNPs) and metal nanocomposites (MNCs) against multidrug-resistant (MDR) bacteria. *Expert Review of Anti-infective Therapy*, **2019**, *17*, 419.

11. A. Allafchian and S.S. Hosseini. Antibacterial magnetic nanoparticles for therapeutics: a review. *IET Nanobiotechnology*, **2019**, *13*, 786.

12. M. Alavi and R. Yarani. ROS and RNS modulation: the main antimicrobial, anticancer, antidiabetic, and antineurodegenerative mechanisms of metal or metal oxide nanoparticles. *Nano Micro Biosystems*, **2022**, *2*, 22.

13. P. Kalakonda, et al. Comparison of Multi-metallic Nanoparticles-Alternative Antibacterial Agent: Understanding the Role of Their Antibacterial Properties. *Journal of Inorganic and Organometallic Polymers and Materials*, **2024**, *34*, 2203.

14. M.I. Anik, et al. Recent progress of magnetic nanoparticles in biomedical applications: A review. *Nano Select*, **2021**, *2*, 1146.

15. K. Zhou, et al. Application of magnetic nanoparticles in petroleum industry: A review. *Journal of Petroleum Science and Engineering*, **2020**, *188*, 106943.

16. M. Bilal, et al. Magnetic nanoparticles as versatile carriers for enzymes immobilization: A review. *International Journal of Biological Macromolecules*, **2018**, *120*, 2530.

17. R. Bushra, et al. Recent advances in magnetic nanoparticles: Key applications, environmental insights, and future strategies. *Sustainable Materials and Technologies*, **2024**, *40*, e00985.

18. Y.A. Fahim, I.W. Hasani, and W. Mahmoud Ragab. Promising biomedical applications using superparamagnetic nanoparticles. *European Journal of Medical Research*, **2025**, *30*, 1.

19. T. Tegafaw, et al. Magnetic Nanoparticle-Based High-Performance Positive and Negative Magnetic Resonance Imaging Contrast Agents. *Pharmaceutics*, **2023**, *15*, 1745.

20. R.V. Stigliano, et al. Alternating magnetic field guiding system for MNP hyperthermia treatment of deep-seated cancers. *International Journal of Hyperthermia*, **2024**, *41*, 2391008.

21. S.K. Chinnaiyan, S. Arthanari, and M. Subramanian, *Nanoparticles in Tissue Engineering Application and Regenerative Medicine*, in *Introduction to Functional Nanomaterials*. **2024**, CRC Press. p. 93.

22. M. Wang, et al. Optimization of Metal-Based Nanoparticle Composite Formulations and Their Application in Wound Dressings. *International Journal of Nanomedicine*, **2025**, *Volume 20*, 2813.

23. N.B. Nandi, et al., *Nanobiotechnology for Sustainable Food Preservations and Shelf-Life Enhancement*, in *Nano-microbiology for Sustainable Development*. **2025**, Springer Nature Switzerland. p. 139.

© 2025 The Authors. This article is licensed under a Creative Commons Attribution 4.0 International License.

24. S. Sahota, et al. Biobased plastics and their nanocomposites: emerging trends in active and intelligent food packaging applications. *Journal of Food Science and Technology*, **2025**, *62*, 1618.

25. H. Hosseinzadeh, H. Oveisi, and A. Meshkini. Functionalized ZnFe2O4@Mesoporous silica nano-support for lipase enzyme immobilization: Enhanced biocatalysis and antibacterial activity for food industry applications. *Food Bioscience*, **2024**, *61*, 104985.

26. E.V. Araújo, et al. Advances in surface design and biomedical applications of magnetic nanoparticles. *Advances in Colloid and Interface Science*, **2024**, *328*, 103166.

27. G.F. Stiufiuc and R.I. Stiufiuc. Magnetic Nanoparticles: Synthesis, Characterization, and Their Use in Biomedical Field. *Applied Sciences*, **2024**, *14*, 1623.

28. P. Kumar, R. Singh, and P. Kush, *Biocompatibility, Toxicity Concerns, Environmental and Safety Considerations, and Legal Aspects of Functionalized Magnetic Nanoparticles*, in *Functionalized Magnetic Nanoparticles for Theranostic Applications*. **2024**, Wiley. p. 533.

29. H. Duman, et al. Silver Nanoparticles: A Comprehensive Review of Synthesis Methods and Chemical and Physical Properties. *Nanomaterials*, **2024**, *14*, 1527.

30. M. Fatemi and Z. Bahrami, *Synthesis of Different Types, Shapes, and Sizes of Nanocarriers Using Synthetic and Biological Approaches*, in *Nano Drug Delivery for Cancer Therapy*. **2023**, Springer Nature Singapore. p. 25.

31. S. Jagdale, et al. Biologically synthesized metallic nanocarriers for efficient therapy of breast cancer. *Expert Review of Anticancer Therapy*, **2025**, *25*, 865.

32. F. Zanbili and A. Poursattar Marjani. Innovative green and bio-based approaches for photosensitive nanoparticle synthesis: a review on methodologies, characterization, and applications. *Micro and Nano Systems Letters*, **2025**, *13*, 3.

33. P. Dahiya, A. Bhatia, and A. Chandra, *Safety and Regulatory Considerations: Navigating the Use of Multifunctional Magnetic Nanoparticles*, in *Multifunctional Magnetic Nanoparticles in Analytical and Environmental Chemistry*. **2025**, Royal Society of Chemistry. p. 346.

34. A. Shah, et al. Synthesis of Iron Oxide Nanoparticles and its Antimicrobial, Anticancer, Anti-inflammatory, Wound Healing, and Immunomodulatory Activities -A Review. *Phytopharmacology Research Journal*, **2025**, *3*, 1.

35. S. Kang, *Electrochemical Microfluidics in Biosensing Applications [PhD thesis]*. **2024**, University of Oxford.

36. E.S. Austria, R.B. Lamorena, and S.D. Arco. Synthesis and functionalization of magnetic nanoparticles for glycoprotein and glycopeptide enrichment: A review. *Microchemical Journal*, **2024**, *201*, 110663.

37. Y. Yu, et al. Microfluidic Synthesis of Magnetic Nanoparticles for Biomedical Applications. *Small Methods*, **2024**, *9*, 2401220.

38. J. Usman, et al., *Hydrothermal and solvothermal methods*, in *Advanced Ceramics for Photocatalytic Membranes*. **2024**, Elsevier. p. 179.

39. H. Hosseinzadeh and H. Oveisi, *Synthesis Factors Dependence of Magnetic Properties of CoFe2O4 and CoFe2-xGdxO4 Semicrystalline Nanoparticles with desired Morphology through Hydrothermal Procedure*. **2022**, Springer Science and Business Media LLC.

40. C. Verma, et al. Green magnetic nanoparticles: a comprehensive review of recent progress in biomedical and environmental applications. *Journal of Materials Science*, **2023**, *59*, 325.

41. R. Soomro, et al. A novel plant-based approach for synthesis of iron oxide nanoparticles and cancer therapy. *Discover Chemistry*, **2025**, *2*, 25.

42. L. Xia, et al. Transforming bone cancer treatment: a comprehensive review of green-synthesized metal nanoparticles. *Cancer Cell International*, **2025**, *25*, 193.

43. A.M. El-Khawaga, et al. Magnetic nanoparticles as a promising antimicrobial agent for combating multidrug resistant bacteria: a review. *Discover Applied Sciences*, **2025**, *7*, 652.

44. J. Li, et al. A new tool to attack biofilms: driving magnetic iron-oxide nanoparticles to disrupt the matrix. *Nanoscale*, **2019**, *11*, 6905.

45. O. Gorobets, et al. Interaction of magnetic fields with biogenic magnetic nanoparticles on cell membranes: Physiological consequences for organisms in health and disease. *Bioelectrochemistry*, **2023**, *151*, 108390.

46. J. Ye, et al. Novel copper-containing ferrite nanoparticles exert lethality to MRSA by disrupting MRSA cell membrane permeability, depleting intracellular iron ions, and upregulating ROS levels. *Frontiers in Microbiology*, **2023**, *14*, 1023036.

47. T. Mai and J.Z. Hilt. Magnetic nanoparticles: reactive oxygen species generation and potential therapeutic applications. *Journal of Nanoparticle Research*, **2017**, *19*, 253.

48. R. Canaparo, et al. Biomedical Applications of Reactive Oxygen Species Generation by Metal Nanoparticles. *Materials*, **2020**, *14*, 53.

49. S. Sabella, et al. A general mechanism for intracellular toxicity of metal-containing nanoparticles. *Nanoscale*, **2014**, *6*, 7052.

50. H. Ma, et al. The Metal Ion Release of Manganese Ferrite Nanoparticles: Kinetics, Effects on Magnetic Resonance Relaxivities, and Toxicity. *ACS Applied Bio Materials*, **2022**, *5*, 3067.

© 2025 The Authors. This article is licensed under a Creative Commons Attribution 4.0 International License.

51. B. Wang, et al. Toxicity of ZnO Nanoparticles to Macrophages Due to Cell Uptake and Intracellular Release of Zinc Ions. *Journal of Nanoscience and Nanotechnology*, **2014**, *14*, 5688.

52. K. Quan, et al. Influence of interaction between surface-modified magnetic nanoparticles with infectious biofilm components in artificial channel digging and biofilm eradication by antibiotics in vitro and in vivo. *Nanoscale*, **2021**, *13*, 4644.

53. N. Eghbalifam, S.A. Shojaosadati, and S. Hashemi-Najafabadi. Role of bioactive magnetic nanoparticles in the prevention of wound pathogenic biofilm formation using smart nanocomposites. *Journal of Nanobiotechnology*, **2023**, *21*, 161.

54. C. Petters, et al. Uptake and Metabolism of Iron Oxide Nanoparticles in Brain Cells. *Neurochemical Research*, **2014**, *39*, 1648.

55. R. Das, et al. Boosted Hyperthermia Therapy by Combined AC Magnetic and Photothermal Exposures in Ag/Fe₃O₄ Nanoflowers. *ACS Applied Materials & Interfaces*, **2016**, *8*, 25162.

56. H. Gavilán, et al. Magnetic nanoparticles and clusters for magnetic hyperthermia: optimizing their heat performance and developing combinatorial therapies to tackle cancer. *Chemical Society Reviews*, **2021**, *50*, 11614.

57. A. Van de Walle, et al. Emergence of magnetic nanoparticles in photothermal and ferroptotic therapies. *Materials Horizons*, **2023**, *10*, 4757.

58. R.K. Manavalan, et al. Review on Medical Applications of Manganese Oxide (Mn2+, Mn3+, and Mn4+) Magnetic Nanoparticles. *Journal of Nanomaterials*, **2024**, *2024*, 1073915.

59. D. Nadhiya, et al. Influence of Cu2+ substitution on the structural, optical, magnetic, and antibacterial behaviour of zinc ferrite nanoparticles. *Journal of Saudi Chemical Society*, **2023**, *27*, 101696.

60. V.C. Anadebe, et al., *Tailoring the Surface of Multifunctional Magnetic Nanoparticles: Modification and Functionalization Strategies*, in *Multifunctional Magnetic Nanoparticles in Analytical and Environmental Chemistry*. **2025**, Royal Society of Chemistry. p. 30.

61. V. Harish, et al. Review on Nanoparticles and Nanostructured Materials: Bioimaging, Biosensing, Drug Delivery, Tissue Engineering, Antimicrobial, and Agro-Food Applications. *Nanomaterials*, **2022**, *12*, 457.

62. H.T.T. Do, et al. Advances in silver nanoparticles: unraveling biological activities, mechanisms of action, and toxicity. *Applied Nanoscience*, **2024**, *15*, 1.

63. R. Feizollah and A. Meshkini. Photochemically enhanced antibacterial activity of polydopamine-coated CeO2@Ag nanocomposites: Surface and colloidal engineering for wound pathogen treatment. *Colloids and Surfaces A: Physicochemical and Engineering Aspects*, **2025**, *725*, 137641.

64. P. Singh, et al. Advanced Nanomaterials for Cancer Therapy: Gold, Silver, and Iron Oxide Nanoparticles in Oncological Applications (Adv. Healthcare Mater. 4/2025). *Advanced Healthcare Materials*, **2025**, *14*, 2403059.

65. N. Mahmed, *Development of Multifunctional Magnetic Core Nanoparticles [Ph.D. Thesis]*. **2013**, Aalto University.

66. A.B. Shatan, et al. Cationic Polymer-Coated Magnetic Nanoparticles with Antibacterial Properties: Synthesis and In Vitro Characterization. *Antibiotics*, **2021**, *10*, 1077.

67. M. Azizi-Lalabadi, F. Garavand, and S.M. Jafari. Incorporation of silver nanoparticles into active antimicrobial nanocomposites: Release behavior, analyzing techniques, applications and safety issues. *Advances in Colloid and Interface Science*, **2021**, *293*, 102440.

68. M.M. Berekaa. Nanotechnology in Food Industry; Advances in Food processing, Packaging and Food Safety. *International Journal of Current Microbiology and Applied Sciences*, **2015**, *4*, 345.

69. E. Fantozzi, et al. Silver Doped Magnesium Ferrite Nanoparticles: Physico-Chemical Characterization and Antibacterial Activity. *Materials*, **2021**, *14*, 2859.

70. M.A. Rabbi, et al. Preparation of stable Fe₂O₃/Ag nanocomposite particles with catalytic, antioxidant and antibacterial properties. *New Journal of Chemistry*, **2024**, *48*, 5278.

71. M. Güneş, et al. Synthesis and Antibacterial Evaluation of Silver-Coated Magnetic Iron Oxide/Activated Carbon Nanoparticles Derived from Hibiscus esculentus. *Magnetochemistry*, **2025**, *11*, 53.

72. X. Liu, et al. Zinc-doped inorganic bioactive materials: a comprehensive review of properties and their applications in osteogenesis, antibacterial, and hemostasis. *Applied Materials Today*, **2024**, *40*, 102393.

73. R. Krishnamoorthy, et al. Antibacterial Mechanisms of Zinc Oxide Nanoparticle against Bacterial Food Pathogens Resistant to Beta-Lactam Antibiotics. *Molecules*, **2022**, *27*, 2489.

74. G. Kasparis, et al. Zn doped iron oxide nanoparticles with high magnetization and photothermal efficiency for cancer treatment. *Journal of Materials Chemistry B*, **2023**, *11*, 787.

75. J.A. Joseph, et al. Zinc-doped iron oxide nanostructures for enhanced photocatalytic and antimicrobial applications. *Journal of Applied Electrochemistry*, **2021**, *51*, 521.

76. M.A.B. Hamid, et al. Enhanced nanofluid stability of Zn-doped iron oxide: Applications of ascorbic acid nanofluid in enhanced oil recovery. *Materials Letters*, **2024**, *377*, 137418.

© 2025 The Authors. This article is licensed under a Creative Commons Attribution 4.0 International License.

77. A. Bigham, et al. Multifunctional nanoporous magnetic zinc silicate-ZnFe2O4 core-shell composite for bone tissue engineering applications. *Ceramics International*, **2018**, *44*, 11798.

78. O. Bakina, et al. New PMMA-Based Hydroxyapatite/ZnFe2O4/ZnO Composite with Antibacterial Performance and Low Toxicity. *Biomimetics*, **2023**, *8*, 488.

79. F. Jabeen, et al. Carrageenan: structure, properties and applications with special emphasis on food science. *RSC Advances*, **2025**, *15*, 22035.

80. A. Kumar, et al. Metal-based nanoparticles, sensors, and their multifaceted application in food packaging. *Journal of Nanobiotechnology*, **2021**, *19*, 256.

81. V.A. Tirado-Kulieva, et al. A Critical Review on The Integration of Metal Nanoparticles in Biopolymers: An Alternative for Active and Sustainable Food Packaging. *Current Research in Nutrition and Food Science Journal*, **2022**, *10*, 01.

82. H. Hosseinzadeh, H. Oveisi, and A. Meshkini. Comprehensive analysis of morphological effects in single and multi-layer zinc oxide and silica coatings on the physicochemical and biological properties of $ZnFe_2O_4$ nanoparticles. *Colloids and Surfaces A: Physicochemical and Engineering Aspects*, **2025**, *718*, 136946.

83. H. Mohd Yusof, et al. Antibacterial Potential of Biosynthesized Zinc Oxide Nanoparticles against Poultry-Associated Foodborne Pathogens: An In Vitro Study. *Animals*, **2021**, *11*, 2093.

84. H. Ghanbari, et al. Synthesis, characterization, and biological activity of a fresh class of sonochemically synthesized Cu2+ complexes. *Scientific Reports*, **2024**, *14*, 21325.

85. Z. Mao, et al. Iron oxide nanoparticles for biomedical applications: an updated patent review (2015–2021). *Expert Opinion on Therapeutic Patents*, **2022**, *32*, 939.

86. J.L.S. de Azevedo Neiva, *Metal-Based Antimicrobial for Orthopedic Devices [M.Sc. Thesis]*. **2021**, Universidade do Minho.

87. D.K. Verma, et al., *Recent Development and Importance of Nanoparticles in Disinfection and Pathogen Control*, in *Smart Nanomaterials Technology*. **2023**, Springer Nature Singapore. p. 83.

88. M.J. Woźniak-Budych, K. Staszak, and M. Staszak. Copper and Copper-Based Nanoparticles in Medicine—Perspectives and Challenges. *Molecules*, **2023**, *28*, 6687.

89. S. Kanagesan, et al. Evaluation of Antioxidant and Cytotoxicity Activities of Copper Ferrite (CuFe2O4) and Zinc Ferrite (ZnFe2O4) Nanoparticles Synthesized by Sol-Gel Self-Combustion Method. *Applied Sciences*, **2016**, *6*, 184.

90. M.-J. Lai, et al. Effect of Size and Concentration of Copper Nanoparticles on the Antimicrobial Activity in Escherichia coli through Multiple Mechanisms. *Nanomaterials*, **2022**, *12*, 3715.

91. J. Ramos-Zúñiga, N. Bruna, and J.M. Pérez-Donoso. Toxicity Mechanisms of Copper Nanoparticles and Copper Surfaces on Bacterial Cells and Viruses. *International Journal of Molecular Sciences*, **2023**, *24*, 10503.

92. N.F. Andrade Neto, et al. Characterization and photocatalytic application of Ce4+, Co2+, Mn2+ and Ni2+ doped Fe3O4 magnetic nanoparticles obtained by the co-precipitation method. *Materials Chemistry and Physics*, **2020**, *242*, 122489.

93. B. Jyothish, U.S. Geethu, and J. Jacob. Influence of the Ag1+ and Co2+ doping on structural, optical and anti-cancer properties of ZnFe2O4 nanoparticles synthesized by co-precipitation method. *Materials Science and Engineering: B*, **2022**, *276*, 115544.

94. O. Cadar, et al., *Progress, Challenges and Opportunities in Divalent Transition Metal-Doped Cobalt Ferrites Nanoparticles Applications*, in *Advanced Functional Materials*. **2020**, IntechOpen.

95. W. Tahir, et al. Impact of silver substitution on the structural, magnetic, optical, and antibacterial properties of cobalt ferrite. *Scientific Reports*, **2023**, *13*, 1.

96. K.K. Keshri, et al. Magnetic, Optical, and Antibacterial Properties of Ag+ and Ti4+ Doped Cobalt Ferrite Nanocrystals. *Physics of the Solid State*, **2024**, *66*, 521.

97. Z.E. Gahrouei, S. Labbaf, and A. Kermanpur. Cobalt doped magnetite nanoparticles: Synthesis, characterization, optimization and suitability evaluations for magnetic hyperthermia applications. *Physica E: Low-dimensional Systems and Nanostructures*, **2020**, *116*, 113759.

98. H. Hosseinzadeh and H. Oveisi. Gadolinium-doped CoFe ₂ O ₄ semi-crystalline nanoparticles with designed morphology: The effect of synthesis parameters on microstructure and magnetic characteristics. *Advances in Applied Ceramics: Structural, Functional and Bioceramics*, **2025**.

99. B. Shobana, et al. Sensing the invisible: Ultra-low-level electrochemical detection of the microbe (Pseudomonas aeruginosa) on cobalt ferrite-doped silver nanocomposite (CoFe2O4/AgNPs) surfaces. *Food Chemistry*, **2024**, *439*, 138073.

100. J. Luo, et al. Review of Cobalt-Based Nanomaterials as Sensors for Water Contaminants. *ACS Applied Nano Materials*, **2024**, *7*, 19784.

101. A.A. Kajani, A. Pouresmaeili, and M. Kamali. Facile one-pot synthesis of the mesoporous chitosan-coated cobalt ferrite nanozyme as an antibacterial and MRI contrast agent. *RSC Advances*, **2024**, *14*, 16801.

102. E. AlMatri, et al. Preparation, Characterization, and Antibacterial Activity of Various Polymerylated Divalent Metal-Doped MF2O4 (M = Ni, Co, Zn) Ferrites. *Polymers*, **2025**, *17*, 1171.

© 2025 The Authors. This article is licensed under a Creative Commons Attribution 4.0 International License.

103. B. Lin, et al. Multifunctional manganese-doped core–shell quantum dots for magnetic resonance and fluorescence imaging of cancer cells. *New Journal of Chemistry*, **2013**, *37*, 3076.

104. W. Montha, et al. Synthesis of doxorubicin-PLGA loaded chitosan stabilized (Mn, Zn)Fe 2 O 4 nanoparticles: Biological activity and pH-responsive drug release. *Materials Science and Engineering: C*, **2016**, *59*, 235.

105. C. R.K, V. Rajagopalan, and N.K. Sahu. Synthesis of manganese doped β-FeOOH and MnFe ₂ O ₄ nanorods for enhanced drug delivery and hyperthermia application. *IET Nanobiotechnology*, **2020**, *14*, 823.

106. A. Hossain, et al. Application of Nanomaterials to Ensure Quality and Nutritional Safety of Food. *Journal of Nanomaterials*, **2021**, *2021*, 1.

107. T. Du, et al. Antibacterial Activity of Manganese Dioxide Nanosheets by ROS-Mediated Pathways and Destroying Membrane Integrity. *Nanomaterials*, **2020**, *10*, 1545.

108. Z. Sobańska, et al. Applications and Biological Activity of Nanoparticles of Manganese and Manganese Oxides in In Vitro and In Vivo Models. *Nanomaterials*, **2021**, *11*, 1084.

109. X. Yu, et al. Design, Preparation, and Application of Magnetic Nanoparticles for Food Safety Analysis: A Review of Recent Advances. *Journal of Agricultural and Food Chemistry*, **2021**, *70*, 46.

110. P. Pageni, et al. Recyclable magnetic nanoparticles grafted with antimicrobial metallopolymer-antibiotic bioconjugates. *Biomaterials*, **2018**, *178*, 363.

111. K. Albinali, et al. <p>A perspective on magnetic core–shell carriers for responsive and targeted drug delivery systems</p&gt. *International Journal of Nanomedicine*, **2019**, *Volume 14*, 1707.

112. S.D. Anderson, V.V. Gwenin, and C.D. Gwenin. Magnetic Functionalized Nanoparticles for Biomedical, Drug Delivery and Imaging Applications. *Nanoscale Research Letters*, **2019**, *14*, 188.

113. R. Mannu, et al. Polyethylene Glycol Coated Magnetic Nanoparticles: Hybrid Nanofluid Formulation, Properties and Drug Delivery Prospects. *Nanomaterials*, **2021**, *11*, 440.

114. C. Turrina, et al. Carboxymethyl-Dextran-Coated Superparamagnetic Iron Oxide Nanoparticles for Drug Delivery: Influence of the Coating Thickness on the Particle Properties. *International Journal of Molecular Sciences*, **2022**, *23*, 14743.

115. J. Bhoopathy, et al. Synthesis and characterization of sericin-based magnetic nanoparticles for MR imaging application - An in vivo study. *International Journal of Biological Macromolecules*, **2025**, *310*, 143415.

116. M.M. Selim, et al. A review of magnetic nanoparticles used in nanomedicine. *APL Materials*, **2024**, *12*.

117. U. Patel and E.C. Hunt. Recent Advances in Combating Bacterial Infections by Using Hybrid Nano-Systems. *Journal of Nanotheranostics*, **2023**, *4*, 429.

118. L.A. Almutairi, *Effects of Mild Magnetic Nanoparticle Hyperthermia on the Susceptibility of Biofilm Infections to Antibiotics*. **2020**, Kent State University.

119. R. Jahani, et al., *Cancer theranostics: recent global advances*, in *Functionalized Nanomaterials for Cancer Research*. **2024**, Elsevier. p. 3.

120. T. Anani, et al. MRI-traceable theranostic nanoparticles for targeted cancer treatment. *Theranostics*, **2021**, *11*, 579.

121. F. Ding, et al. Photothermal nanohybrid hydrogels for biomedical applications. *Frontiers in Bioengineering and Biotechnology*, **2022**, *10*, 1066617.

122. Z. Ahmadian, et al. A review on the impacts of metal/metal nanoparticles on characteristics of hydrogels: Special focus on carbohydrate polymers. *International Journal of Biological Macromolecules*, **2023**, *253*, 126535.

123. M.-H. Kim. Nanoparticle-Based Therapies for Wound Biofilm Infection: Opportunities and Challenges. *IEEE Transactions on NanoBioscience*, **2016**, *15*, 294.

124. N. Nadeem, et al., *Silver-doped metal ferrites for wastewater treatment*, in *Silver Nanomaterials for Agri-Food Applications*. **2021**, Elsevier. p. 599.

125. S.-W. Kim, et al., *Bio-application of Inorganic Nanomaterials in Tissue Engineering*, in *Advances in Experimental Medicine and Biology*. **2020**, Springer Singapore. p. 115.

126. H.M. Khan, et al. Smart biomaterials and their potential applications in tissue engineering. *Journal of Materials Chemistry B*, **2022**, *10*, 6859.

127. B. Rezaei, et al. Magnetic nanoparticles for magnetic particle imaging (MPI): design and applications. *Nanoscale*, **2024**, *16*, 11802.

128. L. Jiang, L. Ding, and G. Liu. Nanoparticle formulations for therapeutic delivery, pathogen imaging and theranostic applications in bacterial infections. *Theranostics*, **2023**, *13*, 1545.

129. V. Madhubala, et al. Influences of superparamagnetic Fe3O4@Ag core-shell nanoparticles on the growth inhibition of Huh-7 cells. *Materials Today Communications*, **2023**, *35*, 106139.

130. F.H. Wisam, et al. Silver and Cobalt nanoparticles as potential antibacterial agents Staphylococcus aureus isolated from wound infections. *Tikrit Journal of Pure Science*, **2020**, *25*, 21.

© 2025 The Authors. This article is licensed under a Creative Commons Attribution 4.0 International License.

131. T.K. Jana, et al. The antibacterial and anticancer properties of zinc oxide coated iron oxide nanotextured composites. *Colloids and Surfaces B: Biointerfaces*, **2019**, *177*, 512.

132. A. Seyfoori, et al. Multifunctional magnetic ZnFe2O4-hydroxyapatite nanocomposite particles for local anti-cancer drug delivery and bacterial infection inhibition: An in vitro study. *Journal of the Taiwan Institute of Chemical Engineers*, **2019**, *96*, 503.

133. B. Ghalib and M. Hessien. Magnetic and antibacterial properties of substituted cobalt spinel ferrite nanocomposites synthesized via henna green microwave hydrothermal method. *Scientific Reports*, **2025**, *15*, 16653.

134. P. Xu, et al. Synthesis of magnetic Cu-Fe3O4/carbon composite microspheres with excellent catalytic and antibacterial properties. *Colloids and Surfaces A: Physicochemical and Engineering Aspects*, **2023**, *676*, 132161.

135. X. Jin, et al. Bimetallic oxide Cu–Fe3O4 nanoclusters with multiple enzymatic activities for wound infection treatment and wound healing. *Acta Biomaterialia*, **2024**, *173*, 403.

136. B. Paz-Díaz, et al. ZnFe2O4 and CuFe2O4 Nanocrystals: Synthesis, Characterization, and Bactericidal Application. *Journal of Cluster Science*, **2021**, *34*, 111.

137. L.B. Anigol, V.P. Sajjan, and P.M. Gurubasavaraj. Evaluation of Antioxidant and Antibacterial Property of Microwave Assisted Green Synthesis of Fe3O4 -MgO Nanocomposites. *Indian Journal Of Science And Technology*, **2023**, *16*, 1777.

138. A. Rai, et al. Innovative Antibacterial Air Filters Impregnated with Photocatalytic MgFe2O4 Nanoparticles for Improved Microbiological Air Quality. *Catalysts*, **2025**, *15*, 365.

139. L. Dong, et al. A review on recent advances in the applications of composite Fe ₃ O ₄ magnetic nanoparticles in the food industry. *Critical Reviews in Food Science and Nutrition*, **2022**, *64*, 1110.

140. C.A. dos Santos, A.P. Ingle, and M. Rai. The emerging role of metallic nanoparticles in food. *Applied Microbiology and Biotechnology*, **2020**, *104*, 2373.

141. J. Wróblewska-Krepsztul, et al. Recent progress in biodegradable polymers and nanocomposite-based packaging materials for sustainable environment. *International Journal of Polymer Analysis and Characterization*, **2018**, *23*, 383.

142. S.M.A.S. Keshk, et al. Synthesis of a Magnetic Nanoparticles/Dialdehyde Starch-Based Composite Film for Food Packaging. *Starch - Stärke*, **2018**, *71*, 1.

143. L.F. Ballesteros, et al., *Active Packaging Systems Based on Metal and Metal Oxide Nanoparticles*, in *Nanotechnology-Enhanced Food Packaging*. **2021**, Wiley. p. 143.

144. B. Socas-Rodríguez, et al. Recent Applications of Magnetic Nanoparticles in Food Analysis. *Processes*, **2020**, *8*, 1140.

145. M. Adampourezare, et al. Iron/iron oxide-based magneto-electrochemical sensors/biosensors for ensuring food safety: recent progress and challenges in environmental protection. *RSC Advances*, **2023**, *13*, 12760.

146. A. Inês and F. Cosme. Biosensors for Detecting Food Contaminants—An Overview. *Processes*, **2025**, *13*, 380.

147. N. Idil, et al. Recent Advances in Optical Sensing for the Detection of Microbial Contaminants. *Micromachines*, **2023**, *14*, 1668.

148. A.S.G.G. Santos, et al. Feasibility of using magnetic nanoparticles in water disinfection. *Journal of Environmental Management*, **2021**, *288*, 112410.

149. A. Najafpoor, et al. Effect of magnetic nanoparticles and silver-loaded magnetic nanoparticles on advanced wastewater treatment and disinfection. *Journal of Molecular Liquids*, **2020**, *303*, 112640.

150. H. Kruse, *Antibacterial effects of silver magnetic nanoparticles against Escherichia coli, Salmonella enterica serovar Typhimurium and S. Anatum*. **2019**, Mississippi State University.

151. B. Pattanasiri and S. Sangjan. ZnO/g-C3N4/Fe3O4 Nanocomposites Embedded Sa-PVA as Photocatalyst Hydrogel Beads for Photodegradation. *Key Engineering Materials*, **2022**, *931*, 99.

152. X. Zhang, et al. Loading Cu-doped magnesium oxide onto surface of magnetic nanoparticles to prepare magnetic disinfectant with enhanced antibacterial activity. *Colloids and Surfaces B: Biointerfaces*, **2018**, *161*, 433.

153. S. Chen, et al. Preparation of composite film with CoFe2O4/MXene/chitosan for extending the shelf life of Kyoho grapes. *Food Bioscience*, **2025**, *64*, 105900.

© 2025 The Authors. This article is licensed under a Creative Commons Attribution 4.0 BY International License.

© 2025 The Authors. This article is licensed under a Creative Commons Attribution 4.0 International License.

Author Biography

Hamid Hosseinzadeh is currently a Ph.D. candidate in Materials Engineering with a specialization in Advanced Materials at Hakim Sabzevari University. He is also the CEO of the technology-based company "Fanavaran Sanat Novin Garsha", located in the Khorasan Razavi Science and Technology Park, Iran. His research interests lie in the field of nanotechnology, with a particular focus on biomedical nanomaterials and antibacterial agents for medical diagnostics and therapeutics. He has published several research articles in reputable international journals in these areas. Currently he is researching the design and fabrication of metal–organic frameworks (MOFs) for applications in skin health and wound healing. He is also committed to translating scientific research into practical, technology-based healthcare solutions.

© 2025 The Authors. This article is licensed under a Creative Commons Attribution 4.0 International License.

Effect of $CoCl_2$ Doping on the Optical and Electrical Properties of PEO Polymer Films for Optoelectronic Applications

Roopa K. V., Subramanya Kilarkaje *

Department of PG Studies and Research in Physics, Kuvempu University, Shivamogga, Karnataka, India

Editor's note: Polyethylene oxide (PEO) films are characterized by their semi-crystalline structure, which imparts several important properties, including hydrophilicity, chemical stability, solubility in alcohols, and flexibility. However, the absence of charge carriers limits their application in various fields. Enhancing the conductivity of these films could lead to advancements in next-generation photonic devices, solar cells, optoelectronics, and sensors. Roopa K. V. and Subramanya K. investigated the doping of PEO films with cobaltous chloride ($CoCl_2$) at various concentrations. Their findings indicated that the interaction between Co^{2+} ions and the ether groups of PEO results in the formation of metal-ligand coordination bonds within the doped PEO films. This interaction significantly enhances the electrical conductivity and ion mobility of the $CoCl_2$-doped PEO films and results in a redshift in the absorption edge of these films.

doi: 10.22034/jams.2025.210147

How to cite: R. K.V. and S. Kilarkaje, *Journal of Applied Material Science*, **2025**, *1*, 210147.

JOURNAL OF
APPLIED
MATERIAL
SCIENCE
jams.hsu.ac.ir

© 2025 *J. Appl. Mater. Sci.* This material is licensed under a Creative Commons Attribution 4.0 International License.

Journal of Applied Material Science **2025**, *1*, 210147
How to cite: R. K.V. and S. Kilarkaje, *Journal of Applied Material Science*, **2025**, *1*, 210147.
Journal homepage: **jams.hsu.ac.ir**

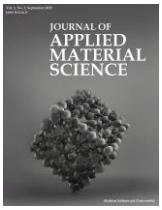

Original Research

Effect of $CoCl_2$ Doping on the Optical and Electrical Properties of PEO Polymer Films for Optoelectronic Applications

Roopa K. V., Subramanya Kilarkaje *

Department of PG Studies and Research in Physics, Kuvempu University, Shivamogga, Karnataka, India

Abstract

Highly porous polymer films were synthesized using the solution casting technique by doping polyethylene oxide (PEO), a semi-crystalline polymer known for its good film-forming ability, chemical stability, ionic conductivity, and optical properties, with varying concentrations of cobaltous chloride ($CoCl_2$) (0, 5, 10, 15, and 20 wt%). $CoCl_2$, a transition metal halide containing Co^{2+} ions, is known for its tunable optical absorption, enhanced electrical conductivity, and strong coordination behavior, making it suitable for improving the performance of polymer matrices. X-ray Diffraction analysis revealed a gradual reduction in crystallinity with increased $CoCl_2$ content, indicating structural disruption and confirming (120) and (032) planes as per JCPDS standards. Fourier transform infrared (FTIR) spectra showed interactions between Co^{2+} ions and PEO ether groups, suggesting the formation of metal-ligand coordination bonds. UV-Visible spectroscopy exhibited a redshift in the absorption edge, and Tauc's plots revealed decreasing direct and indirect band gaps. The extinction coefficient increased significantly (from 1×10^4 to 6.7×10^4), indicating enhanced light absorption and suitability for UV photodetector applications. AC conductivity increased with doping due to enhanced ion mobility, while Nyquist plots confirmed reduced bulk resistance and improved ion transport through hopping mechanisms. The 20 wt% $CoCl_2$-doped film exhibited a bulk resistance of just 33 Ω, indicating potential semiconductor or ionic conductor behavior. SEM images confirmed increased surface porosity and morphological changes, consistent with the semi-crystalline nature of the films. These findings suggest that $CoCl_2$-doped PEO films are promising candidates for flexible electronics, optoelectronic devices, sensors, and solid polymer electrolytes in energy storage applications.

Keywords: Polyethylene oxide; Inorganic metal salt; Polymer composite film; Energy band gap; FTIR; AC Conductivity.

1. Introduction

Polymers have established themselves as unbelievable and non-replaceable across diverse fields due to their physical flexibility, low price, weightlessness, processing ease, and chemical tunability. They are widely used in household products, adhesives, medical, and pharmaceutical industries. Properties such as non-toxicity, porosity behavior, flexibility, and solubility in desired solvents make them particularly suitable for functional applications. Furthermore, their

* Corresponding author.
Email addresses: subbuk17@gmail.com, drskkuphysics@gmail.com (S. Kilarkaje)

Received 30 July 2025
Revised 8 August 2025
Accepted 9 August 2025
Available online 10 August 2025

https://doi.org/10.22034/jams.2025.210147
© 2025 The Authors. This article is licensed under a Creative Commons Attribution 4.0 International License.

covalent backbone allows polymers to interact with dopants and fillers effectively, enabling structural and functional modifications for specific performance requirements [1].

Among many polymers, polyethylene oxide (PEO) is suitable for flexible photonic applications for its chemical structure, covalent bond at the backbone, its semi-crystalline nature, hydrophilicity, chemical stability, solubility in alcoholic groups, and flexibility [2]. Although PEO is electrically not capable of conducting alone, it lacks charge carriers for performing strong optical, electrical responses in advanced applications such as solar cells, optoelectronics [3]. Further development of polymer and combined constituent materials, various strategies have been found. Among these, doping, adding a small portion of metal salts to the main polymer structure, enhances optical, electrical properties. This occurs due to a modification in microlevel structure, which is not much explored in the present era. The ability to solubilize a range of inorganic salts makes it highly adaptable for material blending and conductivity enhancement [4].

To overcome the intrinsic limitations of PEO for electronic applications doped with transition metal salts. Cobaltous chloride ($CoCl_2$), a pink crystalline salt, a transition metal halide containing Co^{2+} ions, due to partially filled d-orbitals, exhibits optical absorption. Modification in structure forming tetrahedral or octahedral complexes is one such candidate known for its conductive properties, transition metal activity, and coordination behavior. $CoCl_2$ dissolves in alcohol also chemically stable, exhibiting partially filled d orbit with stability, and is easy to incorporate into polymer structures [5]. When integrated with PEO, $CoCl_2$ can act as a donor species, modifying the charge distribution, enhancing free carrier density, and improving both structural and electrical performance of the polymer system [3].

Dopant significantly influences the overall work frame of the application chosen and helps in tuning of microstructure property, leading to UV-Vis absorbance, XRD, FTIR, electrical property, and scanning electron microscopy (SEM), leading to the formation of polycrystalline domains that are advantageous for charge transport and mechanical strength. There is no such work framework accessing inter-connected research work accessing with dopant $CoCl_2$ induced with PEO. There exists a narrow gap correlating with multifunctional characteristic studies, enhancing properties [6].

To address the above research gap present study reports on the fabrication and characterization of PEO-$CoCl_2$ films via the solution cast technique, a low-cost, durable method. This is subjected to multi-characterization techniques such as UV-Visible spectroscopy, XRD, FTIR, SEM, and AC electrical conductivity, enhancing photonic applications. In the context of these resulting optical responses, bonding behavior, contact angle-volume measurement, bonding behavior, crystal size, nature of structure, morphology, and charge transport of the film are considered. Their processability at room temperature, compatibility with flexible substrates, and potential for miniaturization make them ideal for next-generation applications such as flexible displays, low-power sensors, optoelectronics, and renewable energy devices [7].

This work reveals Co^{2+} ions of dopant responsible for charge transport, aiming to differ in the result of absorption-extinction coefficient and refractive index by reducing the optical band gap below 3eV. FTIR reveals Co=O bond and C=O coordination bond, XRD reveals (120) and (032) planes, and crystal size. The SEM analysis has been revised to better correlate with the above findings, providing morphological evidence that supports the structural and electrical characteristics discussed. AC conductivity enhances, and the resistance of the material decreases to 0.33Ω. This evidence suggests PEO-$CoCl_2$ films potential candidate for use in photonics applications. The structural, optical, and electrical properties of the composite films are systematically investigated using UV–Visible spectroscopy, FTIR, XRD, SEM, and AC electrical I–V characterization. This study focuses on how varying $CoCl_2$ concentrations affect optical band gap, crystallinity, and conductivity with a view toward applications in photoactive systems, sensors, and energy storage devices [8].

2. Experimental

2.1. Materials

The Solution cast technique method is preferred to achieve Polyethylene Oxide (PEO, Mw = 5.6×10^6 g/mol, Merck) and Cobaltous Chloride ($CoCl_2$, Mw = 237.93 g/mol) doped films, were to its simplicity, cost-effectiveness, and ability to yield uniform films under

© 2025 The Authors. This article is licensed under a Creative Commons Attribution 4.0 International License.

constant temperature 50 °C. A fixed amount of PEO was dissolved in methanol (Mw = 32.04 g/mol; SD Fine Ltd.) under constant stirring to obtain a clear solution at 50 °C. $CoCl_2$ was added in varying concentrations (0%, 5%, 10%, 15%, and 20% by weight of PEO) and stirred thoroughly to ensure homogeneity and uniformity under thermal conditions of 50 °C. The resulting solution was cast into Petri dishes and dried at a temperature of 50 °C to allow solvent evaporation and avoid thermal degradation of the sample. Thus, the obtained samples are sealed in zip cover bags and desiccated. The films were cut into squares of one square centimetre, and characterization was carried out.

2.2. *Measurements*

The optical properties were studied using UV–visible NIR spectroscopy using a Quartz tungsten Halogen lamp as a source for pure and composites between 200 nm to 1500 nm wavelength range to determine band gap values. Fourier-transform infrared (FT-IR) spectroscopy was conducted in KBr medium using a Perkin Elmer IR Spectroscopy in the air medium. The structural properties of the synthesized samples were analyzed using an X-ray diffractometer with Cu-Kα radiation (λ = 1.5406 Å), operating at 40 kV and 30 mA, with a scan range from 5° to 80° (2θ), and a step size of 5° per minute. Surface morphology studies and thickness of the sample were studied using Table top Scanning electron microscope (SEM), with a JEOL JSM-IT500LA microscope operating at 5000V, and at a resolution of 300X magnification was taken under vacuum. AC Electrical property studies were done using a Keithley Source Measure, frequency versus dielectric.

3. Results and discussion

3.1. *UV-Visible spectroscopy results*

UV-Vis spectroscopy, which studies the interaction of electromagnetic radiation with matter, is a primary method for analyzing absorbance, transmittance, band gap, and optical properties of materials. Figure 1 shows

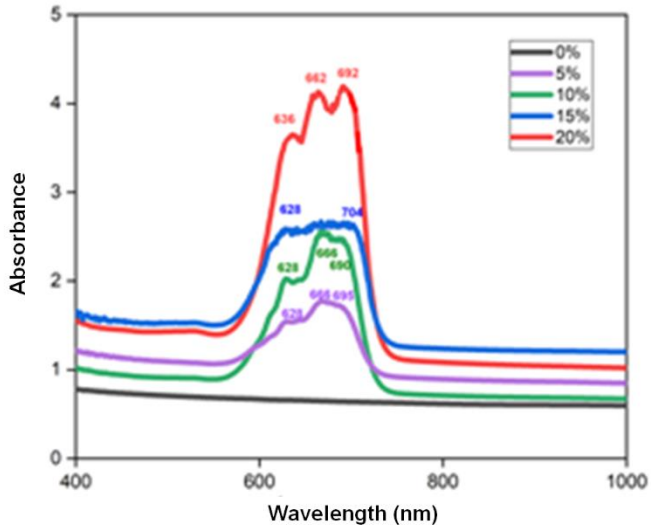

Figure 1. UV-Vis absorption spectra of the samples with varying dopant concentrations (0%, 5%, 10%, 15%, and 20%) in the range of 400–1000 nm.

strong absorbance peaks between 570–750 nm, corresponding to the visible red/near-infrared region, indicating that these wavelengths are absorbed while blue/violet light is reflected, resulting in a bluish-violet film appearance. There is a possibility of forming both tetrahedral (blue/violet) and octahedral (violet/pink) of Co^{2+}ions coordination complexes with the polyethylene oxide (PEO) matrix [9-11].

Table 1 exhibits the data for pure PEO, the $CoCl_2$-doped sample, as observed increased absorbance, absorption coefficient, and extinction coefficient, along with enhanced translucency, indicating higher crystallinity and formation of tetrahedral Co^{2+} complexes [12]. Figure 2 shows correlated Tauc plots and their derivative using equations (1) and (2), showing a reduction in direct band gap (<3 eV) with increased $CoCl_2$ concentration. At longer wavelength absorption, UV sensitivity is seen sensitive at longer wavelength absorption, which makes the material suitable for photosensitive applications [13, 14].

Table 1. Direct and Indirect Band Gap, Absorption Coefficient, Extinction Coefficient, and Refractive Index of doped PEO–$CoCl_2$ films

Dopant Weight Percent (%)	0	5	10	15	20
Direct Band Gap (eV)	3.20	1.93	1.78	1.61	1.55
Indirect Band Gap (eV)	2.40	1.90	1.65	1.51	1.05
Absorption Coefficient (eV)	-	1.688	1.683	1.647	1.632
Extinction Coefficient ($\times 10^{-4}$)	0.95	1.47	1.65	3.21	3.66
Refractive index	0.11	0.18	0.22	0.28	0.66

© 2025 The Authors. This article is licensed under a Creative Commons Attribution 4.0 International License.

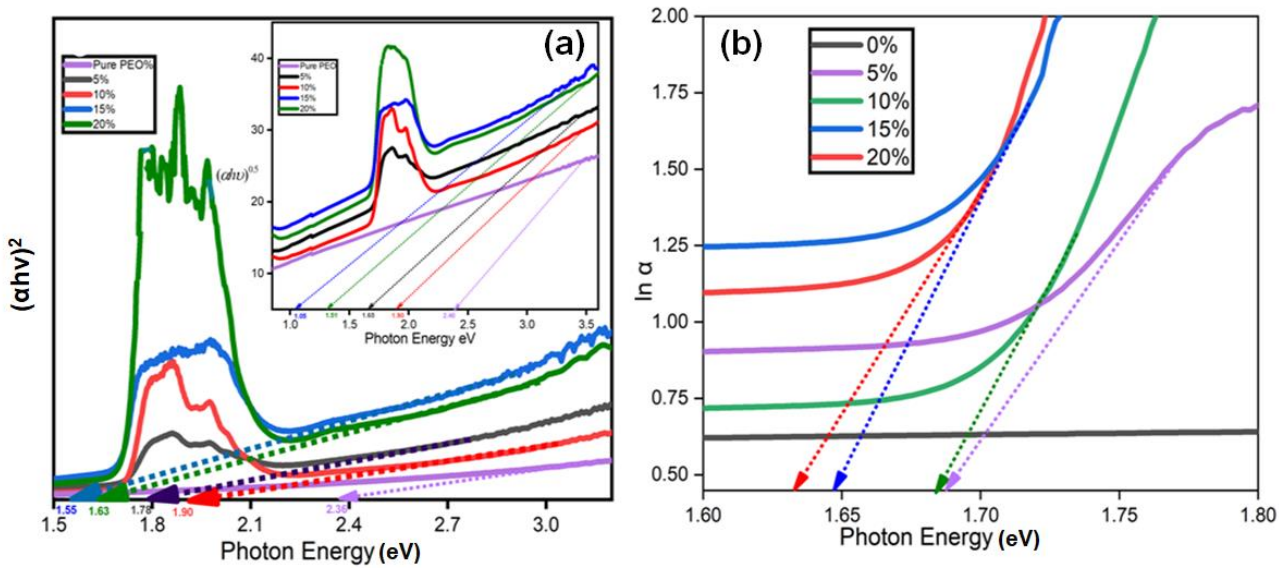

Figure 2. Plots of the direct and indirect band gaps (a), as well as the absorption coefficient (b), as a function of increasing dopant weight percentage.

Beer–Lambert Law address calculation for absorption coefficient (α) via equation (3), showing enhancement, reflecting the material's photon absorption strength as in Figure 2. Figure 3 shows that the extinction coefficient increased from 0.95×10^{-4} to 3.66×10^{-4} with increased doping, calculated using equation (4), indicating photon penetration at higher photon absorption. The refractive index, calculated via equation (5), increased from 0.11 to 0.66 as in Figure 3, implying improved polarizability and photon trapping at grain boundaries, supporting increased optical conductivity [15-17]. A summary of the optical data is presented in Table 1.

$$\alpha h\nu = A(h\nu - E_g)^n \quad (1)$$

$$\alpha = 2.303(t^{-1})log(T)^{-1} \quad (2)$$

$$\alpha = \frac{2.303A}{t} \quad (3)$$

$$k = \frac{\alpha\lambda}{4\pi} \quad (4)$$

$$n = \sqrt{\frac{(1+R)^2 - k^2}{(1-R)^2 + k^2}} \quad (5)$$

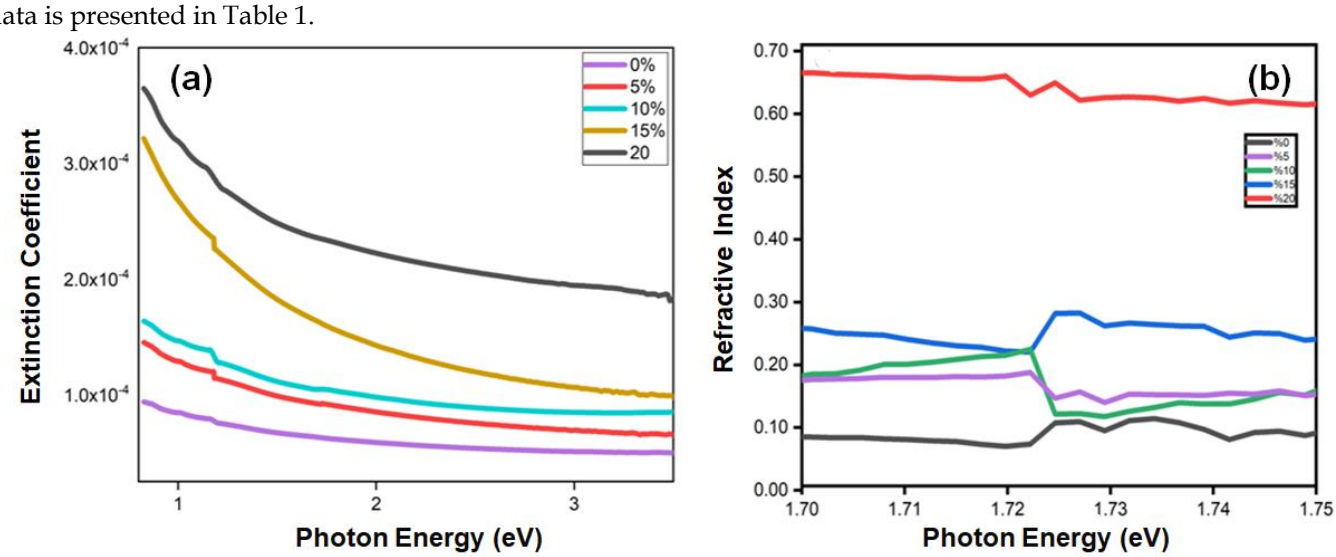

Figure 3. Plots of the extinction coefficient and refractive index as functions of increasing dopant weight percentage.

© 2025 The Authors. This article is licensed under a Creative Commons Attribution 4.0 International License.

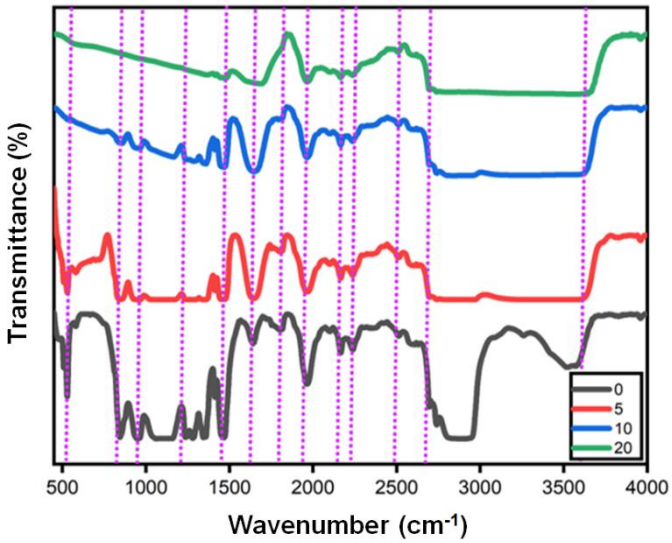

Figure 4. FTIR spectra of samples with varying $CoCl_2$ dopant concentrations (0%, 5%, 10%, and 20%) in the wavenumber range of 500–4000 cm^{-1}.

3.2. Fourier transform infrared spectroscopy studies

FTIR data predicts formation of new bonds in the doped PEO–$CoCl_2$ films at higher concentration, which are absent in pure PEO, evidencing structural modifications upon doping. In Figure 4, the broad O–H stretching band is seen in all the samples around 3500 cm^{-1}, confirming hydroxyl interactions [6, 18]. Similar to OH stretching, symmetric CH_2 stretching vibration characteristic near 2900 cm^{-1} in pure PEO disappears in doped samples, which hinders the structural organization due to coordination between Co^{2+} ions and the PEO matrix [19].

CH bending and stretching vibrations near 2600 cm^{-1} are observed in all samples, indicating a Carbon-Hydrogen bond. C≡C stretching exists around 2100–2260 cm^{-1}, while peaks from 1800–1900 cm^{-1} and near 2250 cm^{-1} are attributed to CO–Co metal carbonyl bonds, confirming the formation of Co^{2+} complexes [20].

An absorption peak around 1900 cm^{-1} is assigned to C=O stretching, and a band near 1600 cm^{-1} indicates symmetric and asymmetric C=C and O=C=O stretches, suggesting the presence of metal carboxylate complexes. Additionally, peaks around 1300 cm^{-1} are related to C–O stretching of alcohol groups and CH_2 wagging. The CH_2–CH_2–O group, prominent in pure PEO, diminishes

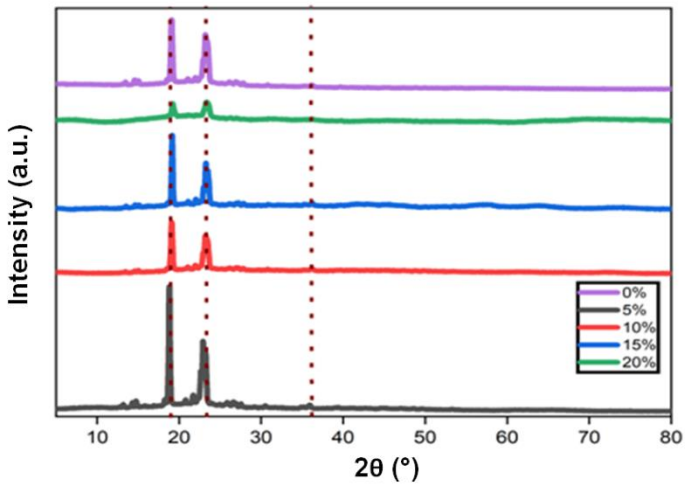

Figure 5. XRD patterns of samples with varying $CoCl_2$ dopant concentrations (0%, 5%, 10%, 15%, and 20%).

© 2025 The Authors. This article is licensed under a Creative Commons Attribution 4.0 International License.

at higher dopant concentrations, suggesting that tetrahedral Co^{2+} complexes interact with the polymer's carbon groups, altering the polymer's local structure [21, 22]. FTIR reveals metal ligand coordination bond with peaks around 2250 cm^{-1} (CO–Co metal carbonyls) and 2100–2260 cm^{-1} (C=C stretching), which were absent in pure PEO.

3.3. X-ray diffraction analyses

Figure 5 shows that the undoped PEO exhibits two sharp peaks at 2θ ≈ 19.2° and 23.3°, corresponding to the (120) and (032) planes, respectively, as per JCPDS standards. These intense reflections confirm the semi-crystalline nature of pure PEO.

The sharp, high-intensity peaks at 2θ ≈ 19.2° and 23.3° in Figure 5 confirm the semi-crystalline nature of pure PEO, indicating well-ordered chain packing. With increasing $CoCl_2$ dopant concentration, these peaks persist but exhibit broadening and reduced intensity, suggesting decreased crystallinity due to structural distortion [23, 24].

This reduction is attributed to Co^{2+} ions interacting with ether oxygen in PEO via coordination bonds, disrupting chain alignment and inducing a shift toward amorphous character.

The reduced crystallinity enhances ion mobility and flexibility, improving charge transport-crucial for applications in flexible electronics, solid-state batteries, and optoelectronic devices.

Table 2, tabulation of structural parameters of XRD, such as degree of crystallinity (Xc), average crystallite size (P), and inter-crystallite separation (R), was calculated using:

$$P = 0.9\lambda / (\beta \cos\theta) \quad (6)$$

$$R = 5\lambda / (8 \sin\theta) \quad (7)$$

where $\lambda = 1.5 \times 10^{-10}$ m and β is the full width at half maximum (FWHM).

This structural evolution aligns with UV-Vis, SEM, and FTIR findings, which show enhanced light absorption, porous morphology, and altered bonding. The reduced crystallinity enhances ion mobility and flexibility, improving charge transport-crucial for applications in flexible electronics, solid-state batteries, and optoelectronic devices.

3.4. SEM morphology studies

Figure 6 presents the scanning electron micrographs of pure PEO and PEO–$CoCl_2$ composites (with 5% and 15% $CoCl_2$) recorded at 5000 V, ×3500 magnification, 5 µm scale, and SEI mode (18 46). Figure 6, Pure PEO has an amorphous appearance, smooth, and looks homogeneous surface. Increased dopant concentration shows a non-homogeneous, spike-like structure, rough surface with an increase in the number of porosities throughout the film also agglomerated Cobalt salt matrix. The linear structure of PEO is evidenced, and the concentration of dopant shows an increased PEO-$CoCl_2$matrix form. The porosity is due to the effect of temperature, which elevates coordination complex formation. Increased Co^{2+} ion and matrix help in evidencing increased conductivity. This is evidenced by the optical property showing particle penetration within

Table 2. Summary of XRD parameters for samples with varying increased $CoCl_2$ dopant weight percentages

Dopant Weight Percent (%)	2θ (°)	θ (°)	d-spacing	P (Å)	R (Å)
0	19.10	9.55	4.645	6.65	7.50
	23.26	11.63	3.841	9.89	1.16
	36.26	18.13	2.466	3.50	1.42
5	18.86	9.43	4.711	8.79	1.79
	22.83	11.41	3.878	3.24	1.02
	36	18	2.492	1.99	1.24
10	18.97	9.48	4.643	6.61	1.55
	23.26	11.63	3.833	1.78	1.16
	36.13	18.06	2.481	6.21	1.32
15	19.23	9.61	4.630	8.95	4.95
	23.26	11.63	3.786	2.22	1.16
	36.26	18.13	2.4776	7.01	1.42
20	19.36	9.68	4.616	6.81	3.71
	23.39	11.69	3.770	2.04	1.22
	36.39	18.19	2.4770	4.75	1.53

© 2025 The Authors. This article is licensed under a Creative Commons Attribution 4.0 International License.

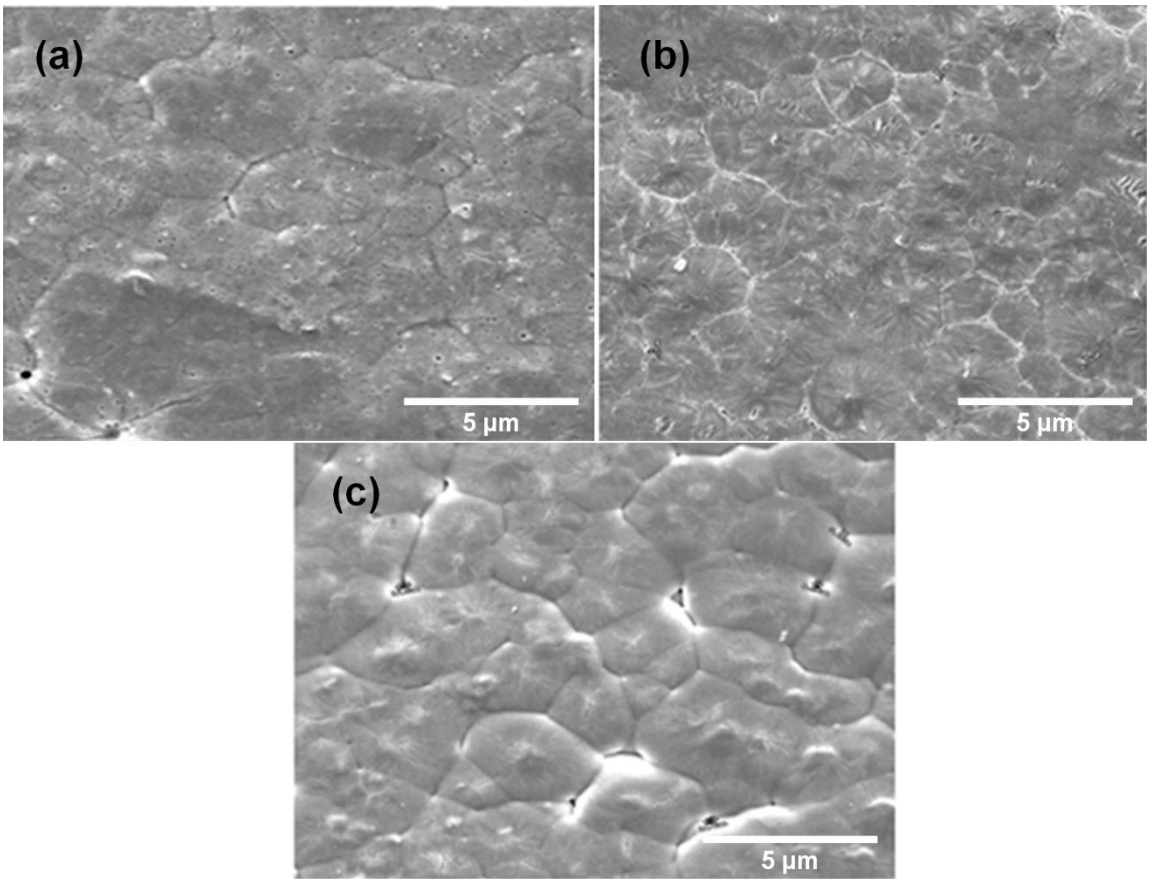

Figure 6. SEM images of Pure PEO (a) and PEO films doped with 5% (b) and 15% (c) $CoCl_2$ concentrations.

the sample is enhanced, allowing charges to pass, hence the conductivity of the sample is possible [25, 26].

3.5. Electrical characterisations

AC conductivity studies confirm enhanced charge transport within the doped PEO–$CoCl_2$ films, as conductivity is inversely proportional to resistivity-reflecting reduced opposition to charge flow. Figures 7 and 8 (Cole–Cole plot) are plotted for Z' versus Z'' as a function of frequency, illustrating the trend of a semicircle that implies the Debye model, showing an increase in bulk resistance at Pure PEO 0.3×10^6 Ω. At a higher weight percentage, it does not follow a semicircle path, hence does not obey the Debye-Model type; also, Bulk resistance decreased to 0.33 Ω, implying that there exists a hopping conduction mechanism. This improvement is attributed to the increased mobility of ionic species introduced by Co^{2+} doping, which facilitates charge transport along the polymer chains.

According to Equation (8), electrical conductivity (σ) is calculated. AC electrical conductivity increases with dopant concentration [6, 27], as tabulated in Table 3. This observation aligns with UV-Vis results, where a reduced band gap and denser film colour-due to higher Co^{2+} content, indicate improved ion transport and enhanced charge flow throughout the film. This is attributed to low-power optoelectronics and sensor devices.

$$\sigma = \frac{d}{RA}^{n} \quad (8)$$

Table 3. Electrical resistance of samples at varying dopant concentrations (0–20 wt%)

Dopant Weight Percent (%)	0	5	10	15	20
Resistance (Ω)	3.88×10^{6}	1.527×10^{3}	2.36×10^{2}	48.01	0.33
Electrical Conductivity (S/cm)	1.55×10^{-8}	3.93×10^{-5}	2.54×10^{-4}	1.25×10^{-3}	1.18×10^{-1}

© 2025 The Authors. This article is licensed under a Creative Commons Attribution 4.0 International License.

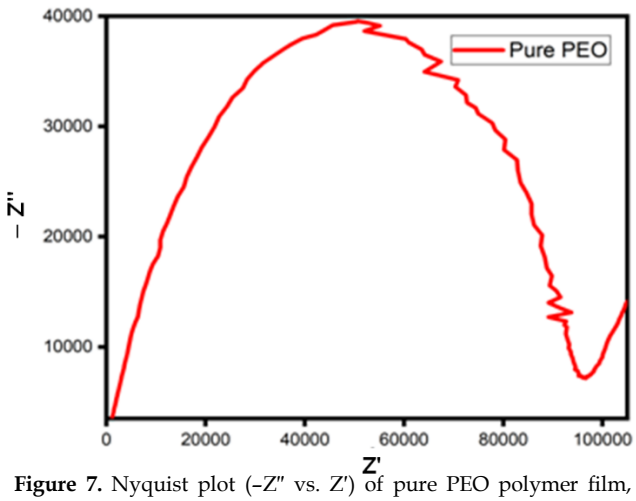

Figure 7. Nyquist plot (–Z″ vs. Z′) of pure PEO polymer film, showing a characteristic semicircular arc, indicating the bulk resistance and conductivity behavior.

4. Conclusions

$CoCl_2$-doped PEO polymer films exhibit enhanced optical and electrical properties, making them strong candidates for use in electronic, optical-sensitive, and optoelectronic applications. The doping process leads to increased absorbance, absorption coefficient, and extinction coefficient from 0.95×10^{-4} to 3.66×10^{-4}, indicating optical sensitivity and significant modifications in direct band gap from 3.20eV to 1.55eV and indirect band gap energies, refractive index found to be 0.66 with 20% dopant concentration, and optical conductivity.

With rising $CoCl_2$ concentrations, improved bonding interactions, greater hydrophilicity, and enhanced dispersion of Co^{2+} ions are observed, as supported by contact angle and colorimetric analyses. FTIR studies confirm the formation of new bonding environments and the incorporation of Co^{2+} ions within the polymer matrix, contributing to improved charge carrier density. Disappearance of peaks of CH_2 symmetric stretches evidencing new bonding interactions induced in the polymer structure. These structural changes are directly correlated with the electronic properties of the sample.

XRD analysis reveals 19° and 23° are seen at all concentration ranges, depicting well-ordered chain packing, reduced crystallinity, variations in crystal size, and changes in interplanar spacing with increased doping, indicating structural transformation within the polymer network. Porosity, grain size, and agglomerated

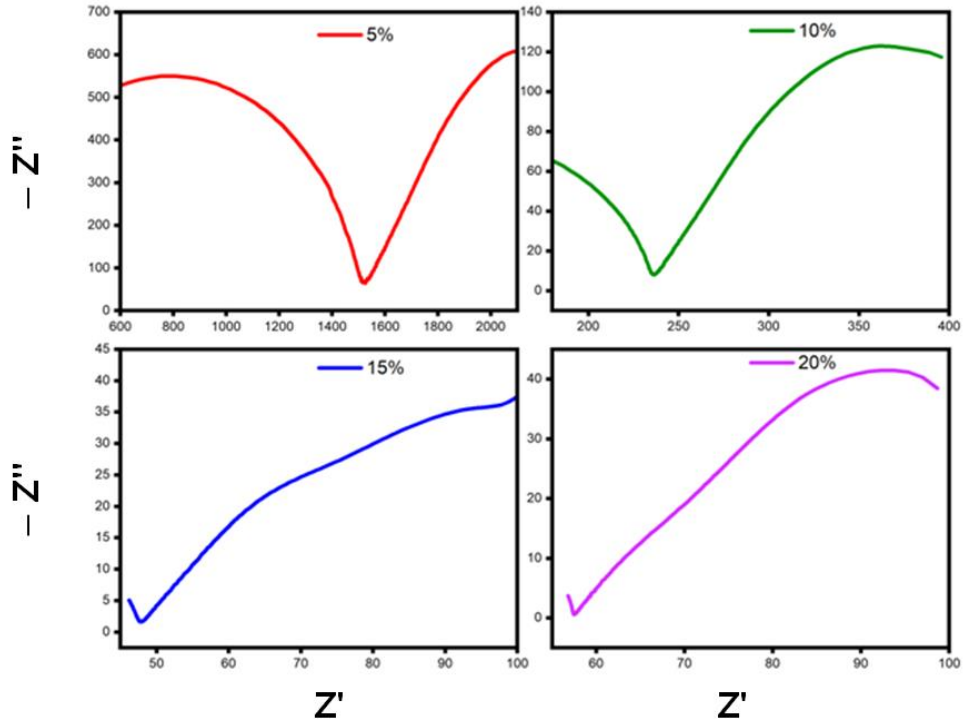

Figure 8. Nyquist plots (–Z″ vs. Z′) of $CoCl_2$-doped PEO films at different doping concentrations (5%, 10%, 15%, and 20%).

© 2025 The Authors. This article is licensed under a Creative Commons Attribution 4.0 International License.

ions of the polymer matrix are enhanced, as verified by SEM analysis. Electrical measurements demonstrate a notable decrease in resistivity and Debye-Model type, which corresponds increase in AC conductivity, suggesting enhanced ionic mobility, disorder in the structural bond, and charge transport.

Overall, the modified PEO–$CoCl_2$ films show promising potential for UV-sensitive, flexible, and cost-effective applications in solar cells, photodetectors, and other optoelectronic devices.

Acknowledgments

The authors acknowledge Sahyadri Science College, Kuvempu University, for fabrication facilities. Appreciation is extended to Dr. Praveen K. C. (LEOS–ISRO) for UV-NIR spectroscopy, Prof. Ganesh Sanjeev (Mangalore University) for AC conductivity studies, and Prof. Balram Sahoo (IISc Bangalore) for XRD analysis.

Conflict of Interest

The authors declare no conflict of interest.

References

1. K.V. Roopa, et al. Study the effect of cobalt chloride (CoCl2) on the structural, optical, and electrical properties of polymer electrolyte (PVA-CoCl2) films. *IOP Conference Series: Materials Science and Engineering*, **2024**, *1300*, 012017.

2. S.S. Siwal, et al. Recent advancements in transparent carbon nanotube films: chemistry and imminent challenges. *Journal of Nanostructure in Chemistry*, **2021**, *11*, 93.

3. A.D. Telfah, et al. Optical, electrical, and structural properties of polyethylene oxide/fullerene nanocomposite films. *Physica B: Condensed Matter*, **2024**, *679*, 415787.

4. S. Kamal, et al. Synthesis of boron doped C3N4/NiFe2O4 nanocomposite: An enhanced visible light photocatalyst for the degradation of methylene blue. *Results in Physics*, **2019**, *12*, 1238.

5. S.B. Aziz, et al. Structural, thermal, morphological and optical properties of PEO filled with biosynthesized Ag nanoparticles: New insights to band gap study. *Results in Physics*, **2019**, *13*, 102220.

6. M.G. Tadesse, A.S. Ahmmed, and J.F. Lübben. Review on Conductive Polymer Composites for Supercapacitor Applications. *Journal of Composites Science*, **2024**, *8*, 53.

7. Z. Gu, et al. From planar structures to curved optoelectronic devices: The advances of halide perovskite arrays. *Matter*, **2023**, *6*, 2666.

8. M. Ahmadi, et al. From Unregulated Networks to Designed Microstructures: Introducing Heterogeneity at Different Length Scales in Photopolymers for Additive Manufacturing. *Chemical Reviews*, **2024**, *124*, 3978.

9. D. Patel, et al. A Review on UV Visible Spectroscopy. *International Journal of Creative Research Thoughts*, **2022**, *10*, 2320.

10. S. Agrahari, S.P. Singh, and A.K. Gupta. DFT analysis of structural and optoelectronic properties of (PEO)8-LiFSI complexes. *Ionics*, **2024**, *31*, 3053.

11. A. Patil and N. Patil. Synthesis, Characterization and Conductance Properties of Cobalt Chloride Doped Polyvinyl Alcohol / Polythiophene (PVA-Co-Pth) Nanocomposite Films. *Journal of Materials Science and Surface Engineering*, **2022**, *9*, 1051.

12. I.N. Perera, et al. Enhanced Electrochemical Properties of Cobalt by Varying the Ethylene Glycol - Choline Chloride Composition in a Deep Eutectic Solvent Mixture. *Journal of The Electrochemical Society*, **2023**, *170*, 052503.

13. J.G. Doremus, et al. Photocatalytic applications of covalent organic frameworks: synthesis, characterization, and utility. *Nanoscale*, **2024**, *16*, 21619.

14. S. Guzman-Puyol, J.J. Benítez, and J.A. Heredia-Guerrero. Transparency of polymeric food packaging materials. *Food Research International*, **2022**, *161*, 111792.

15. K. Charradi, et al. Fabrication and Characterization of Polyvalent Metals/Oxidized Polyvinyl Alcohol Hybrid Films with Improved Proton Conductivity and Optical Performances. *Journal of Polymers and the Environment*, **2023**, *31*, 3167.

16. M. Tüfekçi, et al. Long-term antifouling surfaces for urinary catheters. *Journal of Materials Chemistry B*, **2024**, *12*, 5711.

17. R. Tanwar, et al. Development and characterization of PVA-starch incorporated with coconut shell extract and sepiolite clay as an antioxidant film for active food packaging applications. *International Journal of Biological Macromolecules*, **2021**, *185*, 451.

18. M.S. Anula and C. BeskeyJob. Growth, Spectral, Optical, Thermal, Mechanical and Dielectric properties of CdCl2 added (Na)2 SbF5 Single Crystals. *Journal of Pharmaceutical Negative Results*, **2023**, *14*, 2432.

19. K.-Y. Hsiao, et al. Identification of Hydroxyl and Polysiloxane Compounds via Infrared Absorption Spectroscopy with Targeted Noise Analysis. *Polymers*, **2025**, *17*, 1533.

20. A.S. De León and S.I. Molina. Influence of the Degree of Cure in the Bulk Properties of Graphite Nanoplatelets Nanocomposites Printed via Stereolithography. *Polymers*, **2020**, *12*, 1103.

© 2025 The Authors. This article is licensed under a Creative Commons Attribution 4.0 International License.

21. J.H. Koo, et al. Recent advances in soft electronic materials for intrinsically stretchable optoelectronic systems. *Opto-Electronic Advances*, **2022**, *5*, 210131.

22. A.M. Hawkar, A.M. Pshko, and B.A. Shujahadeen. Investigation of optical band gap in PEO-based polymer composites doped with green-synthesized metal complexes using various models. *RSC Advances*, **2025**, *15*, 23319.

23. M. Khan, et al. Conductive Polymer-Based Electronics in Additive Manufacturing: Materials, Processing, and Applications. *Advances in Polymer Technology*, **2025**, *2025*.

24. S.S. Khasraw, et al. PEO Based Nanocomposite With Improved Structural and Optical Properties. *Journal of Inorganic and Organometallic Polymers and Materials*, **2025**.

25. A. Shahab Marf, R. M. Abdullah, and S. B. Aziz. Structural, Morphological, Electrical and Electrochemical Properties of PVA: CS-Based Proton-Conducting Polymer Blend Electrolytes. *Membranes*, **2020**, *10*, 71.

26. B.A. Abdulkadir, et al. Optimization of the Electrochemical Performance of a Composite Polymer Electrolyte Based on PVA-K2CO3-SiO2 Composite. *Polymers*, **2020**, *13*, 92.

27. A. Kumar, et al. Ion transport, dielectric, and electrochemical properties of sodium ion-conducting polymer nanocomposite: application in EDLC. *Journal of Materials Science: Materials in Electronics*, **2020**, *31*, 10873.

© 2025 The Authors. This article is licensed under a Creative Commons Attribution 4.0 BY International License.

© 2025 The Authors. This article is licensed under a Creative Commons Attribution 4.0 International License.

Investigation of Wear Resistance and Corrosion of Ni-PTFE Composite Coatings Prepared by Electrodeposition Method

Zainab Wetwet *

College of Materials Engineering, University of Babylon, Babylon, Iraq

Editor's note: Composite coatings are recognized for their effectiveness in providing corrosion protection and wear resistance. An investigation was conducted by Wetwet on the impact of varying concentrations of polytetrafluoroethylene (PTFE) particles on the corrosion inhibition and wear resistance of nickel-based coatings applied to a St37 steel substrate. The results indicate that achieving an optimal concentration of PTFE through the electrodeposition coating process significantly enhances the wear resistance and corrosion inhibition performance of nickel-based coatings. This makes the final coating ideal for developing metal-based infrastructures that require corrosion resistance.

doi: 10.22034/jams.2025.210148

How to cite: Z. Wetwet, *Journal of Applied Material Science*, **2025**, *1*, 210148.

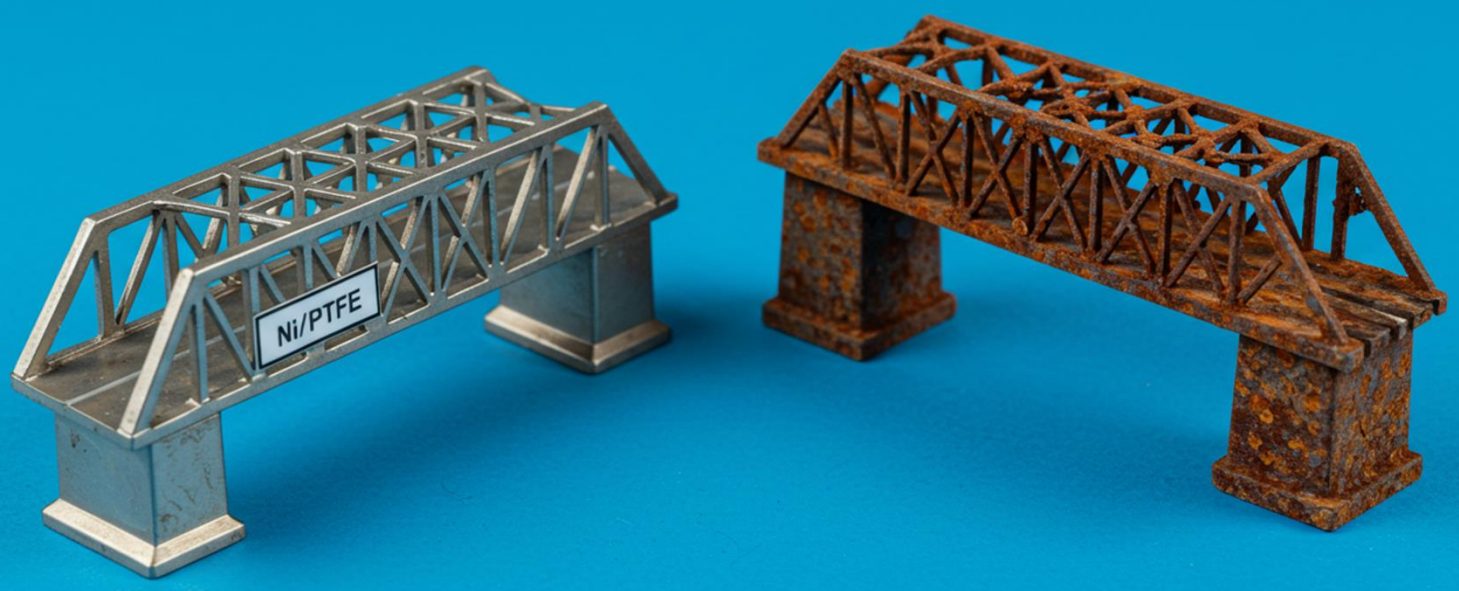

JOURNAL OF
APPLIED
MATERIAL
SCIENCE
jams.hsu.ac.ir

© 2025 *J. Appl. Mater. Sci.* This material is licensed under a Creative Commons Attribution 4.0 International License.

Journal of Applied Material Science **2025**, *1*, 210148
How to cite: Z. Wetwet, *Journal of Applied Material Science*, **2025**, *1*, 210148.
Journal homepage: **jams.hsu.ac.ir**

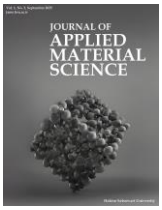

Original Research

Investigation of Wear Resistance and Corrosion of Ni-PTFE Composite Coatings Prepared by Electrodeposition Method

Zainab Wetwet *

College of Materials Engineering, University of Babylon, Babylon, Iraq

Abstract

The results of various research activities have shown that coating is one of the effective ways to increase the corrosion resistance and wear resistance of metallic substrates. Additionally, composite coatings using nanoparticles can also provide further protection to the substrate. In this study, Ni-PTFE coatings were prepared using the electrodeposition process with polytetrafluoroethylene (PTFE) particles at concentrations of 10, 20, or 30 g/L. Their corrosion and wear properties were investigated and compared to those of Ni-P coatings. Using scanning electron microscopy and energy dispersive spectroscopy, the surface morphology and elemental composition of the coatings were analyzed, and finally, by using open circuit potential techniques, electrochemical impedance spectroscopy, and Tafel polarization techniques, the corrosion resistance of the resulting coatings in 3.5 wt.% NaCl solution was evaluated. Microhardness and pin-on-disk tests were also utilized to investigate the effect of PTFE concentration on the tribological properties of the coatings. The results of scanning electron microscopy and energy dispersive spectroscopy studies confirmed the formation of nanocomposites. Electrochemical studies indicated that Ni-PTFE coatings at a concentration of 20 g/L PTFE exhibited the highest electrochemical corrosion resistance. Microhardness decreased as the amount of PTFE particles in the coating increased, reaching its lowest value. By using the wear test, the lowest coefficient of friction was obtained in composite coatings with a concentration of 20 g/L, which shows the applicability of PTFE particles as a solid lubricant in Ni-P coatings.

Keywords: Electrodeposition; Composite coatings; PTFE; Wear; Corrosion; EIS.

1. Introduction

Applying various types of protective coatings is one way to reduce costs associated with corrosion and wear in different industries [1]. Among the various coating methods, such as electroless plating, phosphating, and electrodeposition, nickel coatings have been widely used in the industry [2, 3]. Since 1843, when the first chemical compound of the nickel plating bath was introduced on an industrial scale from nickel-ammonium sulfate solution, until today, many researches have been proposed on improving the properties of these coatings, because these coatings have wide applications in various industries such as aerospace, automotive and chemical industries such as oil and gas [3].

* Corresponding author.
Email addresses: mat.zainab.a@uobabylon.edu.iq (Z. Wetwet)

Received 23 July 2025
Revised 14 August 2025
Accepted 14 August 2025
Available online 20 August 2025

https://doi.org/10.22034/jams.2025.210148
© 2025 The Authors. This article is licensed under a Creative Commons Attribution 4.0 International License.

One of the most important solutions to improve properties is to add secondary elements such as iron [4] or phosphorus [4, 5] or phosphorus [5] or composite the coating by introducing micron-sized particles or nano-like SiC to the field of nickel coating [6, 7]. Adding 10 g/L of graphene oxide to the nickel plating bath has been reported to reduce the corrosion rate by one-fifth [8]. The simultaneous presence of iron and TiC ceramic particles in the nickel coating structure results in a corrosion current density of 0.79 μA/cm² [9].

Several studies have demonstrated that wear and friction are intricate processes influenced by the surface properties of the two sliding objects, the tribological conditions, and their surrounding environment. Many dynamic systems are lubricated with various lubricating fluids. However, one disadvantage of these lubricating liquids is their inability to perform at high temperatures or under vacuum conditions, as they generally lose effectiveness in such environments. Most research has focused on another materials category that reduces the friction coefficient, known as solid lubricants [10, 11].

In recent years, many studies have explored the use of particles such as WS_2 and MoS_2 as solid lubricants in coatings [12, 13]. It has been observed that when solid lubricants are applied to the surfaces of parts operating under slippery conditions, they create a layer between the two surfaces that are in contact. This layer prevents the surfaces from making contact and welding together due to their differing characteristics. Some solid materials exhibit low shear strength, and when they are placed on a slippery surface, they significantly decrease wear and friction. This indicates that the use of solid lubricants, such as protective coatings, is necessary [13, 14]. For example, research results have demonstrated that in the presence of WS_2, the friction coefficient of Ni-P coatings obtained by the electrodeposition method decreases from 0.5 to 0.17 [12]. The presence of MoS_2 in these coatings also reduces the friction coefficient from 0.45 to 0.05 [13]. Another type of solid lubricant is PTFE, whose effect on reducing the friction coefficient of various coatings such as Ni-W has been studied [15]. However, the effect of the presence of this material in the field of Ni-P coatings has not been comprehensively studied. The optimal concentration of PTFE for maximum corrosion resistance, wear resistance, and hardness has not yet been investigated.

In this research, different concentrations of PTFE were deposited on the steel base in Ni-P PTFE electrodeposition baths, and the general characteristics of the coatings, such as chemical composition, participation rate of PTFE in the coating, surface morphology, and hardness of the coating, were evaluated. The effect of the participation percentage of PTFE in the coating on the corrosion behavior was studied using the Tafel polarization test and electrochemical impedance spectroscopy (EIS) in an environment containing 3 to 5% by weight of sodium chloride. Finally, the tribological behavior of the coatings was investigated using the pin test on the disc, and the effect of the participation percentage of PTFE particles in the coating on the friction coefficient was determined. In this study, we utilized soft lubricant particles, specifically PTFE particles, in combination with electroless nickel coating to enhance the friction properties of the surface. The PTFE particles are valued for their chemical stability and unique physical and mechanical properties, which can simultaneously improve the corrosion resistance and tribological behavior of composites.

2. Experimental

2.1. Materials

Sodium phosphate metahydrate and sodium carbonate were purchased from Sigma-Aldrich. Hydrogen peroxide and sulfuric acid were purchased from Merck (Germany). All other reagents and chemicals used were of analytical grade and used without additional purification.

2.2. Preparation of Ni-P-PTFE coatings

In this study, the electrodeposition process was carried out in a 100 ml glass beaker after preparing the substrates of St37 steel and the electrodeposition solution. The anode, which is the positive pole of the electrodeposition bath, was selected from nickel with a geometric area of 20 cm², and the prepared substrates were used as the cathode, which would be the negative pole of the cell. The temperature of the plating baths was set in the range of 40-60 °C. The conditions for the electrodeposition bath used to apply the coatings are presented in Table 1. Each of the cut plates measuring one square centimeter was soldered to a 15 cm long copper wire. To avoid errors during corrosion and electrodeposition tests, the cut parts were mounted in special molds using liquid polyester. After tightening the mount and removing the electrodes from the mold, the present electrodes were mechanically sanded with

© 2025 The Authors. This article is licensed under a Creative Commons Attribution 4.0 International License.

Table 1. Chemical composition and conditions of Ni-P-PTFE plating bath

Cathode	Plates st37
Time (minutes)	30
pH	8-9
Temperature (°C)	45-55
CTAB content	0.033 g/g PTFE
PTFE content	30-0 g/L
Boric acid content	45 g/L
Nickel chloride content	45 g/L
Nickel sulfate content	200 g/L
Sodium hypophosphite monohydrate	25 g/L

600, 800, 2500, and 3000 sandpapers, respectively, until their surface reached a mirror finish.

After the initial preparation, the electrodes are washed in a solvent solution that contains sodium phosphate metahydrate at a concentration of 20 g/L, sodium carbonate at a concentration of 30 g/L, soda at a concentration of 30 g/L, and sodium silicate at a concentration of 15 g/L, at a temperature of 60 °C for 15 minutes and then they were placed in 10 % weighted hydrogen peroxide solution and sulfuric acid 10 % weighted for acid washing. In the deoiling stage, the prepared electrodes were placed in the solvent solution for 15 minutes. Then, the electrodes were washed with distilled water and placed in an acid washing solution for 15 seconds to activate their surface.

2.3. *Measurements*

To study the morphology and substructure of the coatings, the field emission scanning electron microscope (FESEM) MIRA3 FEG-SEM, manufactured by Tescan, Czech Republic, was used at different magnifications. Through energy dispersive spectroscopy (EDS) analysis, the percentage of elements in the coatings was also determined. The micro-hardness test was conducted using the Z-HV1000 device from PACE Technologies Company, employing a Vickers indenter at the center of the coatings' cross-section under a load of 50 grams for 15 seconds. For each sample, three Vickers results were obtained, and the average of these three values was reported as microhardness. The wear test was performed using a pin-on-disc machine of Nasr Sanat Equipment Company (TSN WTC-03 model) based on the ASTM G99 standard. The applied force was 500 grams, the disk rotation speed was 95 rpm, and the travelled distance was 200 meters. The pin used is 52100 steel with 64 Rockwell C hardness. The wear test conditions were consistent across all samples, and the testing was conducted at room temperature. The friction coefficient is determined by measuring the radial force applied to the sensor and continuously recording the data with a computer.

To determine the corrosion rate of coatings, two methods of electrochemical impedance and Tafel polarization were used. In the polarization method, the working electrode is polarized by applying a potential on both sides of the anodic and cathodic potential of the open circuit. The working electrode for the electrodeposition steel sample was placed in a 100 ml beaker containing 3-5 % NaCl by weight. A platinum electrode served as the auxiliary electrode, while a calomel electrode was used as the reference electrode.

The potential curves were constructed based on the logarithm of the current using the Origa Flex device, which was equipped with the Origa Master 5 software. This was done at a scanning speed of 1 mV/s. The curves were then analyzed with the same software to determine the anodic and cathodic slopes, as well as the corrosion potential and corrosion current density. To study EIS, alternating signals with a potential range of ±5 mV were applied to the working electrode within the frequency range of 10 MHz to 100 kHz. The impedance of the sample was measured using the Origa Flex device, and the real and imaginary components of the impedance within the specified frequency range were plotted as a Nyquist diagram. In this method, a three-electrode cell was utilized for the polarization method, and the data were analyzed using Zview II software.

3. Results and discussion

Figure 1 shows the surface morphology of Ni-P coating and Ni-P-PTFE composite coatings that were deposited from solutions containing 10, 20, or 30 g/L of PTFE. It has been suggested that a five-step mechanism exists for the co-deposition of composite particles alongside metals. In the first step, the PTFE particles in the solution absorb the ionic species. In the second and third steps, particles are transported to the cathode through convection and diffusion. In the fourth step, these particles are absorbed onto the surface of the cathode while still being surrounded by a cloud of ions. Finally, in the last step, the particles are incorporated

© 2025 The Authors. This article is licensed under a Creative Commons Attribution 4.0 International License.

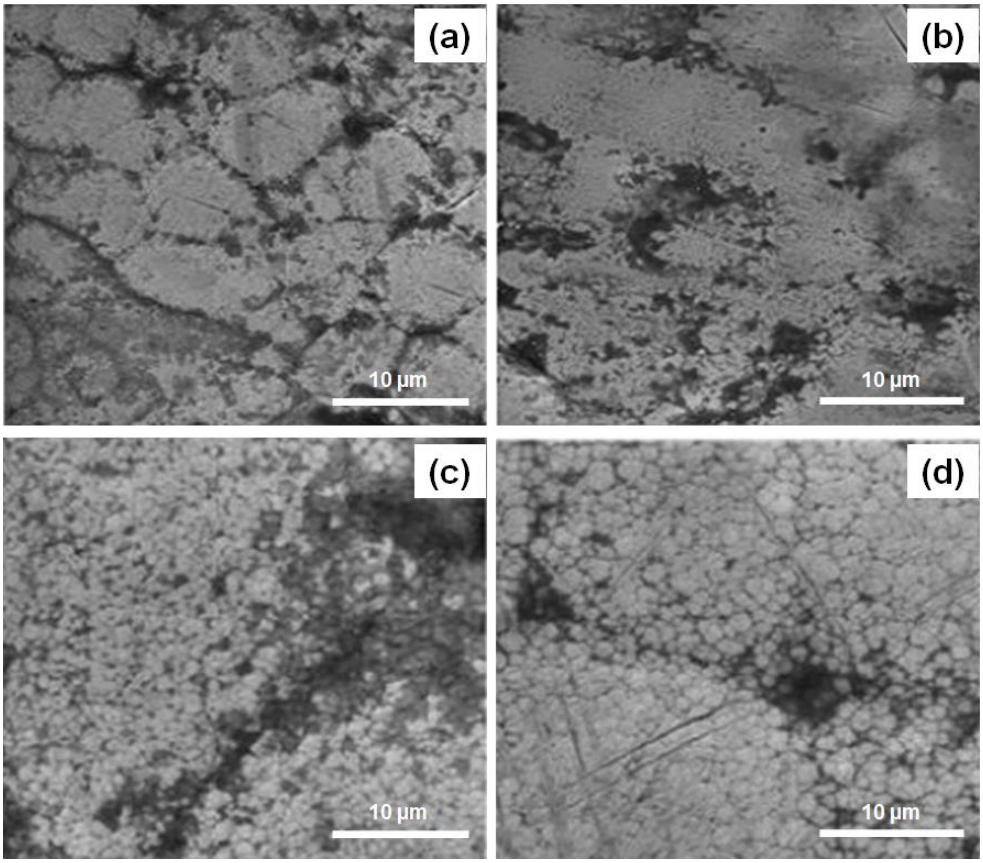

Figure 1. FESEM images of Ni-P-PTFE coatings in baths containing different concentrations of PTFE: (a) 0 g/L, (b) 10 g/L, (c) 20 g/L, and (d) 30 g/L.

into the metal network as a result of the regeneration of certain metal cations [16].

The difference between the surface morphology of Ni-P and the composite containing PTFE is that the particle size of the Ni-P coating is larger, and more intergranular boundaries are observed (Figure 1a). In the case of Ni-P-PTFE composite coatings, the coating's surface exhibits greater uniformity, smaller grain boundaries, and a reduced particle size. However, it is expected that the corrosion resistance of these coatings will increase. The images of nanocomposite coatings indicate that as the concentration of PTFE increases, and as PTFE particles fill the boundaries between the grains in the coating, the surface becomes more uniform. This uniformity is expected to reduce the penetration of corrosive solutions into the substrate. As the concentration of uniformity increases, a point is reached where excessive accumulation of PTFE particles on the surface occurs. This accumulation reduces the uniformity of the coatings, resulting in the formation of islands of Teflon polymers on the surface. Consequently, this leads to an increase in surface roughness.

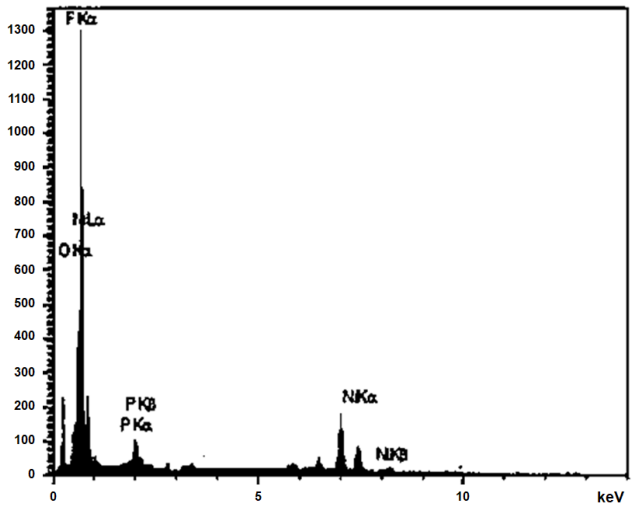

Figure 2. EDS spectrum of Ni-P-PTFE composite coating (20 g/L PTFE)

© 2025 The Authors. This article is licensed under a Creative Commons Attribution 4.0 International License.

Table 2. Weight percentage of elements present in Ni-P and Ni-P-PTFE composite coatings

Samples	PTFE content	Ni (%wt)	F (%wt)	O (%wt)	P (%wt)	C (%wt)
Ni-P	-	91.54	-	0.56	9.02	-
Ni-P-PTFE-1	10 g/L	69.35	3.67	3.95	6.81	20.17
Ni-P-PTFE-2	20 g/L	61.96	4.96	1.07	6.22	26.86
Ni-P-PTFE-3	30 g/L	74.59	3.77	2.83	7.25	11.56

Among the nanocomposite coatings, the concentration at which the coating becomes uniform is found to be at PTFE 20 g/L; beyond this point, the uniformity of the coating decreases with higher concentrations (Figure 1c). EDS analysis was performed for Ni-P coatings and Ni-P-PTFE composite coatings deposited from a solution with different concentrations of PTFE. For example, the presence of peaks related to elements F and C in the spectrum related to the coating obtained from the bath containing 20 g/L of PTFE particles confirms the presence of PTFE particles in the field of Ni-P coatings (Figure 2).

Table 2 shows the percentage of elements present in the deposited coatings. It can be seen that the Ni-P coating contains about 9% by weight of phosphorus. Also, in the presence of 10 g/L of nanoparticles, the amount of phosphorus decreases by 6.22, and the measured amount of fluorine element is 3.67. Increasing the concentration of PTFE nanoparticles from 10 g/L to 20 g/L results in a higher amount of fluorine (F) in the coating. However, when the concentration is raised to 30 g/L, the nanoparticles begin to clump together in the bath. This clumping reduces the ability of the particles to integrate into the crystalline structure of the coating, leading to a decrease in the amount of fluorine detected by EDS analysis.

Ni-P coatings include phosphorus, which results in either an amorphous or nanocrystalline structure, depending on the phosphorus content and deposition conditions. Their corrosion resistance surpasses that of nickel coatings. According to the mentioned table, there is an optimal value for PTFE in Ni-P and Ni-P-PTFE coatings, which is 20 g/L, where smaller crystals are formed due to rapid germination. As a result, a smoother and shinier coating is obtained. Increasing the concentration of PTFE after the optimal point in the bath

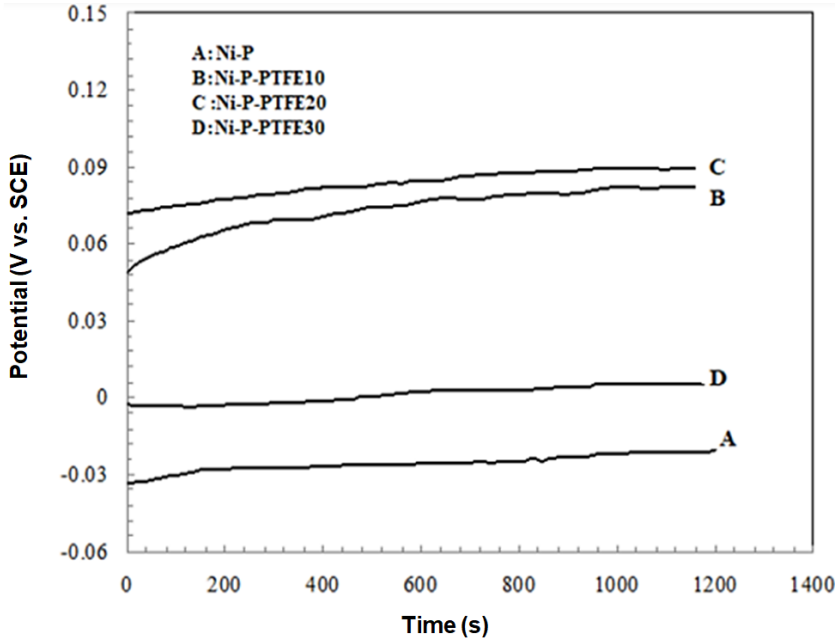

Figure 3. Diagram of open circuit potential changes with time of Ni-P coatings and Ni-P-PTFE nanocomposite in 3.5 %wt NaCl solution.

© 2025 The Authors. This article is licensed under a Creative Commons Attribution 4.0 International License.

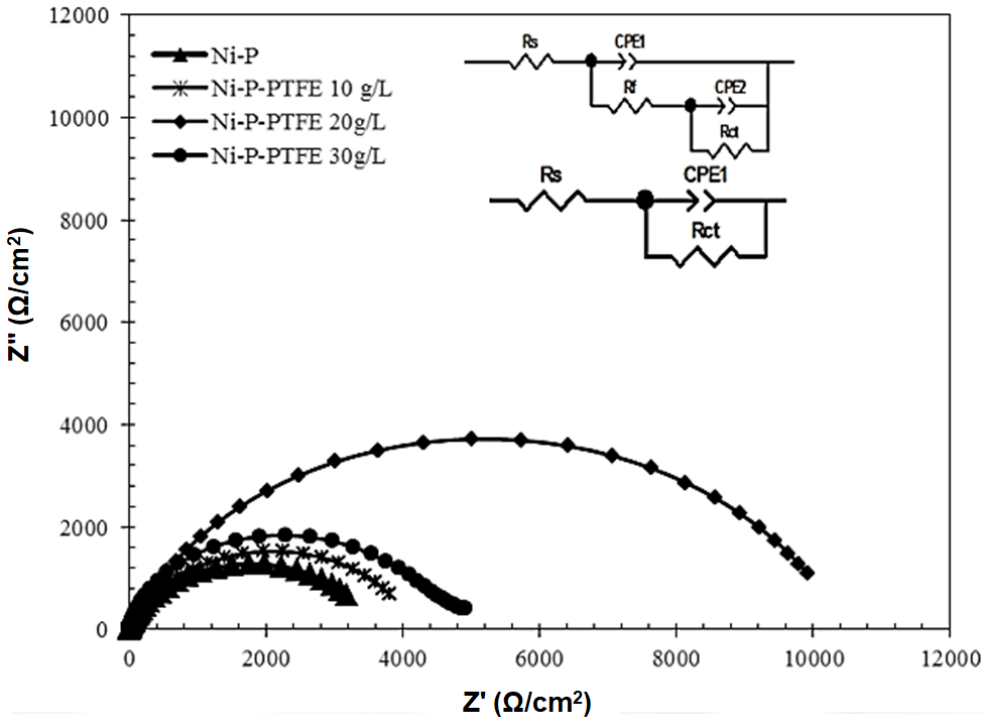

Figure 4. Nyquist diagrams for Ni-P coatings and Ni-P-PTFE composite coatings in 3.5 %wt NaCl solution.

leads to a decrease in the deposition rate. Figure 1 shows that the surface of the Ni-P coating is rougher than that of the Ni-P-PTFE coating, exhibiting extrusions of varying dimensions, with diameters ranging from a few micrometres to several nanometers. But the dimensions of the extrusions in the Ni-P-PTFE coating were smaller than the Ni-P coating.

Figure 3 shows the changes in open circuit potential (OCP) with time for Ni-P and Ni-P-PTFE composite coatings in 3.5 %wt NaCl solution. With an increase in PTFE, the open circuit potential of the samples becomes more positive, likely due to the enhanced corrosion resistance of the resulting composite coatings compared to Ni-P coatings. Various mechanisms have been proposed for the high corrosion resistance of nickel-phosphorus coatings, for example (1) the formation of a protective layer of nickel phosphate that acts as a barrier against the penetration of corrosive solutions, (2) the absorption of hypophosphite ions and the formation of a protective layer that prevents the dissolution of nickel atoms on the surface (3) with the initial dissolution of nickel atoms, a phosphorus-rich layer is created on the surface, which prevents the dissolution of nickel from the underlying layers [17].

The data indicate that the composite coating made from a bath containing 20 g/L of PTFE demonstrates the highest open circuit potential (OCP) value. This indicates that this coating has superior corrosion resistance compared to the others. As summarized in Table 2, the maximum concentration of co-deposited PTFE in the composite coatings is 20 g/L. This addition enhances the open circuit potential of the coating by forming a protective barrier, which prevents corrosive ions from penetrating the base coating and the substrate. The increase in the open circuit potential of metal coatings due to the composite with nanoparticles has also been observed in other research [18].

Figure 4 presents the Nyquist diagrams and the equivalent circuit for Ni-P coatings and Ni-P-PTFE nanocomposites in a 3.5% wt NaCl solution. The two proposed equivalent circuits exhibit the best alignment with the experimental results. By analyzing the impedance data presented in Table 3 along with the Nyquist diagrams, we can conclude that the inclusion of PTFE significantly affects the load transfer resistance (Rct), which reflects the coating's resistance to corrosion. Specifically, when the concentration of PTFE increases from 10 to 20 g/L, Rct increases sharply. However, with

© 2025 The Authors. This article is licensed under a Creative Commons Attribution 4.0 International License.

Table 3. The values of the equivalent circuit elements obtained from fitting the diagrams related to the Nyquist diagram for Ni-P coatings and Ni-P-PTFE composite coatings in 3.5 %wt NaCl solution

Element	Ni-P	Ni-P-PTFE (10 g/L)	Ni-P-PTFE (20 g/L)	Ni-P-PTFE (30 g/L)
R_s	7.572	7.376	10.41	7.603
CPE_1-T	0.0000562	0.0000389	0.0000108	0.0000309
CPE_1-P	0.792	0.897	0.893	0.872
R_2	3575	267.5	324.9	251
CPE_2-T	-	0.0000739	0.0000193	0.000213
CPE_2-P	-	0.7703	0.712	0.0438
R_3 (Ω cm^2)	-	3890	10141	5569

further increases in nanoparticle concentration beyond this point, the values of Rct gradually decrease.

In general, due to the smoothness of nanocomposite coatings compared to Ni-P coating, the load transfer resistance values for all nanocomposite coatings are higher than Ni-P coating. It can be suggested that composite coatings have increased corrosion resistance compared to pure Ni-P alloy coatings. The first reason is that the co-deposition of PTFE particles results in a uniform and dense coating. This density minimizes cracks and voids in the coating, preventing the electrolyte from penetrating and accelerating the corrosion of the substrate metal. The second reason is that PTFE is a non-polar particle and hence, the presence of these particles in the coating reduce the availability of the active metal surface to the corrosive solution and, as a result, the corrosion resistance of the composite increases [15].

The polarization curve of Ni-P coatings and Ni-P-PTFE composite coatings in 3.5 %wt NaCl solution is shown in Figure 5. Increasing the concentration of PTFE has decreased the corrosion current density of

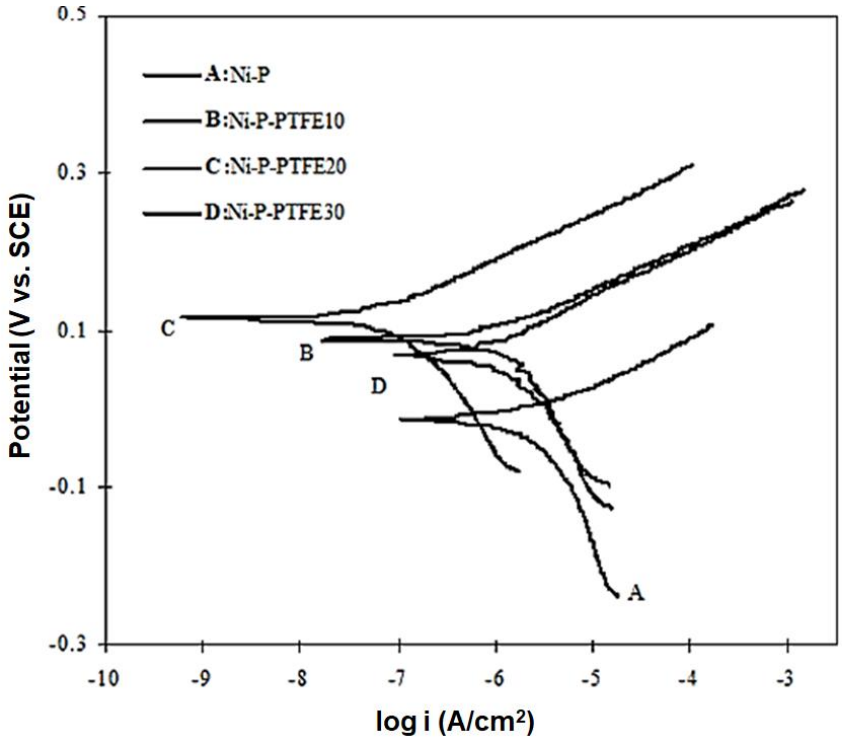

Figure 5. Tafel polarization curves of Ni-P and Ni-P-PTFE coatings in 3.5 %wt NaCl solution with a scan speed of 0.2 mV/s.

© 2025 The Authors. This article is licensed under a Creative Commons Attribution 4.0 International License.

Table 4. Values of i_{corr} and E_{corr} of Ni-P and Ni-P-PTFE composite coatings in 3.5 %wt NaCl solution

Samples	E_{corr} (mV vs. SCE)	i_{corr} (A cm^{-2})
Ni-P	-11.23	5.0×10^{-6}
Ni-P-PTFE (10 g/L)	89.06	1.0×10^{-6}
Ni-P-PTFE (20 g/L)	116.47	1.0×10^{-7}
Ni-P-PTFE (30 g/L)	69.92	1.0×10^{-6}

nanocomposite coatings, shifted the corrosion potential to more positive values, and enhanced the corrosion resistance of these coatings. Table 4 shows the corrosion potential (E_{corr}) and corrosion density (i_{corr}) of these coatings. Data indicate that the lowest corrosion current and highest corrosion resistance are associated with the coating applied from a solution containing 20 g/L of polytetrafluoroethylene. In this concentration, the nucleation is fast, and the crystal growth rate is reduced. This itself makes the coating smoother and more uniform and increases its corrosion resistance compared to other coatings. The results of polarization measurements support the findings from the EIS studies.

Microhardness results shown in Figure 6 indicate that as the concentration of PTFE in the coating increases, the hardness initially decreases to a minimum value before beginning to rise again. In optimal amounts (concentration of 20 g/L) due to the presence of the largest amount of PTFE particles in the structure of the micro-hardness coating, the hardness has decreased, and in the concentration of 30 g/L of PTFE, it has increased again due to the decrease in the number of particles in the micro-hardness coating. Soft particles, such as PTFE and PVDF, reduce the hardness of composite coatings. As the volume fraction of these lubricant particles in the coating increases, the hardness decreases. This reduction in hardness contributes to an increase in the plastic deformation of the coating, primarily due to the presence of the softer particles. This effect has been documented in studies examining microhardness changes in Ni-Cu-P-PTFE coatings deposited through the electroless method [18].

To evaluate the wear resistance and friction coefficient of coatings created with varying concentrations of PTFE, a pin-on-disk test was conducted on the samples. The results of this test to investigate the effect of PTFE concentration on wear and friction coefficient are given below. Figure 7 shows that the lowest friction coefficient is associated with the composite coating derived from a 20 g/L PTFE bath. As expected, with the addition of reinforcing particles inside the composite coating, the

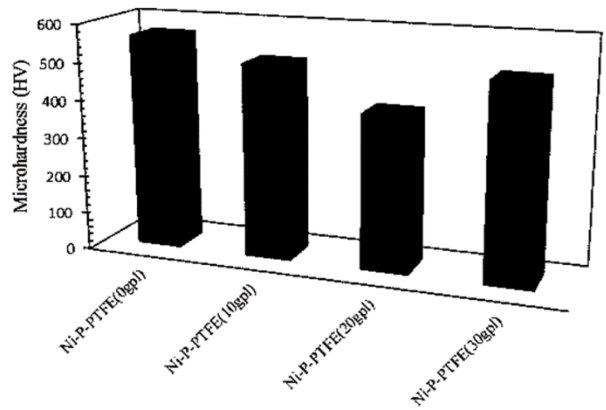

Figure 6. The effect of the concentration of PTFE particles in the plating bath on the microhardness of the Ni-P-PTFE coating.

friction coefficients have decreased from about 0.6 in the absence of PTFE particles to about 0.15 in the composite coating obtained from the 20 g/L PTFE bath. PTFE, being a soft particle, serves as a solid lubricant, effectively reducing the friction coefficient. This issue has also been observed concerning the reduction of the hardness of composite coatings, with the lowest hardness value obtained at a concentration of 20 g/L.

In the presence of 10 g/L of PTFE particles, the decreasing trend of the friction coefficient has been observed to a value of 0.4. In the presence of 30 g/L, the agglomeration of particles in the plating bath and the accumulation of PTFE particles in various areas of the coating have led to an increasing trend in the friction coefficient. In general, it can be stated that one of the factors of changes in wear resistance is the friction coefficient, and the interaction of two factors, hardness and friction coefficient, causes changes in wear resistance. Analysis of the friction coefficients indicates that the coating with 20 g/L of PTFE exhibits the best wear resistance. Similarly, improved wear resistance of electroplated Bronze coatings in the presence of PTFE particles has also been reported [19].

4. Conclusions

Ni-P-PTFE coatings were fabricated using electroplating in a watt bath, incorporating the cationic surfactant CTAB and varying concentrations of PTFE. It was observed that the morphology and electrochemical properties of these coatings depend on the amount of PTFE particles. Electrochemical and tribological studies

© 2025 The Authors. This article is licensed under a Creative Commons Attribution 4.0 International License.

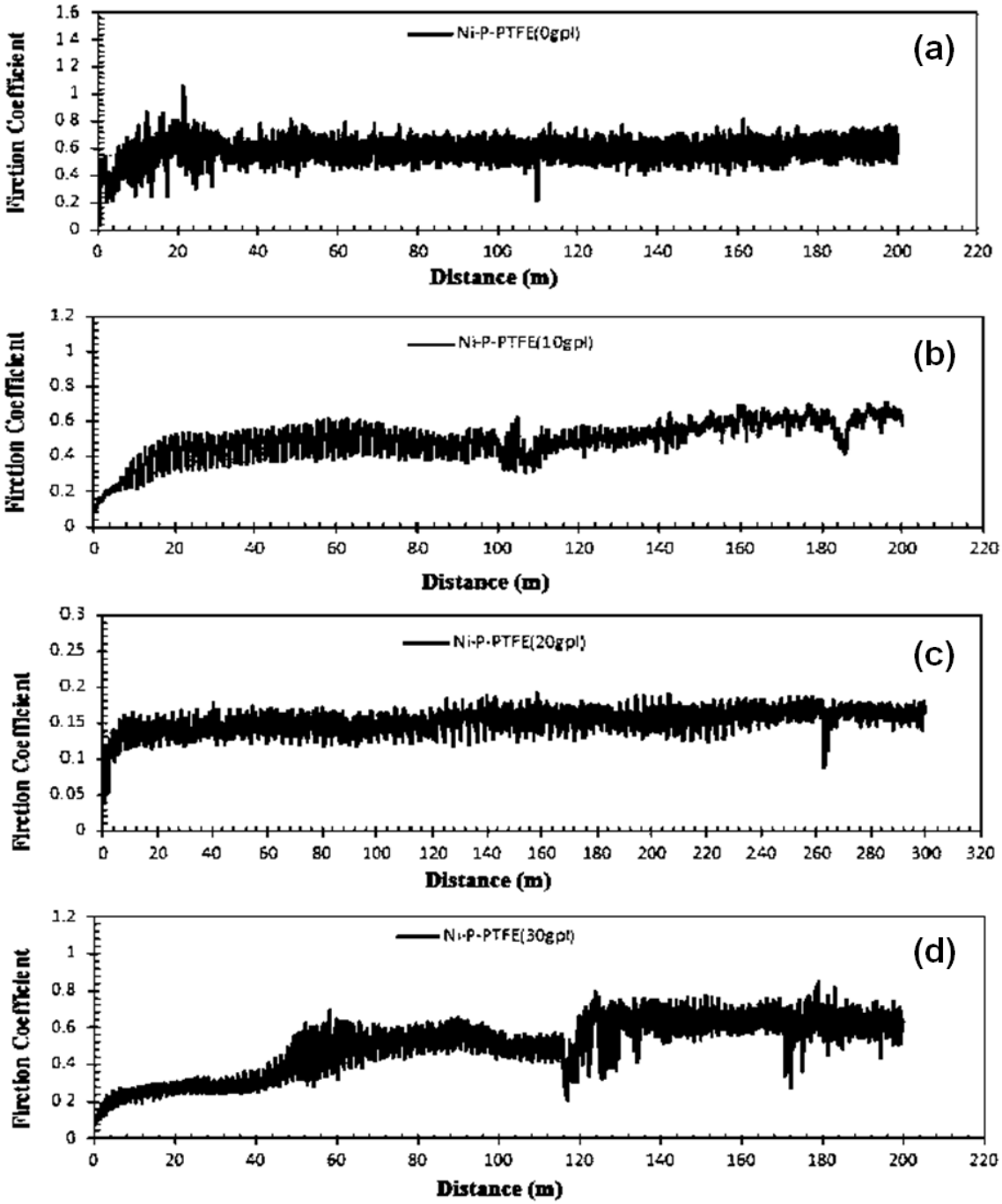

Figure 7. Changes in the friction coefficient and wear resistance of Ni-P-PTFE coating containing different amounts of PTFE particles according to wear distance: (a) 0 g/L, (b) 10 g/L, (c) 20 g/L, and (d) 30 g/L.

revealed that Ni-P-PTFE composite coatings, with a concentration of 20 g/L of PTFE particles, exhibit the highest corrosion resistance in terms of electrochemical performance. The investigation into the microhardness of the coatings indicated that the Ni-P-PTFE coating exhibited the lowest microhardness at an optimal PTFE concentration of 20 g/L. By using the pin on disc test, the lowest coefficient of friction was obtained in Ni-P-PTFE

© 2025 The Authors. This article is licensed under a Creative Commons Attribution 4.0 International License.

composite coatings at a concentration of 20 g/L, and with an excessive increase of these values due to particle clumping and aggregation (agglomeration) of PTFE particles, the coefficient of friction increases.

Conflict of Interest

The authors declare no conflict of interest.

References

1. A. Lelevic and F.C. Walsh. Electrodeposition of Ni P alloy coatings: A review. *Surface and Coatings Technology*, 2019, *369*, 198.

2. M.G. Hosseini, M. Abdolmaleki, and S.A. Seyed Sadjadi. Electrodeposition and mechanical properties of Ni-W-B composites from tartrate bath. *Protection of Metals and Physical Chemistry of Surfaces*, **2010**, *46*, 117.

3. M. Sheydaei and M. Edraki. Orange Peel-impregnated Sodium Montmorillonite as a Sustainable Corrosion Inhibitor for Mild Steel. *Journal of Applied Material Science*, **2025**, *1*, 210136.

4. V. Torabinejad, et al. Electrodeposition of Ni-Fe alloys, composites, and nano coatings–A review. *Journal of Alloys and Compounds*, **2017**, *691*, 841.

5. V. Hasannaeimi and S. Mukherjee. Highly Catalytic Amorphous Ni–P Synthesized via Pulsed Electrodeposition. *Advanced Engineering Materials*, **2019**, *21*, 1801122.

6. M.G. Hosseini, M. Abdolmaleki, and J. Ghahremani. Investigation of corrosion resistance of electrodeposited Ni–W/SiC composite coatings. *Corrosion Engineering, Science and Technology*, **2013**, *49*, 247.

7. C.R. Raghavendra, S. Basavarajappa, and I. Sogalad. Electrodeposition of Ni-nano composite coatings: a review. *Inorganic and Nano-Metal Chemistry*, **2018**, *48*, 583.

8. V. Tseluikin, et al. Electrodeposition and Corrosion Properties of Nickel–Graphene Oxide Composite Coatings. *Materials*, **2021**, *14*, 5624.

9. M. Ganji, et al. The corrosion behavior of Ni–Fe and Ni–Fe–TiC nanoparticles deposited using pulse electrodeposition on low-carbon steel. *Journal of the Australian Ceramic Society*, **2022**, *58*, 1283.

10. D. Almonti, et al. Enhanced wear resistance in Nickel-graphene-PTFE composite coatings: Fabrication and characterisation. *Surface Engineering*, **2025**, *41*, 383.

11. R. Kumar, et al. An outline on modern day applications of solid lubricants. *Materials Today: Proceedings*, **2020**, *28*, 1962.

12. Y. He, et al. An electrodeposited Ni-P-WS2 coating with combined super-hydrophobicity and self-lubricating properties. *Electrochimica Acta*, **2017**, *245*, 872.

13. S. Jeyaraj and P.S. Sivasakthivel. Prediction of Process Parameters for Electrodeposited Ni-PTFE Composite Coating: A Multi-Response Analysis Using ANFIS Model. *Transactions of the Indian Institute of Metals*, **2024**, *77*, 3991.

14. S. Shiri. Exploring Corrosion Protection Potential of Sustainable and Green Morus alba 'Pendula' Fruit Extracts. *Journal of Applied Material Science*, **2025**, *1*, 210139.

15. S. Sangeetha, G.P. Kalaignan, and J.T. Anthuvan. Pulse electrodeposition of self-lubricating Ni–W/PTFE nanocomposite coatings on mild steel surface. *Applied Surface Science*, **2015**, *359*, 412.

16. N. Zhou, *Investigation of Ni-MoS2 self-lubricating composite coating via electrodeposition as a potential alternative for Ni-PTFE coating [PhD Thesis]*, in *Key Engineering Materials*. **2024**, University of Southampton.

17. S. Li, et al. Graphene-Reinforced Zn–Ni Alloy Composite Coating on Iron Substrates by Pulsed Reverse Electrodeposition and Its High Corrosion Resistance. *ACS Omega*, **2021**, *6*, 13728.

18. C. Yanhai, et al. Effect of PTFE Addition on the Properties of Electroless Ni-Cu-P-PTFE Deposits. *Rare Metal Materials and Engineering*, **2014**, *43*, 1025.

19. M. Shamsaee Zafarghandi and N. Pirhady Tavandashti. Electrodeposition of Hierarchically Structured Superhydrophobic Ni-PTFE Composite Coating with Remarkable Corrosion Resistance, Chemical and Mechanical Stability. *Scientia Iranica*, **2023**, *31*, 907.

© 2025 The Authors. This article is licensed under a Creative Commons Attribution 4.0 BY International License.

© 2025 The Authors. This article is licensed under a Creative Commons Attribution 4.0 International License.